

# We are IntechOpen, the world's leading publisher of Open Access books Built by scientists, for scientists

6,300

Open access books available

171,000

International authors and editors

190M

Downloads

Our authors are among the

154

Countries delivered to

TOP 1%

most cited scientists

12.2%

Contributors from top 500 universities



WEB OF SCIENCE™

Selection of our books indexed in the Book Citation Index  
in Web of Science™ Core Collection (BKCI)

Interested in publishing with us?  
Contact [book.department@intechopen.com](mailto:book.department@intechopen.com)

Numbers displayed above are based on latest data collected.  
For more information visit [www.intechopen.com](http://www.intechopen.com)



# Introductory Chapter: Application of Optical Fiber for Sensing

Christian Cuadrado-Laborde

## 1. Introduction

The history of the use of optical fiber for sensing applications began with two different, but interrelated, discoveries: laser light and optical fibers. The first laser was built in 1960 by T. H. Maiman at Hughes Research Laboratories, based on the theoretical work by C. H. Townes and A. L. Schawlow. A laser provides a source of an intense coherent light, highly collimated, and quasi-monochromatic; its potential for data transfer was immediately envisaged. Naturally, first experiments involved the transmission of the laser beam through the air. However, a communication channel cannot be practically sustained propagating freely through the air, owing to atmospheric attenuation and weather influence. Researchers also conducted experiments by transmitting the laser beam through glass fibers, which soon became the preferred medium for transmission of light. First, optical fibers were not practical to sustain a communication channel mainly due to the presence of impurities in the fiber material, resulting in very high transmission losses ( $>1000$  dB/km), until Corning presented at the beginning of the 1970s optical fibers with (in comparison) very lower transmission losses, with only a few dB/km. Today, typical transmission losses are below 0.2 dB/km. This represents an extraordinary improvement as compared with electrical signal transmission through coaxial cables, not to mention the wider bandwidth available, which is several orders of magnitudes higher.

These developments paved the way to a plethora of different works on fiber optic sensing. But, what is an optical fiber sensor? **Figure 1** shows a block diagram of a typical optical fiber sensor. It is composed of a light source (which not only can be a laser, but also a broad band light source like a light emitting diode, etc.), the optical fiber itself transmits the light from the light source to the sensing area

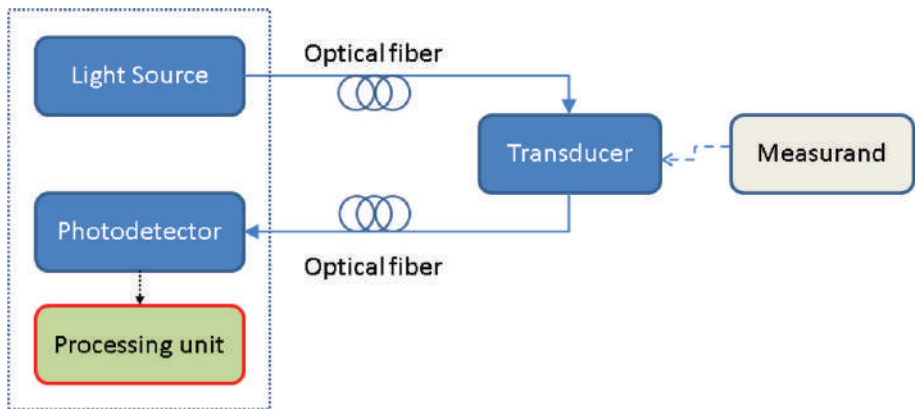


**Figure 1.**  
General block diagram for an optical fiber sensor.

(forward optical fiber), the sensing element (which can be the same optical fiber, or another specially designed optical fiber, or not fiber at all, see below the differences between intrinsic and extrinsic optical fiber detectors), another optical fiber, which carry the light with the information of the measurand of interest (in some case, backward or return optical fiber; in this case, forward and backward fibers are the same fiber; it typically used some additional optical fiber element like an optical circulator), a photo-detector, which converts light in an electrical signal, and an end-processing device or processing unit (which converts this electric signal, eventually digitized in the measurand of interest; in a research laboratory environment, it would be an optical-spectrum analyzer, oscilloscope, etc.; and in a final user environment, the processing unit is simplified in order to provide more easy access to the measurand information, and of course, in order to reduce costs).

Compared with other types of sensors, fiber optic sensors exhibit a number of advantages, among them are the following:

- Possibility of use in high-voltage environments, since an optical fiber is made fundamentally of silica, which is an electrically insulating material.
- Possibility of use in explosive environments, since electricity is not present, there is no risk at all of electrical sparks.
- Optical fibers are chemically passive (the object to be measured can hardly be contaminated).
- Immunity to corrosion.
- Immunity to electromagnetic interference, no matter how much intense they were. Because an optical fiber is electrically nonconductive, it becomes impossible to act as an antenna.
- Very wide operating temperature range.
- Easy integration into a wide variety of structures, including composite materials, with little interference due to their small size and cylindrical geometry.
- Lightweight, which is fundamental in aero spatial applications.
- Robust and resistant to harsh environments.
- Material cost is relatively low, which in turn prevents theft (as compared with copper wires).
- Security of information passed down the cable.
- Highly sensitive sensing capabilities.
- Multiplexing capability to form sensing networks, multiple sensors in a single fiber can be simultaneously interrogated.
- Remote sensing capability.
- Multifunctional sensing capabilities such as strain, pressure, corrosion, temperature, and acoustic signals.

- No need for power amplifiers in a broad length range, since the attenuation losses can be very low, even over long distances.

Optical fiber sensor can be divided into intrinsic or extrinsic. In the first, intrinsic, the measurand of interest interacts itself with the optical fiber; that is, the optical fiber structure is modified under the influence of the measurand and the fiber itself plays an active role in the sensing function. As a consequence, there is some kind of modulation of light inside the fiber (this modulation can affect the intensity, wavelength, phase, or polarization), which carries the information of the performed measurement. Thus, by detecting these parameters and their changes, the external perturbations can be sensed. This is the reason why they are also called all-fiber sensors. A typical example of this kind of sensors is a fiber Bragg grating working as a strain sensor; under different strains, the Bragg reflection shifts to a different wavelength. On the other hand, in an extrinsic sensor, the measurand does not act on the fiber itself, it acts outside the fiber. In this case, the optical fiber merely acts as a transmission medium, and of course light collection. Some fiber optic Fabry-Perot interferometers are good examples of this kind.

The aforementioned division is not unique, and optical fiber sensors can be divided according to other characteristics. One especially useful is according to the point of measurement. Therefore, we can distinguish single-point sensing, quasi-distributed sensing, and continuous distributed sensing. In the former, there is one single point of measurement; for example, a LPG measuring the concentration of some organic compound at a specific place. On the contrary, in quasi-distributed sensing, there are integer numbers of point sensors along the optical fiber; for example, when several fiber Bragg gratings are employed as sensing elements distant some length between them (in this case, some kind of multiplexing is necessary). Finally, in continuous distributed sensing, there is

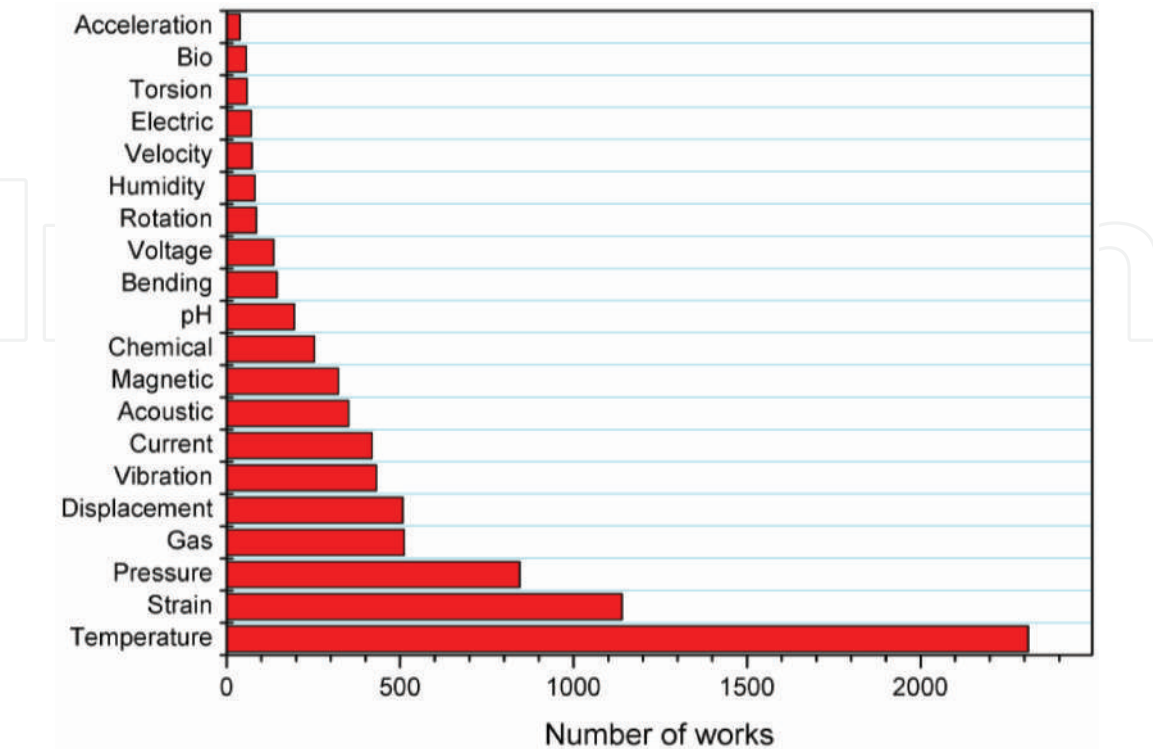


**Figure 2.**  
*Published works along all years distributed according to the nature of the measurands. Patents are not included. In those cases, where the work deals with more than one measurand; for example, temperature and strain, the work counts for both.*

a continuous, real-time measurement along the entire length of an optical fiber cable; not only there are theoretically infinite numbers of measurement points, but also the optical fiber itself is the sensing element (as an example in Raman distributed optical sensing).

Optical fiber sensors have attracted the attention of several research groups around the world along all these years. **Figure 2** shows the result of a rapid search of those published works with the simultaneous presence in their titles of three words: fiber + sensor + measurand of interest (i.e., temperature, strain, pressure, gas concentration, etc.). Temperature and strain are the most frequent physical quantities measured through optical fiber sensors, which is not surprising at all, since first efforts were focused in this direction.

The optical fiber sensors in turn, can be constructively performed in several ways, either by using: short (Bragg) or long period gratings, interferometers (Fabry-Perot, Mach-Zehnder, etc.), by detecting different scattered light signals (Raman, Brillouin, and Rayleigh), photonic crystal fibers, surface plasmon resonance (SPR) etc. **Figure 3** shows the number of those published works with the simultaneous presence in their titles of three words: fiber + sensor + operation principle (i.e., Bragg grating, photonic crystal fiber, Fabry-Perot, etc.). It should not be surprising that the most used fiber optic sensor is the fiber Bragg grating, which is motivated firstly by its versatility.

To resume, the optical fiber sensing technology is today a successful and mature technology after a half-century of development [1–5], with a year-to-year increasing market participation. It is expected that in the near future arose new emerging applications offering new opportunities for research and exploitation.

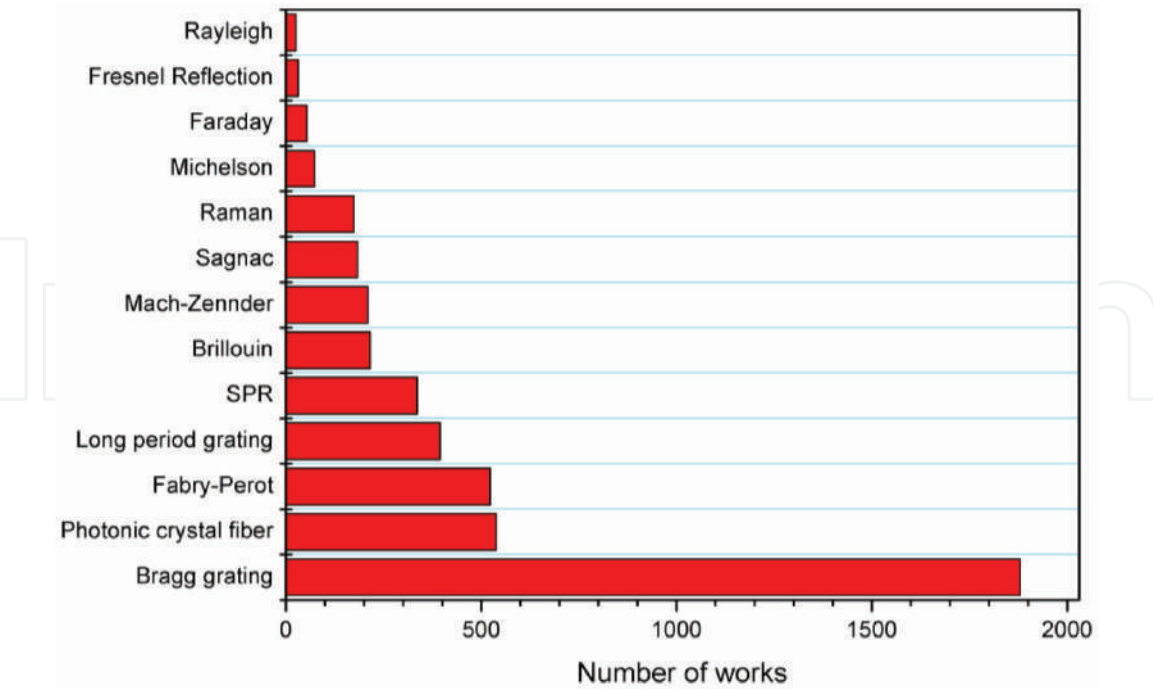


**Figure 3.** Published works along all years distributed according to the operation principle. Patents are not included. In those cases, where the work deals with more than one operation principle (e.g., fiber Bragg grating and long-period grating), the work counts for both.

IntechOpen

## Author details

Christian Cuadrado-Laborde<sup>1,2\*</sup>

1 Instituto de Física Rosario (CONICET-UNR), Rosario, Argentina

2 Facultad de Química e Ingeniería, Pontificia Universidad Católica Argentina,  
Rosario, Argentina

\*Address all correspondence to: [christian.cuadrado@uv.es](mailto:christian.cuadrado@uv.es)

## IntechOpen

© 2019 The Author(s). Licensee IntechOpen. This chapter is distributed under the terms of the Creative Commons Attribution License (<http://creativecommons.org/licenses/by/3.0>), which permits unrestricted use, distribution, and reproduction in any medium, provided the original work is properly cited. 

## **References**

- [1] Lee B. Review of the present status of optical fiber sensors. *Optical Fiber Technology*. 2003;**9**(2):57-79. DOI: 10.1016/S1068-5200(02)00527-8
- [2] Lopez-Higuera JM, editor. *Handbook of Optical Fibre Sensing Technology*. New York: John Wiley & Sons Inc.; 2002. 828 pp. ISBN 0-47182-053-9
- [3] Di Sante R. Fibre optic sensors for structural health monitoring of aircraft composite structures: Recent advances and applications. *Sensors*. 2015;**15**(8):18666-18713. DOI: 10.3390/s150818666
- [4] Culshaw B. Optical fibre sensors: A current perspective. *The Open Optics Journal*. 2013;**7**(Suppl-1, M2):21-31. DOI: 10.2174/1874328501307010021
- [5] Culshaw B, Kersey A. Fiber-optic sensing: A historical perspective. *Journal of Lightwave Technology*. 2008;**26**(9):1064-1078. DOI: 10.1109/JLT.0082.921915



# We are IntechOpen, the world's leading publisher of Open Access books Built by scientists, for scientists

6,300

Open access books available

171,000

International authors and editors

190M

Downloads

Our authors are among the

154

Countries delivered to

TOP 1%

most cited scientists

12.2%

Contributors from top 500 universities



WEB OF SCIENCE™

Selection of our books indexed in the Book Citation Index  
in Web of Science™ Core Collection (BKCI)

Interested in publishing with us?  
Contact [book.department@intechopen.com](mailto:book.department@intechopen.com)

Numbers displayed above are based on latest data collected.  
For more information visit [www.intechopen.com](http://www.intechopen.com)





# Minimalist Approach for the Design of Microstructured Optical Fiber Sensors

*Jonas H. Osório and Cristiano M. B. Cordeiro*

## Abstract

We report on recent investigations regarding ultra-simplified designs for microstructured optical fiber sensors. This minimalist approach relies on the utilization of capillary-like fibers—namely embedded-core fibers, surface-core fibers, and capillary fibers—as platforms for the realization of sensing measurements. In these fibers, guidance of light is accomplished in an embedded or surface germanium-doped core or in the hollow part of capillaries. External stimuli can alter fiber wall thickness and/or induce birefringence variations, allowing, for the embedded-core and capillary fibers, to operate as pressure or temperature sensors. For the surface-core fiber design, the interaction between the guided mode and external medium allows the realization of refractive index sensing either by using fiber Bragg gratings or surface plasmon resonance phenomenon. Also, we report the realization of directional curvature sensing with surface-core fibers making use of the off-center core position. The attained sensitivities are comparable to the ones obtained with much more sophisticated structures. The results demonstrate that these novel geometries enable a new route toward the simplification of optical fiber sensors.

**Keywords:** fiber optics, fiber optics sensors, fiber Bragg gratings, surface plasmon resonance, microstructured optical fibers

## 1. Introduction

The increasing need for the development of optical sensors motivates intense research in this area. Particularly, great efforts have been observed in the field of optical fiber sensors since they can provide numerous advantages such as high sensitivity and improved resolution. Moreover, fiber optics are immune to electromagnetic interference and suitable to be used in harsh environments.

In this context, microstructured optical fibers have much contributed to the development of sensors due to their huge design freedom. Thus, numerous sensing configurations have been reported in the literature to be able to probe variations of a great diversity of parameters such as temperature, strain, hydrostatic pressure, curvature, and refractive index. Regarding pressure sensors, for example, successful approaches are to use photonic-crystal fibers (PCFs) with triangular-shaped microstructures [1] or side-hole PCFs [2]. In these configurations, the hydrostatic pressure application generates asymmetric stresses distributions within the fiber

structure and changes its birefringence via the photoelastic effect. Additionally, metal-filled side-hole PCFs have been demonstrated to act as high-sensitivity temperature sensors [3, 4]. In this approach, the metal expansion inside the fiber structure induces an asymmetric stress distribution within the same (due to the different thermal expansion coefficients of silica and of the metal). It entails changes in the fiber birefringence which can be optically probed and related to the temperature variation through a suitable calibration.

Microstructured optical fibers can also be used as refractive index sensors. Among those ones, plasmonic sensors acquire great importance due to the high sensitivities they can achieve. In these platforms, selected regions of the fiber structure are coated with a nanometric-thick metallic layer to provide coupling between the optical mode and a plasmonic mode. Possible approaches are to coat the inner holes of microstructured fibers [5] or to open up a channel in the fiber structure to expose the fiber core for metallic nanospheres immobilization [6].

However, the microstructured optical fibers usually employed in the sensing schemes described above are sophisticated, which demand great technical efforts for their fabrication. Here, alternatively, we present sensors which are endowed with ultra-simplified microstructures based on capillary-like fibers (embedded-core fibers [7, 8], surface-core fibers [9, 10], and capillary fibers [11]). As it will be shown in the following, even though these configurations are very simple, the attained sensitivities are high when compared to other fiber sensors based on more complex structures. Thus, we can identify the use of capillary-like fibers as a new avenue for obtaining highly sensitive fiber sensors with simplified fabrication process.

## 2. Capillary-like fiber designs for sensing applications

**Figure 1** shows the fiber designs we present here. In **Figure 1a**, a diagram of the embedded-core fiber is shown [7, 8]. This structure consists of a silica capillary endowed with a germanium-doped core, which is placed inside the wall of the capillary. The embedded-core fiber can be employed for pressure or temperature sensing measurements. Specifically, when the embedded-core fiber acts as a temperature sensor, the capillary hollow part must be filled with metal (**Figure 1b**). The principle of operation of these sensors is centered on the capillary wall displacements that occur when the hollow embedded-core fiber is pressurized or when the metal-filled embedded-core fiber experiences temperature variations. These wall displacements within the capillary wall entail asymmetric stress distributions in the

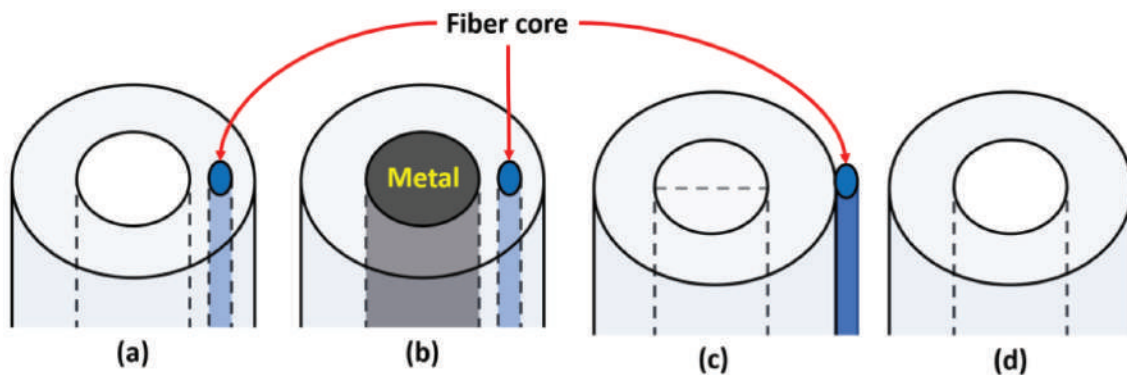


**Figure 1.**

(a) Embedded-core fiber, (b) metal-filled embedded-core fiber, (c) surface-core fiber and (d) capillary fiber.

fiber structures, which generate, by virtue of the photoelastic effect, birefringence variations in the fiber core.

**Figure 1c** shows a diagram of the so-called surface-core fiber [9]. In this structure, the fiber core is placed on the fiber external surface. As here the core directly interfaces the external medium, the evanescent field of the guided optical mode permeates the external environment. Surface-core fibers are, then, a suitable platform for refractive index sensing. A possible approach is to imprint fiber Bragg gratings (FBGs) in the fiber core and measure the sensor spectral response as the external refractive index is altered [9]. A second approach is to perform plasmonic sensing by metal-coating the surface-core fiber with a nanometric metallic layer [10]. Additionally, the off-center position of the fiber core permits the surface-core fibers to act as directional curvature sensors. In this case, the curvature-induced strain levels within the core can be probed by a FBG [9].

**Figure 1d** presents a forth structure, which is simply a capillary fiber [12]. Here, we study the guidance of light in the hollow part of the capillary and investigate how the optical response of the fiber is changed when it experiences temperature variations. It is worth saying that, in this investigation, we employed polymethyl methacrylate (PMMA) capillaries. This choice was due to the higher thermal expansion and thermo-optic coefficients of PMMA when compared to silica.

In the next sections, we specifically describe the principle of operation of each configuration. Moreover, we present theoretical and experimental results and compare them with the ones available in the literature.

### 3. Embedded-core capillary fibers for pressure sensing

The application of pressure to capillary fibers generates displacements on their walls. This, in turn, induces an asymmetric stress distribution within the capillary structure which, due to the stress-optic effect, entails birefringence variations in it. As described in [7], an analytical model can be used to account for the material birefringence variations ( $\Delta B_{mat}$ ) in pressurized capillaries. To do that, we can employ Eq. (1), where  $C_1$  and  $C_2$  are the elasto-optic coefficients ( $C_1 = -0.69 \times 10^{-12}$  and  $C_2 = -4.19 \times 10^{-12} \text{ Pa}^{-1}$  for silica), and  $\sigma_x$  and  $\sigma_y$  are the pressure-induced stresses on the horizontal and vertical directions, respectively [13, 14].

$$\Delta B_{mat} = (C_2 - C_1)(\sigma_x - \sigma_y) \quad (1)$$

The stresses  $\sigma_x$  and  $\sigma_y$  can be obtained from Lamé solution inside thick-walled tubes subjected to pressure [15]. The resulting expression for the material birefringence at a position  $x$  on the horizontal axis is shown in Eq. (2), where  $r_{in}$  and  $r_{out}$  are the inner and outer radius of the capillary, and  $p_{gauge} = p_{out} - p_{in}$  ( $p_{in}$  and  $p_{out}$  are the inner and outer pressure levels) [7].

$$\Delta B_{mat} = 2(C_2 - C_1)p_{gauge} \left[ 1 - \left( \frac{r_{in}}{r_{out}} \right)^2 \right]^{-1} \frac{r_{in}^2}{x^2} \quad (2)$$

By observing Eq. (2), we see that, when maintaining  $r_{in}$  constant,  $|\Delta B_{mat}|$  will be greater for higher  $r_{in}/r_{out}$  ratios. It means that the analytical model predicts that the change in the birefringence is increased for thin-walled capillaries. Moreover, we see that, for fixed  $r_{in}$  and  $r_{out}$  values, the change in the birefringence is higher for positions ( $x$ ) which are closer to the inner wall of the capillary [7].

Although the analytical model for the material birefringence can provide important information on the most important geometrical parameters that affects the sensitivity of the sensor, it is necessary to account for the modal birefringence dependence on the applied pressure for a broader understanding of the sensor characteristics. To do this, a numerical simulation of the embedded-core fiber structure was carried on. **Figure 2** presents the results for  $dB_{\text{modal}}/dP$  (derivative of the modal birefringence as a function of the pressure) as a function of the core position within the capillary. In the simulations,  $r_{\text{in}} = 40 \mu\text{m}$  and  $r_{\text{out}} = 67.5 \mu\text{m}$ . The core dimensions were considered to be  $5.7$  and  $11.4 \mu\text{m}$ .

The results presented in **Figure 2** show, as could be expected from the analytical model, that  $dB_{\text{modal}}/dP$  values are higher for core positions which are closer to the inner wall of the capillary. However, we note that, very interestingly, the trend that is expected from the analytical model is verified only when the whole core is within the capillary wall. When the the core has part of its area outside of the capillary wall, a strong decrease in  $dB_{\text{modal}}/dP$  is observed (core region is represented as dark blue ellipses in **Figure 2**). This allows observing that, for maximizing  $dB_{\text{modal}}/dP$  in embedded-core fibers, it is crucial that the whole core is inside the capillary wall.

In order to obtain an experimental demonstration of the proposed design acting as a pressure sensor, we performed the fabrication of the embedded-core fiber. The fabrication process is simple and with few steps. Initially, a germanium-doped silica rod is merged to a silica tube. In sequence, the resulting preform is inserted in another silica tube, which acts as a jacket. The preform is then drawn in a fiber tower facility [7]. **Figure 3a** shows the cross-section of the embedded-core fiber.

**Figure 3b** exposes a diagram of the experimental setup used for pressure measurements. Light from a broadband source (BLS) is launched in the fiber and detected with an optical spectrum analyzer (OSA). Polarizers ( $P_1$  and  $P_2$ ) are used to excite the orthogonal modes of the fiber and to recombine them after traveling along the fiber. A pressure chamber is used to subject the fiber to different pressure levels.

By using the configuration of **Figure 3b**, an interference spectrum is measured in the OSA. Since the embedded-core fiber is sensitive to pressure variations, the spectral position of the interferometric fringes is shifted when the external pressure level is altered. A sensitivity coefficient,  $C_S$ , is defined to account for the spectral shift of the fringes as a function of the pressure variation,  $\frac{d\lambda_F}{dP}$ . The  $C_S$  value can also be written as a function of the wavelength,  $\lambda$ , the fiber group birefringence,  $G$ , and

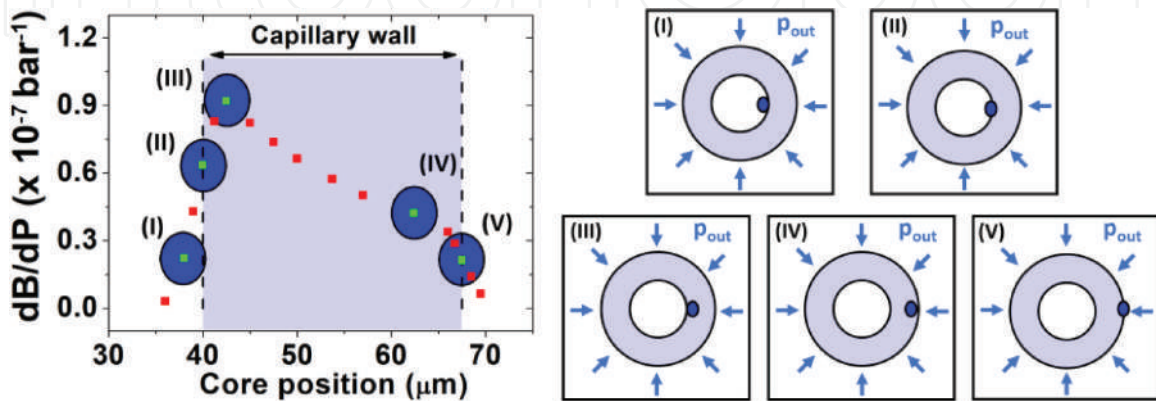


**Figure 2.** Modal birefringence derivative as a function of pressure for different core positions inside the capillary wall. Light blue region represents the capillary wall, and dark blue ellipses represent the core region. Insets illustrate the core position within the capillary.



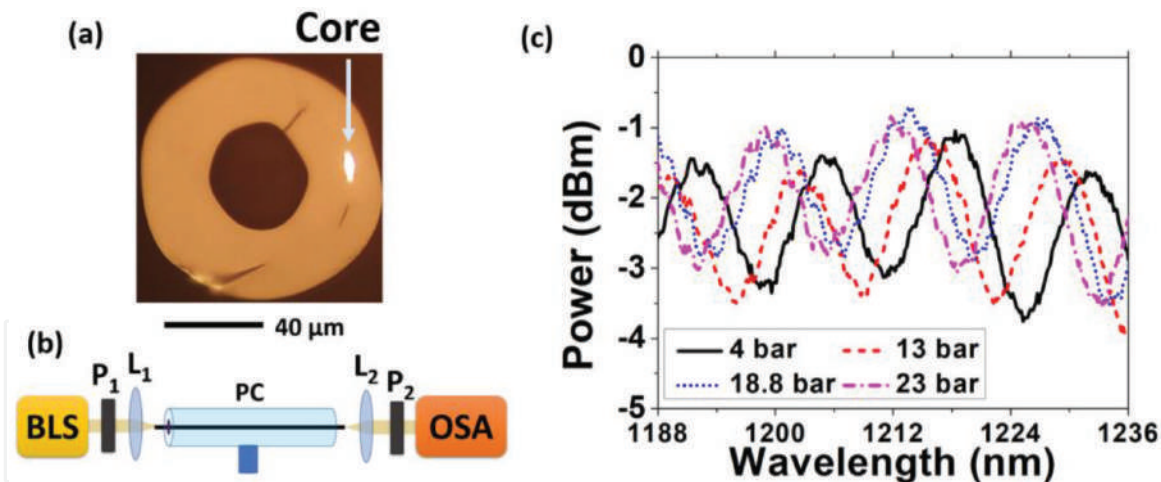


**Figure 3.** (a) Embedded-core fiber. (b) Experimental setup for pressure sensing measurements. BLS: broadband light source.  $P_1$  and  $P_2$ : polarizers.  $L_1$  and  $L_2$ : objective lenses. PC: pressure chamber. (c) Spectral response of the embedded-core fiber for different pressure levels.

of the modal phase birefringence derivative with respect to the pressure,  $\frac{\partial B_{\text{modal}}}{\partial P}$  — Eq. (3) [2].

$$C_s \equiv \frac{d\lambda_{\text{IF}}}{dP} = \frac{\lambda}{G} \frac{\partial B_{\text{modal}}}{\partial P} \quad (3)$$

**Figure 3c** presents the measured optical response of the embedded-core fiber for different pressurization conditions. It is seen that when the pressure level increases, the fringes blueshift. After performing an appropriate correction on the fiber pressurized and nonpressurized lengths [2, 16], we can estimate a sensitivity value of  $(1.04 \pm 0.01)$  nm/bar [7]. This value is high when compared to other results measured in polarimetric measurements reported in the literature. For example, in [17], a sensitivity of 0.342 nm/bar was measured for a commercial photonic-crystal fiber. Additionally, in [18, 19], the sensitivities of 0.30 and 0.52 nm/bar were reported for specially designed microstructured fibers.

Moreover, the  $\frac{\partial B_{\text{modal}}}{\partial P}$  value for the embedded-core fiber can be estimated from Eq. (3). The resulting value is  $(2.33 \pm 0.02) \times 10^{-7} \text{ bar}^{-1}$ , which is in the same magnitude order of the ones found for much more sophisticated microstructured fibers [1]. Therefore, we see that the embedded-core fiber structure allows achieving high sensitivity ( $C_s$ ) and  $\frac{\partial B_{\text{modal}}}{\partial P}$  even with a nonoptimized fiber. It also allows recognizing embedded-core fiber as a promising platform for the realization of pressure sensing using optical fibers and a novel route for the design of microstructured optical fiber pressure sensors.

#### 4. Embedded-core capillary fibers for temperature sensing

Embedded-core fibers can also act as highly sensitive temperature sensors if a metal is inserted into the hollow part of the capillary (**Figure 1b**). In analogy to the embedded-core fiber pressure sensor, the principle of operation is based on the induction of stresses inside the capillary and on the consequent variation of the fiber birefringence [8].

In this configuration, the metal expansion inside the capillary causes its volume elements to displace and to compress the silica capillary structure. This, in turn,

entails an asymmetric stress distribution within the capillary wall and induces birefringence variations. An analytical model can be used to predict the most relevant parameters that contribute to the sensor response. This analytical model provides Eq. (4), which accounts for the variation in the material birefringence of the capillary,  $\Delta B_{mat}$ , for a given temperature variation,  $\Delta T$  ( $r_{in}$  and  $r_{out}$  are the capillary inner and outer radii, and  $C_1$  and  $C_2$  are the silica elasto-optic coefficients). The parameter  $\delta$  in Eq. (4) is given by Eq. (5), where  $\nu$  is the Poisson ratio,  $E$  is the Young modulus, and  $\alpha$  is the thermal expansion coefficient. In Eq. (5), index 1 refers to the filling metal and index 2 refers to silica [8]. By observing Eq. (4) and Eq. (5), it is possible to realize that  $|\Delta B_{mat}|$  will be greater for positions closer to the inner radius and when the filling metal has a larger thermal expansion coefficient.

$$\Delta B_{mat} = -2\delta\Delta T(C_2 - C_1)\frac{r_{out}^2}{x^2} \quad (4)$$

$$\delta = \frac{(1 + \nu_2)\alpha_2 - (1 + \nu_1)\alpha_1}{\frac{(1 + \nu_1)}{E_1}\left(\nu_1 - \frac{1}{2}\right) + \frac{(1 + \nu_2)}{E_2}\left(\nu_2 - \frac{1}{2} - \frac{r_{out}^2}{r_{in}^2}\right)} \quad (5)$$

Thus, indium was chosen to be the filling metal due to its high thermal expansion coefficient ( $32.1 \times 10^{-6} \text{°C}^{-1}$ ) and reasonably low melting point ( $156^\circ\text{C}$ ) [3]. The low melting point is an important property since it simplifies the metal filling process. To insert the metal inside the embedded-core fiber, the metal is molten and pressure is applied to push it into the hollow region.

**Figure 4a** shows the indium-filled embedded-core fiber. To measure its temperature sensitivity, the same experimental setup as represented in **Figure 3b** was used. The unique difference is that, for the temperature sensing measurements, the pressure chamber was substituted by a water reservoir placed on a hot plate in order to adequately alter the fiber temperature.

**Figure 4b** shows the spectra measured for different temperature conditions. We see that there is a spectral shift toward longer wavelengths as the temperature is increased. After performing a suitable correction on the heated and unheated fiber lengths, the sensitivity was calculated to be  $(8.40 \pm 0.06) \text{ nm/°C}$  [8]. This sensitivity value compares well to the highest temperature sensitivity values reported in the literature such as  $9.0$  [4],  $6.6$  [20], and  $16.49 \text{ nm/°C}$  [21], which were measured for photonic-crystal fibers filled with indium, ethanol, and index matching liquid, respectively. This once again demonstrates that embedded-core fibers are a very promising platform for the realization of high-sensitivity optical sensing.

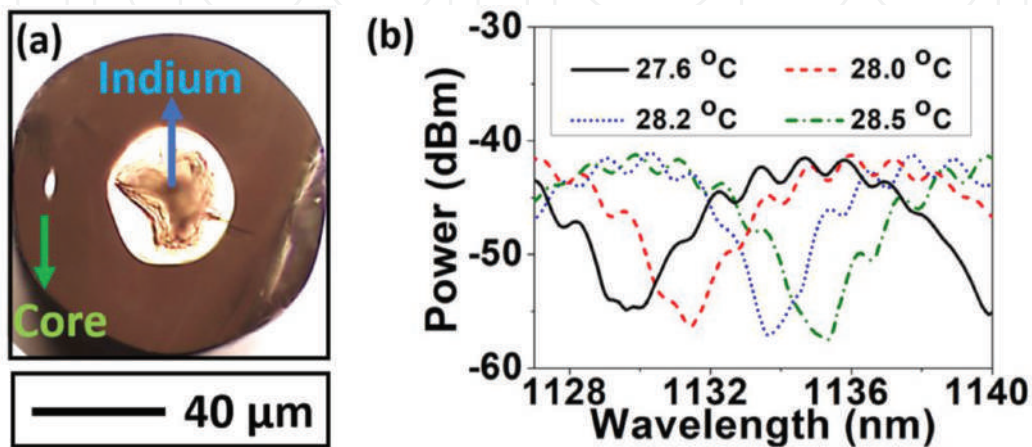


**Figure 4.**  
(a) Indium-filled embedded-core fiber. (b) Spectral response of the indium-filled embedded-core fiber for different temperature conditions.

### 5. Surface-core fibers for refractive index sensing

A third sensing opportunity under the approach of simplified optical fiber sensors is the employment of surface-core fibers [9]. In this kind of fibers, the core is placed on the outer surface of the same (Figure 1c). The proximity of the core to the external environment makes surface-core fibers suitable to be used as refractive index sensors, and the off-center position of the core allows these fibers to operate as directional curvature sensors. Figure 5a presents the cross-section of the surface-core fiber.

In order to explore the refractive index sensitivity of surface core fibers, fiber Bragg gratings (FBGs) can be inscribed in the fiber core [9]. FBGs consist of a refractive index modulation in the core of the fiber able to couple the propagating core mode to a contra-propagating one. The coupling between the modes is achieved at a specific wavelength,  $\lambda_B$ , which can be accounted by Eq. (6), where  $n_{eff}$  is the effective refractive index of the core mode and  $\Lambda$  is the pitch of the grating. Experimentally, the response of FBGs is seen as a reflection peak at  $\lambda_B$ .

$$\lambda_B = 2n_{eff}\Lambda \tag{6}$$

As the optical mode guided in the core directly interfaces the external medium, the effective refractive index of the core mode will be dependent on the external refractive index variations. Thus, if the refractive index of the external environment is altered, a shift in the spectral position of the Bragg peak is expected.

Figure 5b presents the measured wavelength shift of the Bragg peak as a function of the external refractive index. As can be seen in Figure 5b, the results for the surface-core fiber showed low sensitivity. To improve the sensor response, tapers from the surface-core fiber were prepared prior to grating inscription. By doing this, it is possible to enhance the interaction between the guided mode evanescent

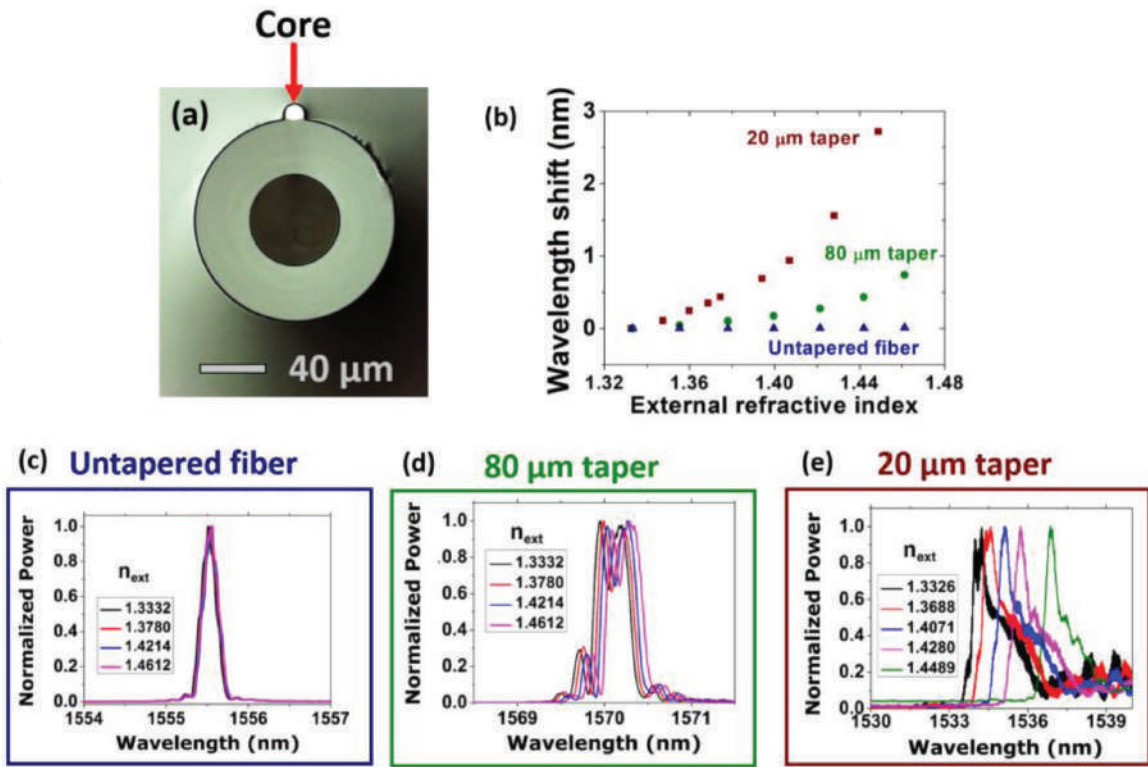


Figure 5.  
(a) Surface-core fiber. (b) Wavelength shift of the Bragg peak as a function of the external refractive index. Reflected Bragg peaks in the (c) untapered surface-core fiber and in the (d) 80 μm and (e) 20 μm tapers.



field and the external medium and improve the sensitivity. The results measured for tapers with 80 and 20  $\mu\text{m}$  diameter are also shown in **Figure 5b**. The Bragg peaks for the untapered surface-core and for the 80 and 20  $\mu\text{m}$  tapers are shown in **Figure 5c–e**—the gratings were imprinted via phase-mask technique by employing phase masks with pitches 1075.34 nm (for the 80  $\mu\text{m}$  taper) and 1071.2 nm (for the untapered fiber and for the 20  $\mu\text{m}$  taper). Around 1.42 RIU (refractive index unit), the measured sensitivities were 8 and 40 nm/RIU for the 80 and 20  $\mu\text{m}$  tapers, respectively. These sensitivity values compare well with other results for FBG-based refractive index sensors. In [22], it is reported a sensitivity of 15 nm/RIU for a Bragg grating inscribed in a 6- $\mu\text{m}$ -thick taper (measured around 1.326 and 1.378 RIU) and, in [23], a sensitivity of 30 nm/RIU was measured for a 8.5- $\mu\text{m}$  taper (in the same refractive index range). It is worth observing that the results for surface-core fibers were attained for thicker tapers, which implies in sensor robustness improvement.

Another possibility for exploring the sensitivity of surface-core fibers to variations in the refractive index of the external medium is to functionalize the core with a metallic nanolayer and make the fiber to act as a plasmonic sensor. In this approach, the core mode can be resonantly coupled to a plasmonic mode when phase-matching occurs between them (surface plasmon resonance—SPR). The coupling between these modes is seen as a spectral dip at the wavelength where the phase matching condition is achieved. As the fiber core directly interfaces the external medium, the spectral position of the plasmonic resonance will be dependent on the refractive index of the external environment. The sensitivity of the configuration is, therefore, accounted from the spectral shift of the plasmonic resonance as a function of the external refractive index variation.

**Figure 6a** presents a simulation on the transmittance of the surface-core fiber plasmonic sensor for different refractive index values. In the simulations, the fiber core is assumed to have a 10  $\mu\text{m}$  diameter and to be coated with a gold layer of 50 nm thick. It is seen that the plasmonic resonance is shifted toward longer wavelengths as the external refractive index increases. The sensitivity accounted from the simulations is 1290 nm/RIU. In addition, in **Figure 6b**, the core mode intensity profiles are shown when it is not phase-matched (off-resonance) and when it is phase-matched (in resonance) with the plasmonic mode. We can observe that, when the modes are in resonance, they hybridize. The intensity profiles in **Figure 6b** were calculated for an external refractive index of 1.39. The phase-matched intensity profile was accounted at 600 nm and the one for the off-resonance condition was accounted at 720 nm.

To experimentally test the proposed sensor, the fiber core was coated with a gold layer of 50 nm thick, and sensing measurements were performed at the Aalto

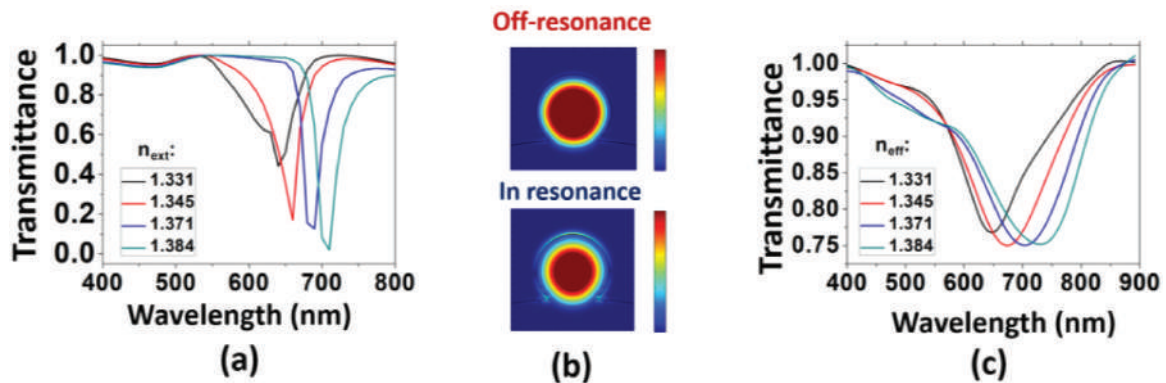


**Figure 6.** (a) Simulated transmittance for different external refractive indexes ( $n_{\text{ext}}$ ). (b) Intensity profiles of the core mode when off-resonance and when in resonance with the plasmonic mode. (c) Experimental transmittance for different external refractive indices.

University (Finland) [10] by immersing the sensor into glycerol-water solutions at different concentrations. **Figure 6c** shows the transmittance spectra as a function of the external refractive index. By following the spectral position of the spectral dip, we could measure a sensitivity of 1380 nm/RIU. This sensitivity value is comparable to the ones reported for other plasmonic sensors, which employ fragile fiber tapers and more sophisticated microstructured optical fibers [24, 25]. Thus, we can visualize that the plasmonic sensor based on a gold-coated surface-core fiber is a powerful platform for the realization of highly sensitive refractive index sensing. Moreover, the setup presents the advantages of increased robustness when compared to fragile fiber tapers and simpler preparation than the sensors, which demand metal coating of the inner holes of microstructured fibers.

## 6. Surface-core fibers for directional curvature sensing

Besides refractive index sensing using Bragg gratings or surface plasmon resonance, surface-core fibers also offer the possibility of the realization of directional curvature sensing. This is possible because the off-center position of the fiber core allows it to experience compression or expansion depending on the curvature direction. In this context, a FBG can be inscribed in the core of the surface-core fiber for probing the bend-induced strain levels inside the core and determine the direction of the curvature.

Compression and expansion of the core introduces strain levels in it. The induced strain in a bent fiber,  $\varepsilon$ , is proportional to the curvature,  $C$  ( $\equiv 1/\text{curvature radius}$ ). If the core is at a distance  $y$  from the fiber neutral axis, the induced strain level can be calculated from Eq. (7) [26]. Since the existence of a strain level in a fiber entails variations in its refractive index (by virtue of the strain optic effect) and length, the spectral response of a FBG in this fiber is expected to shift when it is subjected to strain increments. Eq. (8) describes the dependence of the Bragg peak shift as a function of the curvature. In Eq. (8),  $P_\varepsilon$  is the photoelastic coefficient of silica ( $P_\varepsilon = 0.22$ ) [27].

$$\varepsilon = y C \quad (7)$$

$$\Delta\lambda_B = (1 - P_\varepsilon)\lambda_B\varepsilon = [(1 - P_\varepsilon)\lambda_B y]C \quad (8)$$

To experimentally test the response of the proposed sensor, a FBG was imprinted in the surface-core fiber (by using a phase mask with 1071.2 nm pitch) and the fiber was subjected to curvature increments. The results of the curvature sensing measurements are exposed in **Figure 7**. It is seen that when the fiber experiences expansion, the Bragg peak spectral position redshifts (positive spectral shift). Otherwise, when the fiber is compressed by the bending, the Bragg peak blueshifts (negative spectral shift). The measured sensitivities were  $(188 \pm 5)$  and  $(202 \pm 5)$  pm/m<sup>-1</sup> for the expansion and compression conditions, respectively.

The achieved sensitivity values are high when compared to other FBG-based sensors whose performance is reported in the literature (sensitivities from 50 to 100 pm/m<sup>-1</sup>) [28–30]. Additionally, the sensitivity for the surface-core fiber sensor is greater than the one obtained for FBGs sensors in eccentric core polymer optical fibers [31]. It is worth saying, however, that greater sensitivity values can be attained in other configurations. For example, we find in the literature that fibers with two or three cores can provide sensitivities of hundreds of nanometers per inverse meter [32, 33]. Nevertheless, the spectral features whose spectral shifts are considered in [32, 33] are much broader than the Bragg peak in the surface-core fiber we measured. This has an important impact on the sensor resolution. For the

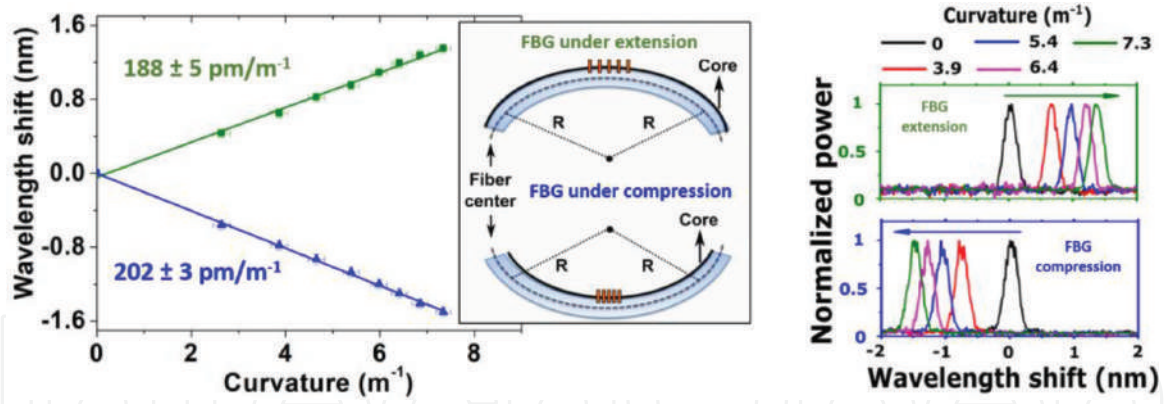


Figure 7.

Wavelength shift as a function of the curvature, representation of the curvature direction and spectral response of the directional curvature sensor based on a FBG inscribed in a surface-core fiber.

sensor reported in [32], for example, one can estimate a resolution limit of  $0.01 \text{ m}^{-1}$ , which is similar to the one we can find in our results ( $0.02 \text{ m}^{-1}$ ).

## 7. Polymer capillary fibers for temperature sensing

A simpler structure, which can be employed in sensing measurements, is capillary fibers [12]. In our approach, we investigated the sensitivity of polymer capillary fibers to temperature variations by studying the spectral characteristics of the light that is transmitted through its hollow part.

The typical transmission spectra through the hollow part of capillaries have wavelengths of high loss,  $\lambda_{\min}$ . These wavelengths encounter high leakage during propagation because they are resonant with the capillary wall. At these wavelengths, which are given by Eq. (9), transmission minima are observed. In Eq. (9),  $n_1$  is the refractive index of the hollow core,  $n_2$  is the refractive index of the capillary material,  $d$  is the thickness of the capillary wall, and  $m$  is the order of the minimum. Eq. (9) tells that if the thickness and the refractive index of the capillary are altered, the minima spectral locations are expected to shift. As temperature variations are able to change both these parameters, capillary fibers can act as temperature sensors.

$$\lambda_{\min} = \frac{2n_1d}{m} \sqrt{\left(\frac{n_2}{n_1}\right)^2 - 1} \quad (9)$$

Taking this into account, polymethyl methacrylate (PMMA) capillaries were chosen to be used in this investigation. This decision was due to the high thermal expansion coefficient of PMMA ( $2.2 \times 10^{-4} \text{ }^\circ\text{C}^{-1}$ ) and its high thermo-optic coefficient ( $-1.3 \times 10^{-4} \text{ }^\circ\text{C}^{-1}$ ).

An analytical model can be used to investigate the influences of the thermal expansion and of the thermo-optic effect in the sensor [11, 34]. Eq. (10) presents an expression for calculating the output power ( $P_{\text{out}}$ ) as a function of the wavelength ( $\lambda$ ). In Eq. (10),  $P_{\text{in}}$  is the input power,  $L$  is the fiber length,  $d$  is the capillary wall thickness,  $n_1$  and  $n_2$  are refractive indexes of the hollow core and of the capillary material, and the parameter  $\Gamma$  is given by Eq. (11). In Eq. (10) and Eq. (11),  $\theta_1$  is the angle of incidence of the light rays on the capillary wall for a specific leaky mode—given by  $\theta_1 = \sin^{-1}\left(\frac{n_{\text{eff}}}{n_1}\right)$ . In the expression for  $\theta_1$ , the effective refractive index of the leaky mode guided in the core,  $n_{\text{eff}}$ , can be found by  $n_{\text{eff}} = 1 - \frac{1}{2} \left(\frac{u_{\text{eff}} \lambda}{\pi d_{\text{in}}}\right)^2$ ,



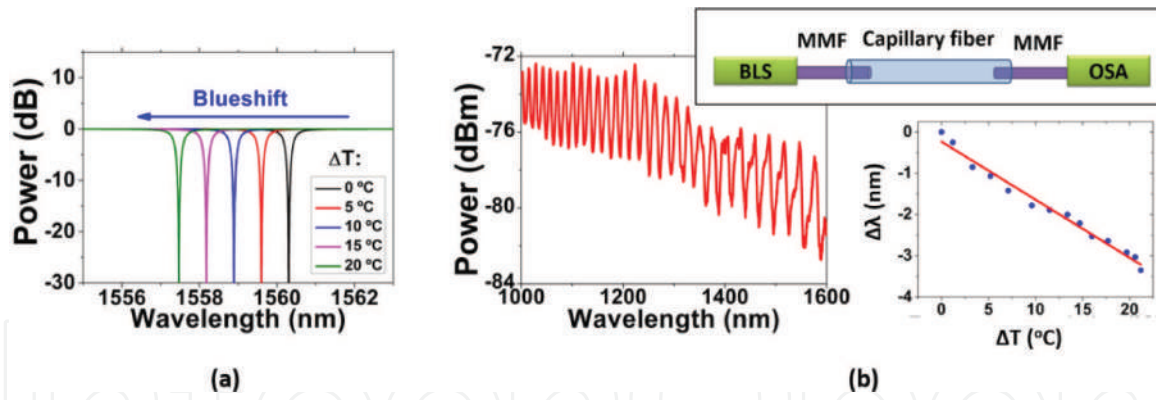


**Figure 8.** (a) Simulated transmittance of a capillary fiber 2 cm long and with 160  $\mu\text{m}$  inner diameter and 240  $\mu\text{m}$  outer diameter. (b) Experimental transmitted spectrum for a 13 cm long PMMA capillary fiber. Insets stands for the experimental setup (BLS: broadband light source; MMF: multimode fiber; OSA: optical spectrum analyzer) and for the wavelength shift ( $\Delta\lambda$ ) as a function of the temperature variation ( $\Delta T$ ).

where  $D_{\text{in}}$  is inner diameter of the capillary and  $u_{\mu\nu}$  is a root of the equation  $J_{\nu-1}(u_{\mu\nu}) = 0$ , where  $J$  is the Bessel function [34, 35].

$$P_{\text{out}} = P_{\text{in}} \exp \left\{ \left( \frac{L}{D_{\text{in}} \tan \theta_1} \right) \ln \left[ 1 - \frac{(1 - \Gamma^2)^2}{(1 - \Gamma^2)^2 + 4\Gamma^2 \sin^2 \left( \frac{2\pi n_2 d}{\lambda} \sqrt{1 - \left( \frac{n_1}{n_2} \right)^2 \sin^2 \theta_1} \right)} \right] \right\} \quad (10)$$

$$\Gamma = \frac{\sqrt{1 - \sin^2 \theta_1} - \frac{n_2}{n_1} \sqrt{1 - \left( \frac{n_1}{n_2} \right)^2 \sin^2 \theta_1}}{\sqrt{1 - \sin^2 \theta_1} + \frac{n_2}{n_1} \sqrt{1 - \left( \frac{n_1}{n_2} \right)^2 \sin^2 \theta_1}} \quad (11)$$

**Figure 8a** presents the simulation for a transmission minimum of a PMMA capillary with 2 cm length, inner diameter 160  $\mu\text{m}$ , and outer diameter 240  $\mu\text{m}$  for different temperature conditions. In the simulation, both thermal expansion and thermo-optic effects are considered. It is seen that, when the temperature increases, the transmission dip is expected to blueshift. It is worth saying that, for the considered capillary fiber, the thermo-optic effect is the dominant effect.

To experimentally test the proposed sensor, a PMMA capillary fiber was fabricated (with inner diameter 160  $\mu\text{m}$  and outer diameter 240  $\mu\text{m}$ ) and its performance as a temperature sensor was measured. In the experimental setup, light from a broadband light source was coupled to the capillary fiber (13 cm length) and collected from it by using silica multimode fibers, as shown in the inset of **Figure 8b**. A typical transmission spectrum is shown in **Figure 8b**, and the wavelength shift ( $\Delta\lambda$ ) as a function of the temperature variation ( $\Delta T$ ) is shown in the inset in **Figure 8b**. A sensitivity of  $(-140 \pm 6) \text{ pm}/^\circ\text{C}$  was measured. This sensitivity is around 14 times higher than conventional Bragg gratings-based temperature sensors [36].

## 8. Conclusions

In this chapter, we presented the recent research yields of our group in the State University of Campinas (Unicamp, Brazil) regarding ultra-simplified

microstructured optical fibers designs for sensing applications. In this context, we firstly discussed hollow and metal-filled embedded-core fibers as pressure and temperature sensors. We showed that the achieved sensitivities with this structure are high when compared to other sensors which employ much more sophisticated fiber designs. Additionally, we described surface-core fibers as refractive index and directional curvature sensors by employing fiber Bragg gratings and a plasmonic configuration. Finally, polymer capillary fibers were presented as an even simpler structure for temperature sensing.

The results presented herein demonstrate the great potential of capillary-like fibers to act as sensors for multiple purposes. Hence, it is possible to identify that this minimalist approach for the design of microstructured fiber sensors consists of a novel and very promising avenue for obtaining sensors with simplified structures and optimized performances.

## **Acknowledgements**

We thank M. A. R. Franco, V. A. Serrão, G. Chesini, S. Aristilde, R. Oliveira, T. H. R. Marques, A. Matikainen, and H. Ludvigsen for their contributions to the development of the research reported herein.


This work was funded by the São Paulo Research Foundation (Fapesp, grant #2014/50632-6), the Financiadora de Estudos e Projetos (Finep, grant #01.12.0393.00), and the National Council for Scientific and Technological Development (CNPq).

## **Author details**

Jonas H. Osório\* and Cristiano M. B. Cordeiro  
“Gleb Wataghin” Physics Institute, State University of Campinas, Brazil

\*Address all correspondence to: [cmbe@ifi.unicamp.br](mailto:cmbe@ifi.unicamp.br)

## **IntechOpen**

© 2018 The Author(s). Licensee IntechOpen. This chapter is distributed under the terms of the Creative Commons Attribution License (<http://creativecommons.org/licenses/by/3.0>), which permits unrestricted use, distribution, and reproduction in any medium, provided the original work is properly cited. 

## References

- [1] Anuszkiewicz A, Statkiewicz-Barabach G, Borsukowski T, Olszewski J, Martykien T, Urbanczyk W, et al. Sensing characteristics of the rocking filters in microstructured fiber optimized for hydrostatic pressure measurements. *Optics Express*. 2012; **20**(21):23320-23330
- [2] Osório JH, Hayashi JG, Espinel YAV, Franco MAR, Andrés MV, Cordeiro CMB. Photonic-crystal fiber-based pressure sensor for dual environment monitoring. *Applied Optics*. 2014; **53**: 3668-3672
- [3] Kim BH, Lee SH, Lin A, Lee A, Lee J, Han W. Large temperature sensitivity of Sagnac loop interferometer based on the birefringent holey fiber filled with metal indium. *Optics Express*. 2009; **17**: 1789-1794
- [4] Reyes-Vera E, Cordeiro CMB, Torres P. Highly sensitive temperature sensor using a sagnac loop interferometer based on a side-hole photonic crystal fiber filled with metal. *Applied Optics*. 2017; **56**(2):156-162
- [5] Hautakorpi M, Mattinen M, Ludvigsen H. Surface-plasmon-resonance sensor based on three-hole microstructured optical fiber. *Optics Express*. 2008; **16**:8427-8432
- [6] Doherty B, Thiele M, Warren-Smith S, Schartner E, Ebendorff-Heidepriem H, Fritzsche W, et al. Plasmonic nanoparticle-functionalized exposed-core fiber – an optofluidic refractive index sensing platform. *Optics Letters*. 2017; **41**(21):4395-4398
- [7] Osório JH, Chesini G, Serrão VA, Franco MAR, Cordeiro CMB. Simplifying the design of microstructured optical fibre pressure sensors. *Scientific Reports*. 2017; **7**:2990
- [8] Chesini G, Osório JH, Serrão VA, Franco MAR, Cordeiro CMB. Metal-filled embedded-core capillary fibers as highly sensitive temperature sensors. *IEEE Sensors Letters*. 2018; **2**(2)
- [9] Osório JH, Oliveira R, Aristilde S, Chesini G, Franco MAR, Nogueira RN, et al. Bragg gratings in surface-core fibers: refractive index and directional curvature sensing. *Optical Fiber Technology*. 2017; **34**:86-90
- [10] Matikainen A, Osório JH, Nyman M, Juntunen T, Cordeiro CMB, Ludvigsen H. Plasmonic surface-core fibers for high sensitivity refractive index sensing. In preparation
- [11] Osório JH, Marques THR, Figueredo IC, Serrão VA, Franco MAR, Cordeiro CMB. Optical sensing with antiresonant capillary fibers. In: 25th International Conference on Optical Fiber Sensors, Proc. SPIE 10323. 2017. p. 103233U
- [12] Rugeland P, Sterner C, Margulis W. Visible light guidance in silica capillaries by antiresonant reflection. *Optics Express*. 2013; **21**:29217-29222
- [13] Szpulak M, Martynkien T, Urbanczyk W. Effects of hydrostatic pressure on phase and group birefringence in microstructured holey fibers. *Applied Optics*. 2004; **43**: 4739-4744
- [14] Primak W, Post D. Photoelastic constants of vitreous silica and its elastic coefficient of refractive index. *Journal of Applied Physics*. 1959; **30**:779
- [15] Timoshenko S, Goodter JN. *Theory of Elasticity*. New York: McGraw-Hill; 1969
- [16] Osório JH, Cordeiro CMB. Optical sensor based on two in-series

birefringent optical fibers. *Applied Optics*. 2013;**52**:4915-4921

[17] Fu HY, Tam HY, Shao L, Dong X, Wai PKA, Lu C, et al. Pressure sensors realized with polarization-maintaining photonic crystal fiber-based Sagnac interferometer. *Applied Optics*. 2008;**47**(15):2835-2839

[18] Martynkien T, Szpulak M, Statkiewicz G, Golojuch G, Olszewski J, Urbanczyk W, et al. Measurements of sensitivity to hydrostatic pressure and temperature in highly birefringent photonic crystal fibers. *Optical and Quantum Electronics*. 2007;**39**:481-489

[19] Martynkien T, Statkiewicz-Barabach G, Olszewski J, Wojcik J, Mergo P, Geernaert T, et al. Highly birefringent microstructured fibers with enhanced sensitivity to hydrostatic pressure. *Optics Express*. 2010;**18**(14):15113-15121

[20] Xin Y, Dong X, Meng Q, Qi F, Zhao C. Alcohol-filled sidehole fiber Sagnac interferometer for temperature measurement. *Sensors and Actuators A: Physical*. 2013;**193**:182-185

[21] Naeem BH, Kim B, Kim YC. High-sensitivity temperature sensor based on a selectively-polymer-filled two-core photonic crystal fiber in-line interferometer. *IEEE Sensors Journal*. 2015;**15**(7):3998-4003

[22] Liang W, Huang Y, Xu Y, Lee RK, Yariv A. Highly sensitive fiber Bragg gratings refractive index sensors. *Applied Physics Letters*. 2005;**86**:151122

[23] Iadicicco I, Cusano A, Cutolo A, Bernini R, Giordano M. Thinned fiber Bragg gratings as high sensitivity refractive index sensor. *Photonics Technology Letters*. 2004;**16**(4):1149-1151

[24] Esteban O, Díaz-Herrera N, Navarrete M, González-Cano A. Surface-plasmon resonance sensors based on uniform-waist tapered fibers in a reflective configuration. *Applied Optics*. 2006;**45**:7294-7298

[25] Hautakorpi M, Mattinen M, Ludvigsen H. Surface-plasmon-resonance sensor based on three-hole microstructured fiber. *Optics Express*. 2008;**16**:8427-8432

[26] Hibbeler RC. *Mechanics of Materials*. 8th ed. Boston: Pearson Prentice Hall; 2011. 978-0-13-602230-5

[27] Kreuzer M. *Strain Measurement with Fiber Bragg Gratings Sensors*. Darmstadt, Germany: HBM; 2006

[28] Gander MG, Mac Pherson WN, McBride R, Jones JDC, Zhang L, Bennion I, et al. Bend measurement using Bragg gratings in multicore fibre. *Electronics Letters*. 2000;**36**(2):120-121

[29] Flockhart GMH, Mac Pherson WN, Barton JS, Jones JDC. Two-axis bend measurement with Bragg gratings in multicore optical fiber. *Optics Letters*. 2003;**28**(6):387-389

[30] Araújo FA, Ferreira LA, Santos JL. Simultaneous determination of curvature, plane of curvature, and temperature by use of a miniaturized sensing head based on fiber Bragg gratings. *Applied Optics*. 2002;**41**(13):2401-2407

[31] Chen X, Zhang C, Webb DJ, Peng G, Kalli K. Bragg grating in a polymer optical fiber for strain, bend and temperature sensing. *Measurement Science and Technology*. 2010;**21**:094005

[32] Villatoro J, Newkirk AV, Antonio-Lopez E, Zubia J, Shülzgen A, Amezcua-Correa R. Ultrasensitive vector bending



sensor based on multicore optical fiber.  
Optics Letters. 2016;**41**:832-835

[33] Guzman-Sepulveda JR, May-Arrioja DA. In-fiber directional coupler for high-sensitivity curvature measurement. Optics Express. 2013;**21**: 11853-11861

[34] Lai C, You B, Lu J, Liu T, Peng J, Sun C, et al. Modal characteristics of antiresonant reflecting pipe waveguides for terahertz waveguiding. Optics Express. 2010;**18**(1)

[35] Marcatili EAJ, Schmeltzer RA. Hollow metallic and dielectric waveguides for long distance optical transmission and lasers. The Bell System Technical Journal. 1964;**43**(4)

[36] Oliveira R, Osório JH, Aristilde S, Bilro L, Nogueira RN, Cordeiro CMB. Simultaneous measurement of strain, temperature and refractive index based on multimode interference, fiber tapering and fiber Bragg gratings. Measurement Science and Technology. 2016;**27**:075107

# We are IntechOpen, the world's leading publisher of Open Access books Built by scientists, for scientists

6,300

Open access books available

171,000

International authors and editors

190M

Downloads

Our authors are among the

154

Countries delivered to

TOP 1%

most cited scientists

12.2%

Contributors from top 500 universities



WEB OF SCIENCE™

Selection of our books indexed in the Book Citation Index  
in Web of Science™ Core Collection (BKCI)

Interested in publishing with us?  
Contact [book.department@intechopen.com](mailto:book.department@intechopen.com)

Numbers displayed above are based on latest data collected.  
For more information visit [www.intechopen.com](http://www.intechopen.com)



# Fiber Bragg Gratings as e-Health Enablers: An Overview for Gait Analysis Applications

*Maria de Fátima Domingues, Cátia Tavares, Tiago Leite, Nélia Alberto, Cátia Leitão, Carlos Marques, Ayman Radwan, Eduardo Rocon, Paulo Antunes and Paulo André*

## Abstract

Nowadays, the fast advances in sensing technologies and ubiquitous wireless networking are reflected in medical practice. It provides new healthcare advantages under the scope of e-Health applications, enhancing life quality of citizens. The increase of life expectancy of current population comes with its challenges and growing health risks, which include locomotive problems. Such impairments and its rehabilitation require a close monitoring and continuous evaluation, which add financial burdens on an already overloaded healthcare system. Analysis of body movements and gait pattern can help in the rehabilitation of such problems. These monitoring systems should be noninvasive and comfortable, in order to not jeopardize the mobility and the day-to-day activities of citizens. The use of fiber Bragg gratings (FBGs) as e-Health enablers has presented itself as a new topic to be investigated, exploiting the FBGs' advantages over its electronic counterparts. Although gait analysis has been widely assessed, the use of FBGs in biomechanics and rehabilitation is recent, with a wide field of applications. This chapter provides a review of the application of FBGs for gait analysis monitoring, namely its use in topics such as the monitoring of plantar pressure, angle, and torsion and its integration in rehabilitation exoskeletons and for prosthetic control.

**Keywords:** fiber Bragg gratings, e-Health enablers, gait analysis, plantar pressure, foot shear pressure, gait joint monitoring, instrumentation of prosthetic limbs

## 1. Fiber Bragg gratings: an introduction

Fiber Bragg gratings (FBGs) are sensing elements based on the longitudinal modulation of the refractive index of the optical fiber core. This type of device has all the advantages associated with optical fiber sensors, with the added feature of easily multiplexing several sensing points along one single fiber.

The production methodology of FBGs has evolved significantly since its initial approach. In the late 1970s, it was shown that optical fibers can be photosensitive, opening the door for FBGs production and its applications, both as sensing devices and in optical communications [1]. In 1981, Lam and Garside suggested that the formation of the FBGs was related to the interaction between UV light with defects

in the doped silica core. Such findings lead to the later confirmation that the refractive index changes could be induced by doping the optical fibers core with germanium, given a new insight on the FBGs production [2, 3].

One decade has passed since new breakthroughs emerged regarding the FBGs production methodology. In 1989, Meltz et al. reported an FBG external inscription technique. The authors used a split 244 nm beam, which was later recombined in order to produce an interference pattern in the optical fiber core [4, 5]. With this technique, the authors were able to create a periodic and permanent change in the optical fiber core refractive index [5]. The reflected Bragg wavelength can be adjusted by changing the angle between the two split beams. In that way, the period of the interference pattern and the refractive index will change accordingly.

Alternatively, FBGs can be inscribed using phase masks, which are periodic patterns usually etched onto fused silica. In this technique, when the radiation from a UV laser is incident in the phase mask, the diffracted orders +1 and -1 are maximized, while the remaining ones are suppressed, creating an interferometric reflective pattern along the optical fiber core [6]. In **Figure 1**, the FBG inscription based on the phase mask technique as well as a representation of the FBG sensing mechanism is shown.

The FBG operational principle consists in monitoring the Bragg wavelength ( $\lambda_{\text{Bragg}}$ ) shift reflected by the grating, as a function of the monitored parameter. The Bragg wavelength is dependent on the effective refractive index of the fiber core ( $n_{\text{eff}}$ ) and the grating period ( $\Lambda$ ) by the relation [4]:

$$\lambda_{\text{Bragg}} = 2 n_{\text{eff}} \Lambda \quad (1)$$

Therefore, the Bragg wavelength can be actuated by variations in the grating period or in optical fiber core effective refractive index. So, the Bragg wavelength dependence on strain and temperature can be translated by:

$$\Delta\lambda_{\text{Bragg}} = \lambda_{\text{Bragg}}(1 - \rho\alpha)\Delta\varepsilon + \lambda_{\text{Bragg}}(\alpha + \xi)\Delta T, \quad (2)$$

where the first term refers to the strain influence on the  $\lambda_{\text{Bragg}}$  and the second describes the temperature effect. Hence, in Eq. (2),  $\Delta\lambda_{\text{Bragg}}$  represents the shift of the Bragg wavelength, while  $\rho$ ,  $\alpha$ , and  $\xi$  are the photoelastic, thermal expansion,

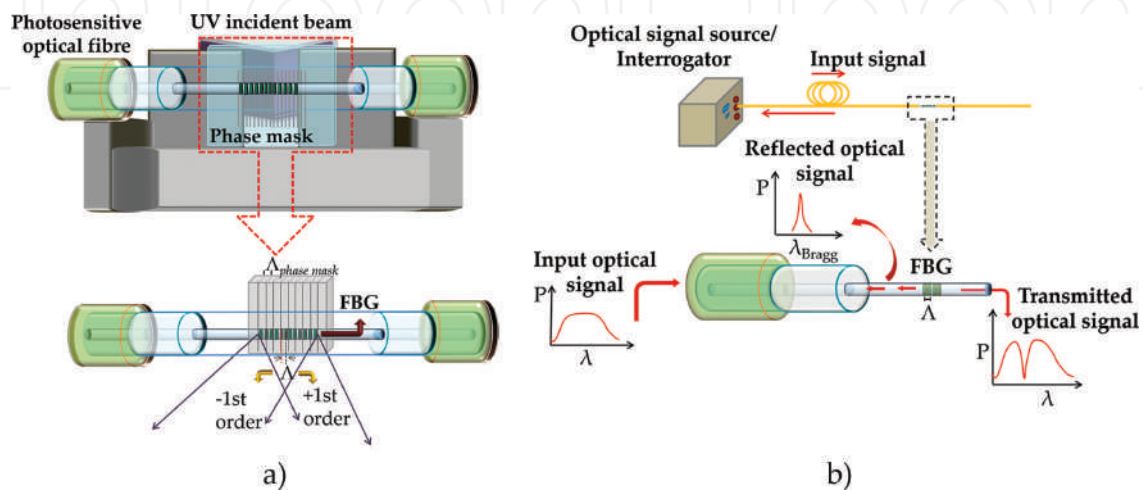


**Figure 1.**  
(a) Schematic representation of the setup typically used to inscribe FBG sensors in photosensitive optical fiber using the phase mask methodology; and (b) working principle of an FBG sensor.

and thermo-optic coefficients of the fiber, respectively;  $\Delta\epsilon$  and  $\Delta T$  corresponds to strain and temperature variations.

The FBG sensing mechanism comprises of a spectral broadband optical signal launched into the fiber, and an optical spectra analyzer to monitor the Bragg wavelength shifts. At the grating region, the Bragg wavelength component of the spectrum will be reflected, while in the transmitted optical signal that same Bragg wavelength component will be missing, as illustrated in **Figure 1b**.

Based in the described mechanisms, FBG sensors have a wide field of applications that range from their use for structural health monitoring, in oil and aeronautic industry and also as biomedical sensors and e-Health enablers, among others. Moreover, as the FBGs are elements with only few millimeters long, several gratings can be inscribed along the same optical fiber, allowing to multiplex a diverse network of sensing elements.

## 2. Gait analysis: relevance and impact in an e-Health scenario

Gait analysis research was given a pilot role in the nineteenth century, when the study of gait parameters started to be relevant in sports and medicine [7]. Regarding the medical point of view, from gait pattern analysis, a change in its normal parameters can reveal key information on patient's quality of life and/or in the evolution of different diseases. Gait disorders affect a large number of world population, since they are direct consequence of neurodegenerative diseases, such as spinal amyotrophic, multiple sclerosis, amyotrophic lateral sclerosis, neuromuscular diseases, cerebrovascular and cardiovascular pathologies, or even the physiological aging process [8–12]. Neurodegenerative diseases can be reflected in gait by showing a poor balance, a slower pace, shorter steps, lower free speed, and higher cadence [8–11].

The study of dynamic characteristics of human gait for clinical purposes has been widely reported lately. It aims to enhance the life's quality of patients suffering from gait disorders, and also, for their early detection, to enable early diagnosis and an adaptable treatment according to the evolution of the diseases or disorders [7, 13–16].

### 2.1 Gait analysis: gait cycle pattern

Gait analysis can be seen as the comprehensive study of the human locomotion, which as previously mentioned, has a major role in physical rehabilitation assessment, disorder diagnosis, surgical decision, and recovering follow up. Such study comprises the kinematic analysis (joint angles, angular velocities, and accelerations) and the kinetic analysis (ground reaction and joint forces) during the gait cycles [17, 18].

One gait cycle is the period of time between two consecutive contacts of the heel of the same foot with the floor. Generally, a cycle can be divided in two major phases: the stance phase, corresponding to the period in contact with the ground, which lasts for ~60% of the cycle; and the swing phase, corresponding to the period when there is no contact with the floor, and has a duration of ~40% of the total gait cycle [12, 19]. In **Figure 2**, the different phases are illustrated, along with events and periods that characterize a gait cycle.

The gait cycle can be further subdivided into six periods and eight functional events, five during the stance phase and three in the swing phase. Considering only one limb, the stance phase encompasses three different support periods. The first consists in a period of a double support, which is followed by single



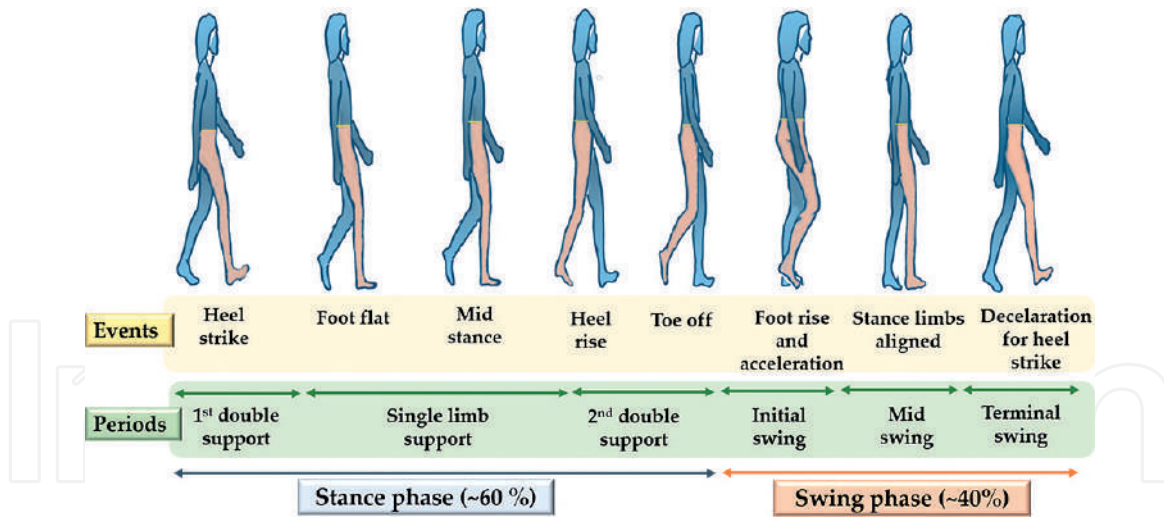


**Figure 2.**  
Representation of the stance and swing phases of a gait cycle.

support and ends with the second double support period [18–20]. The double support period corresponds to the percentage of the cycle when both feet are simultaneously in contact with the floor and it describes the smooth transition between the left and the right single limbs support [18]. During the first double support, the heel strikes the floor (heel strike), marking the beginning of the gait cycle. The cycle evolves then toward the single period support, with the foot moving down toward the floor into a foot-flat position, where a stable support base is created for the rest of the body. Within the single support phase, the body is propelled over the foot, with the hip joint vertically aligned with ankle joint in the event characterized as the mid stance. From that point onward, the second double support phase starts, with the lower limb moving the body center of mass forward during the heel rise event, where the heel loses contact with the floor. The last contact of the foot with the floor is made by the big toe (hallux), at the toe off event, which also marks the end of the stance phase and the beginning of the swing phase [20].

During the swing phase, there is no contact between the plantar foot and the floor, and the limb continues its movement forward, which can be divided into three different periods: initial swing, mid swing, and terminal swing. In the initial swing, the lower limb vertical length should be reduced, for the foot to clear the floor and to accelerate forward by flexing the hip and knee, together with ankle dorsiflexion. The mid swing is characterized by the alignment of the accelerating limb with the stance limb. In this phase, the ankle and the hip joints are aligned. During the terminal swing, the limb undergoes a deceleration while it prepares for the contact with the floor, in the heel strike of the start of a new cycle [19–21]. As described, the swing phase is characterized by accelerations and decelerations of the lower limb, which require a more demanding muscular effort at the hip level [18].

## 2.2 Gait parameters

Gait analysis is a systematic procedure that allows the detection of negative deviations from normal gait pattern, as well as their causes. Based on such analysis, it is possible to quantify the parameters involved in the movement of the lower limbs and retrieve the mechanisms that rule the human body movement [22]. Based on the gait cycle pattern described earlier, there are several parameters that can be physically monitored in order to assess the patient's health: anthropometric,

spatio-temporal, kinematic, kinetic, and dynamic electromyography (EMG), as shown in **Table 1** [22]. From such parameters, the ones that require a more specialized technology to be monitored outside the clinical environment, and therefore passible of being monitored in a gait e-Health architecture, are [7, 23, 24]:

- the stance and the swing phases duration for each foot;
- the walking velocity and gait cadence (number of steps per unit of time);
- The step length, width (distance between two equivalent points of both feet), and angles (direction of the foot during gait);
- the body posture (bending and symmetry) and the existence of tremors;
- the shear and the foot plantar pressure during the stance phase; and
- the direction and alignment of the limb segments with the ankle, knee, and hip joints.

The act of walking implies the movement of the whole body, and specifically, it requires a synchronized movement of each lower limb apart. Therefore, the gait pattern of an individual can be affected by a disorder in any segment of the body, like for instance, problems in the spinal cord or from a reduced knee flexion in patients with an anterior cruciate ligament reconstruction [25]. For that reason, the analysis of the gait cycle is a vital tool for the biomechanical mobility monitoring, as it can give crucial information not only about the lower limbs health condition, but also allows to infer details about other possible pathologies related to the dynamic movement of the body [26]. So, by monitoring the parameters previously listed, it is possible to assess the health conditions for the body parts involved in walking, namely the lower limbs and its joint. These parameters can be analyzed using objective and subjective techniques [7, 27, 28].

The subjective analysis is based on the observation of the patient while walking, and is generally performed in clinical environment under the supervision

Parameters	Definition	Evaluation of:
Anthropometric	Related to the corporal dimensions of the human body.	Age, gender, height, weight, limb length, and body mass index.
Spatio-temporal	General gait parameters used for a simple objective gait evaluation, considering the time-distance characteristics.	Step and stride length, step width, cadence, velocity, stance and swing phases, and gait cycle events (for instance, heel strike).
Kinematic	Quantification of movements and geometric description of the lower limbs motion, without reference to forces.	Joint and segments angles, angular motion, acceleration, and segment trajectory.
Kinetic	Evaluation of the forces involved in the body locomotion.	Ground reaction forces, torque, and momentum.
EMG	Refers to the analysis of muscular activity, generally performed by using EMG surface electrodes.	Motor unit action parameters.

**Table 1.**  
*Parameters generally used for gait analysis (adapted from [22]).*



of a doctor or a therapist. For this analysis, the patient is asked to vary several gait-related parameters, while walking in a predetermined circuit [7]. This type of analysis is bit limited in the information that can be retrieved, nevertheless, this could be useful for an initial evaluation and posterior decision on which objective techniques should be used. In contrast to the subjective techniques, objective gait analysis is more of a quantitative evaluation of the parameters listed above. This type of analysis requires the use of different types of equipment and procedures to measure the gait parameters. These methodologies can be categorized according to the technology used, varying from the ones based on imaging, instrumented walking platforms or floor sensors, and wearable sensors [7, 24, 29].

For an e-Health architecture, the most suitable technology would be the one built using wearable sensors, which would be able to acquire the patient gait parameters, everywhere and under any conditions. Among those, FBGs can be considered as an objective technique for gait analysis (allows the quantification of parameters during gait analysis), which could be used in instrumented platforms or as wearable sensors [30]. Recently, the use of FBGs as wearable sensors for remote monitoring of patients has been reported [12, 31, 32].

### **2.3 Gait pattern monitoring: e-Health architecture**

The Internet of Things (IoT) concept is the fusion between pervasive network connectivity and the computing capability expanded to sensing devices and objects, able to acquire and exchange data autonomously. In recent years, due to the potential gains brought to the citizens' quality of life, IoT is seen as a whole platform able to bridge people and objects by integrating the smart concept into people's life, namely, smart cities, homes, wearables, and mobility [33].

Within the vast field of applications provided by IoT, e-Health stands out as one of the most influential topics on life-quality of humans, as smart and connected healthcare services have been requested more enthusiastically. e-Health is gaining too much attention mainly due to the joint effect of the increase of insufficient and ineffective healthcare services, allied to the change in population demographics and the increasing demand of such change entails. The world's population aged over 60 years is expected to reach 2 billion by 2050 [34], which implies the rise of chronic diseases that may be translated on different degrees of mobility impairments, requiring a close monitoring and a patient-centered healthcare service, where the healthcare providers and patients are pervasively connected [12, 33]. Also aligned with such demands, the market for home medical devices is set to significantly grow from \$27.8 billion in 2015 up to nearly \$44.3 billion by 2020 [35]. The increase in available e-Health solutions is a remarkable step toward improving the healthcare services, along with the autonomy of debilitated or impaired citizens. Fundamentally, e-Health can be seen as the solution to help the elders and patients with chronic illness to live an active life, without compromising their mobility or daily routine [32].

e-Health systems use remote monitoring architectures composed of sensing devices responsible to collect patients' physiological information, analyze and store such data in the cloud. The information can afterward be wirelessly sent to the healthcare professionals for a decision/action. The continuous flow of information on the patient's condition improves the provided service at a lower cost, while simultaneously enhancing the life quality of patients, who need continuous attention [33].

The patients' physiological information can be collected by networked sensors, integrated in smart wearable systems, or placed within the patients living

environment. Considering the specific case of gait analysis, the continuous, automatic, and remote monitoring of gait of impaired or under rehabilitation citizens allows the objective assessment for preventive and proactive supervision of the pathologies, as well as to closely assist the therapies in progress [36]. In this scenario, wearable sensing architecture allows not only the evaluation of the patients in the course of daily life activities, but also provides the feedback on the recovering/rehabilitation therapy to patients and medical staff through ubiquitous connectivity. Based on that feedback, new therapeutic instructions can be given remotely to the patient, maximizing the efficiency of the provided healthcare services [31, 32].

An e-Health architecture to monitor the gait pattern of a citizen/patient comprises three key elements: the monitoring system composed of a sensors' network (preferably wearable); a computer/analysis system to collect, analyze, and store the data; and finally, the wireless mobile gateway, responsible for data processing and wireless transmission to medical servers and decision centers [31, 32]. **Figure 3** schematizes the typical architecture involved in an e-Health scenario.

The first part of the considered architecture is responsible for the data sensing and consequently, for the information given to action centers. Therefore, it is crucial that the sensing network is as accurate and reliable as possible. The use of FBGs as IoT and e-Health enablers is becoming increasingly common, due to their sensing characteristics, when compared with the ones of their electronic counterparts, namely small size (in the order of micrometers), biocompatibility, multiplexing capability, immunity to electromagnetic interference, in addition to their high accuracy and sensitivity, even for applications in challenging environments [37–39]. Consequently, FBGs can be used as a reliable solution for the integration in e-Health architectures, as for monitoring sensing systems in biomechanics and physical rehabilitation. Some examples can be mentioned, covering the detection of bone strains, mapping of gait plantar and shear pressures, measuring of pressures in orthopedic joints and angles between the body segments, as have already been successfully reported [12, 30].

In the following sections, the use of FBGs to monitor different body segments involved in gait will be explored.

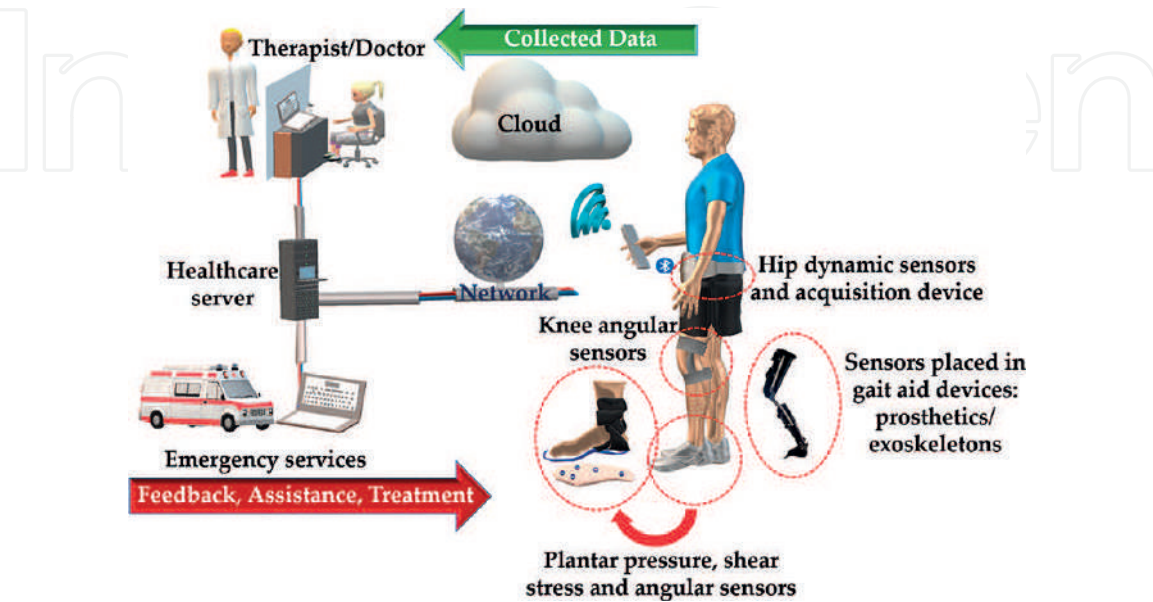


**Figure 3.**  
*Possible architecture for a gait e-Health monitoring system.*

### **3. Plantar pressure and shear analysis**

The assessment of plantar and shear pressures is of great importance for the gait health evaluation analysis, aiming to understand the effects induced in/by the body and to prevent the ulceration of the foot [40]. The pressure ulcers occur when tissue is compressed during prolonged periods of time, resulting in a wound that can infect and cause amputation, or in more severe cases, the patient's death [41]. An early identification of individuals at risk of foot ulceration (people with diabetes mellitus and peripheral neuropathy) is one of the primary means to reduce its incidence [40, 41]. Due to the poor load distribution, resulting from the reduced sensitivity of the foot, abnormally high plantar pressures occur in certain areas of the foot, and when that happens, it can lead to the growth of pressure sores in these locations [42]. The most affected areas are those with bony prominences, such as under the metatarsal bones, where the majority of plantar neuropathic ulcers occur [43]. Correct and continuous mapping of plantar pressure can prevent the occurrence of these pathologies, with the adoption of different walking habits or the use of correction equipment. On the other hand, in the case of the existence of ulcers, a redistribution of the forces imposed on the foot during walking aids healing and prevents further ulceration.

The force applied to the skin surface by a supporting structure has two components: the pressure acting normal to the surface and the shear stress acting in a tangential direction. Many authors have suggested that shear stresses have a pathogenic factor in the development of plantar ulcers [40–43]. This shear stress exists if there is sliding between two surfaces (foot and shoe), and it is closely related to friction [44]. Despite the importance of shear monitoring in assessing gait patterns, only normal pressure is widely reported. The lack of a validated and commercially available shear stress sensor is one of the main reasons why shear analysis is not as referenced as plantar pressure.

There are several solutions in the market for measuring plantar pressure, static in the form of fixed platforms, and wearable as shoes insoles. In regards of the importance of gait-related pathologies in the general population, and in the elder generation in particular, several works have been developed to improve the state-of-the-art. The literature reports the use of various technologies of plantar pressure and shear sensors, such as magneto-resistors, strain gauges, piezoelectric materials, capacitive sensors, and micro-strip antennas and coils.

As an alternative to these electronic devices, optical fiber-based sensors stand out due to their small diameter (hundreds of micrometers) and robustness, biocompatibility, high precision, electromagnetic insensitivity, as well as being electrically free at the point of measurement and owning the property of being able to multiplex several sensors in the same fiber, which allows to simultaneously monitor different parameters [45, 46].

Following such path, research studies have been carried out with FBG-based sensors used to measure not only plantar pressure but also shear parameters.

#### **3.1 Plantar pressure sensors**

The plantar pressure monitoring devices can be presented as fixed platforms or as insoles to be used directly in the footwear. Platform systems are typically constructed of several pressure sensors arranged in an array embedded in the floor or in a rigid platform. These systems can be used for static and dynamic studies, but are generally restricted to clinics and laboratories. In the case of the static tests, the patient stands still on the platform. On the other hand, for the dynamic tests, the platform is placed on the floor and the patient walks through it.



The application of these types of measuring systems has the advantage of being easy to use, since the platforms are flat and stationary. Nevertheless, these systems also present disadvantages, since they are influential to the patient's gait, once during the examination, he/she will have to tread specific areas of the platform surface [47].

Insole sensors can be incorporated into shoes, so that the measurements truly reflect the interface between the foot and the shoe. These systems, as they are flexible and portable, allow a greater accuracy of the acquired data, regarding the natural gait of the patient, and also greater variety of studies with different walking tasks, footwear, and even diverse floors/terrains [47]. However, insoles usually have a reduced number of sensors compared to platforms. The main requirements for the development of wearable/in-shoe sensors are: mobility, reduced number of cables, low power consumption, low cost, high acquisition frequency, proper sensitivity, noninvasiveness, and do not represent any danger to the user. Therefore, fiber optic sensors, due to their characteristics, have proven to be a reliable solution in this type of applications. Also, within the range of fiber optic sensors, the FBGs seem to be the best solution, since their multiplexing capability allows to have multiple sensors into a single fiber, reducing the number of cables needed in the insole. In this section, some recently developed work using optical fibers with Bragg gratings, as plantar pressure sensors in fixed platforms and in-shoe equipment, will be described.

The first work with FBG sensors incorporated in platforms for the measurement of plantar pressure was published in 2003, when Hao's team developed an insole shaped device with a silica optical fiber with five FBGs [48]. The insole was constituted of 10 layers of carbo-epoxy, among which the optical fiber was placed. The sensing FBG units were placed strategically at the main pressure points (heel and metatarsal areas). The device was tested in static tests to determine which areas have the greatest and lowest pressure at different user positions. The results showed that the sensors had an average sensitivity of 5.44 pm/N.

In 2014, Suresh et al. published a work comparing the use of FBGs and piezoelectric (PZT) sensors for gait monitoring at low and high speeds [49]. To manufacture the optical sensing platform, the FBGs were embedded between layers of a carbon composite material (CCM) in the form of an arc. After that, both types of sensors were placed on the underside of a commercial shoe (**Figure 4a**). For the dynamic test and to verify the behavior of both types of sensors, a healthy male walked on a treadmill wearing those shoes at various speeds. For the FBGs sensors, a mean pressure sensitivity of 1.3 pm/kPa was obtained. The study revealed that the FBG sensors have a better performance in the static moments and at lower speeds, while the piezoelectric sensors had greater performance for higher speeds.

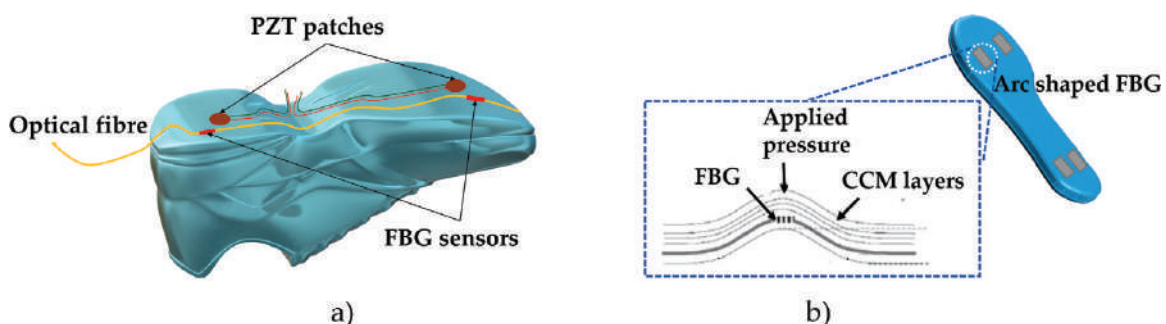


**Figure 4.**  
 (a) Scheme of the shoe with the attached FBG and PZT sensors (adapted from [49]); and (b) schematic representation of an arc shaped FBG pressure sensor (left) and the insole sensing scheme (right) (adapted from [50]).

Other approach was made by the same team, in which similar FBG cells were incorporated in an insole structure, as can be verified in the **Figure 4b**. The device was constituted by four arc-shaped cells, strategically placed in the forefoot and heel area. In this study, the plantar pressure was analyzed in both the fixed platform and the in-shoe systems. An average pressure sensitivity of 1.2 pm/kPa was obtained [50].

In 2016, Liang et al. proposed a sensing system based on six FBGs inscribed into a single fiber, which was embedded in silicone rubber [51]. The data registered by the optical sensors were compared to the ones collected through an i-Step P1000 digital pressure plate with 1024 barometric sensors. For the sensors' validation, 11 participants were tested, and according to the results, the viability of the optical sensor for this kind of measurement was demonstrated. Additionally, four different foot supporting types were successfully identified.

In 2017, Domingues et al. reported the development of two noninvasive solutions with FBGs in silica optical fiber incorporated in cork to monitor the body center of mass displacements and vertical ground reaction forces induced in the foot plantar surface during gait [12, 32]. One of the solutions, containing five FBGs, was developed to act as a fixed platform, and the other, with six FBG sensors, to be used as an instrumented insole to be adapted in a shoe as shown in **Figure 5**. Although the insole is made of five FBGs multiplexed in the same fiber, a clear isolation of each sensing point was also demonstrated, as seen in **Figure 6a**. Upon the calibration of the sensors located at point 1 (heel area), when the increasing load is applied in that point, only the FBG 1 shows a Bragg wavelength shift, proportional to the load applied (**Figure 6b**) [12].

The obtained results demonstrated the accuracy and reliability of the proposed systems to monitor and map the vertical active forces on the foot's plantar area during gait, **Figure 7**, with a sensitivity up to 11.06 pm/N.

The top graphic representation corresponds to the values independently registered by the five FBGs along time during two gait cycles, where the sum of the forces acquired by each FBG corresponds to the typical gait pattern [12]. In more detail, in the bottom graphic representation, it is possible to see which points of the insole are more actively pressed during the stance phase of the gait cycle. The dark blue representations in the foot, corresponds to the foot area that supports a higher load in the different stages of the stance phase [12, 32].

In the same year, a polymer optical fiber (POF) sensing system based on FBGs to measure foot plantar pressure was also described [52]. The plantar pressure signals were detected by five FBGs recorded in a cyclic transparent optical polymer (CYTOP) fiber, which was embedded in a cork platform in the form of an insole to monitor plantar pressure during gait. Initially, two studies were made with the insole as a fixed platform, one in which the user walked through the sensing

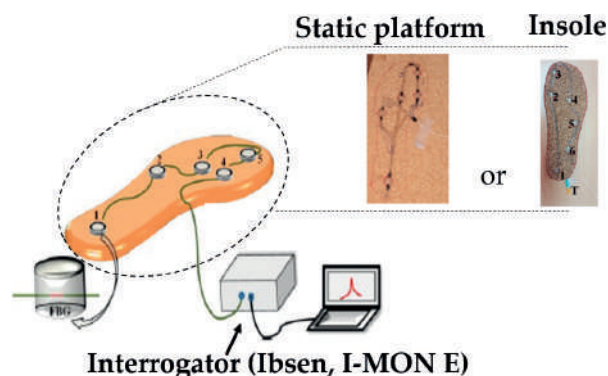


**Figure 5.**  
Schematic representation of the cork insole FBG monitoring system (adapted from [12]).

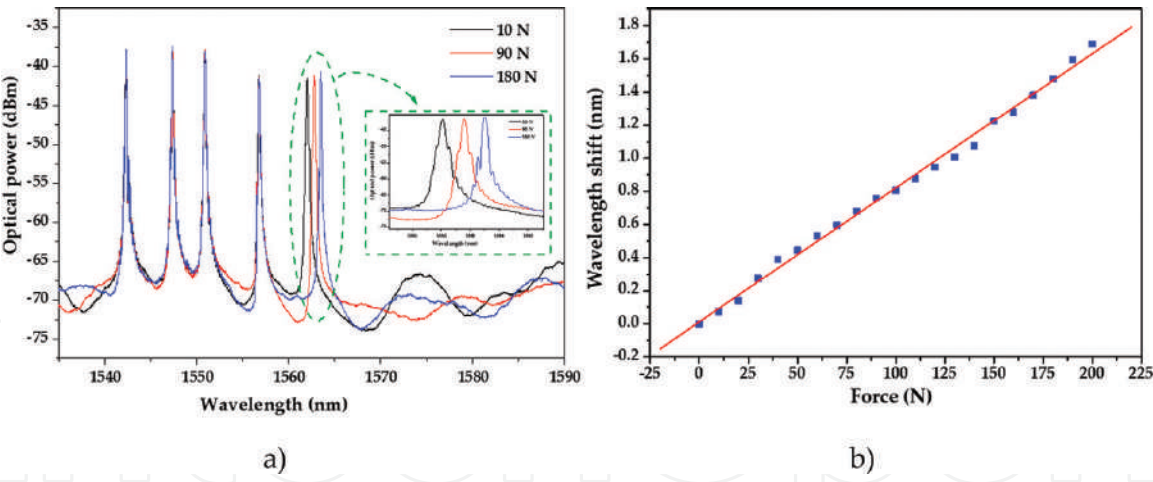


**Figure 6.**  
(a) Reflection spectra of the five FBGs multiplexed in the cork insole for three different load values; and (b) Bragg wavelength shift dependence on the load applied for FBG1 (adapted from [12]).

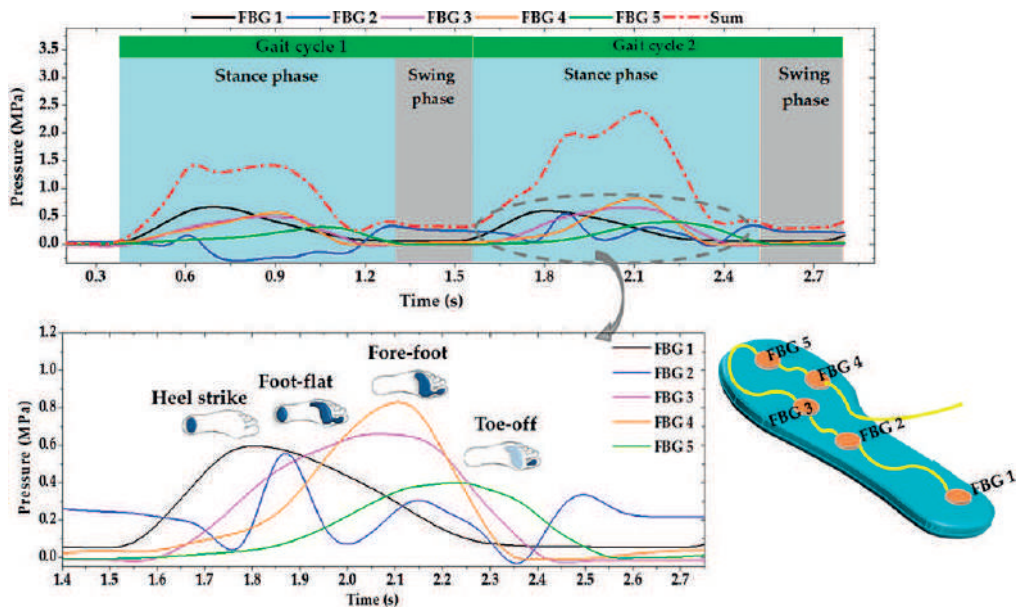


**Figure 7.**  
Representation of two complete gait cycles registered using a cork insole instrumented with five multiplexed FBGs (adapted from [12, 32]).

structure and another where he stood in the platform just moving the body center of mass. The data obtained from this device in both tests showed good repeatability and a sensitivity twice as high as the solutions based on silica optical fiber. Additionally, a team of researchers from Shanghai presented a sensing platform based on FBGs using the fused deposition modeling (FDM) method for the construction of the structure [53]. This platform was composed of several cylindrical structures in polylactic acid (PLA) with the FBG inside them. This device was designed to be used as a fixed broad platform for plantar pressure monitoring, which demonstrated to have a reliable mechanical performance.

Finally, a noninvasive and efficient insole FBG-based architecture for monitoring plantar pressure was presented in [32]. This work stands out from the others, because the authors introduced a whole IoT solution with the insole sensors integrated with a wireless transceiver, exhibited high energy efficiency and secured data transmission, to ensure the mobility and privacy of user data. The presented data reflected the precision of the proposed system, with the sensors having sensitivities up to 7.8 pm/kPa.



### 3.2 Plantar pressure and shear sensors

FBGs have also great potential for measuring shear stresses in the shoe. Although there are reports of sensors developed for shear measurement [54, 55], measuring plantar and shear pressure simultaneously is more attractive and provides more insights about the wellbeing of the foot and the overall health of the person. Due to the advantages of fiber optics, and FBGs in particular, several researchers have been working on the design of FBG-based cells able to measure these two forces simultaneously. Although the main objective is the measurement of these parameters during gait, none of the studies refers the introduction of the developed sensing cells in insoles or platforms, presenting only the cells in its isolated form.

The first work published with simultaneous shear and vertical forces sensing with FBGs goes back to the year of 2000. The team of Koulaxouzidis developed a cell, using three optical fibers with an FBG each, embedded in a block of elastic material, as schemed in **Figure 8a** [56]. The developed sensor was able to measure the vertical stress, as well as the magnitude and direction of the shear stress on its top surface. The experimental results showed a good repeatability and a resolution near to 5 kPa in the measurement of both forces. Later, in 2013, Zhang et al. developed an identical sensor to the previous one. In this case, two POFs with one FBG each were used, one of them was placed horizontally (hPOF, hFBG), while the other was tilted (tPOF, tFBG). Both fibers were embedded in a soft polydimethylsiloxane (PDMS) matrix, as shown in **Figure 8b** [57]. The sensor had a 27 mm length and width, and a 22 mm height. In this work, the obtained pressure sensitivity was 0.8 pm/Pa in a full range of 2.4 kPa, and the shear stress sensitivity was 1.3 pm/Pa for a full range of 0.6 kPa.

In 2015, Chethana et al. developed an optical sensor ground reaction force measurement platform for gait and geriatrics studies [58]. The developed system consisted of eight FBGs to measure the respective soil reaction forces on the three axes (x, y, and z). Four of the FBGs were placed at the vertices of the measuring platform, monitoring the shear motions on the x and y-axes (two for the x-axis and two for the y-axis motions detection). The remaining four FBGs were placed one on each frame supporting leg to measure the plantar pressure exerted on these zones. According to the authors, the optical fiber sensors platform for ground reaction force measurements presented a zero cross-force sensitiveness in all three loading axes [58].

In 2018, Tavares et al. developed a cell with the same operating principle as previously reported, but using only one silica optical fiber with two FBGs placed individually in two adjacent cavities, one made of cork and another of polylactide acid (PLA), as shown in **Figure 9** [59]. For the cells' calibration, the used method was similar to the one described in Ref. [57], and the obtained values were

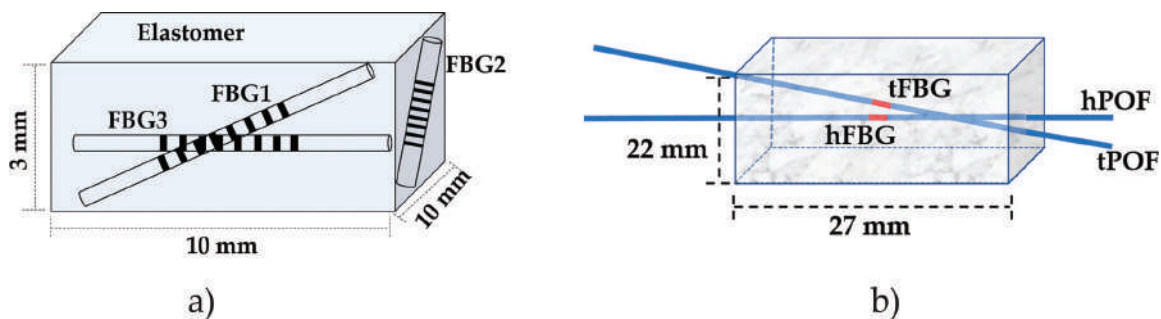


**Figure 8.** Schematic representation of the FBG-based sensor cell developed in (a) silica (adapted from [56]) and (b) POF (adapted from [57]) fibers.



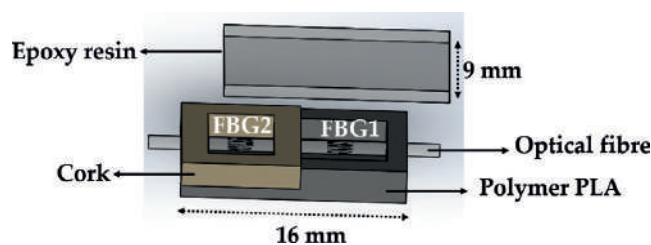


**Figure 9.**  
 Scheme of the shear and pressure sensing cell with its different components and respective dimensions (adapted from [59]).

compared with a 3-axial electronic force sensor. The results demonstrated that the developed device is a reliable solution for simultaneous measurement of shear and vertical forces. This solution has a great advantage over previous ones, since it only requires one optical fiber, which facilitates its incorporation into insoles. Therefore, several points, along the foot plantar surface, can be measured with a single optical fiber [12, 51, 52], with the advantage of being able to simultaneously differentiate the two different forces (shear and pressure).

There are also studies using FBGs for vertical and shear forces measurements, but in which shear measurement is indirectly inferred from temperature variations. The authors argue that a rise in temperature in a certain area of the foot presupposes that there was friction between the surface of the foot and the shoe (shear force) [44, 60]. Najafi's team published a work in 2017 with the validation of a smart-textile based on fiber-optics with FBGs (SmartSox) for simultaneous measurement of temperature, pressure, and joint angles in patients with diabetic peripheral neuropathy (PND), where irregular temperature increase suggested the presence of shear forces [44]. In this study, FBG sensors were placed in socks that were successfully tested in a clinical setting by 33 individuals with PND to evaluate plantar pressure and temperature during normal gait velocity in a clinical setting.

#### 4. Lower limb joints monitoring

The knee, hip, and ankle have a key role in gait, as it allows the body locomotion with muscles' minimum energy consumption and provides stability to walk in different terrain relief. During gait, the lower limb joints act together in order to provide the smoothest locomotion for the body. In **Figure 10**, the kinematics of the lower limbs in the different phases of gait are represented, namely the stance (a) and the swing phases (b) [14, 28].

At the beginning of the stance phase, in first double support and at the heel strike, the hip is flexed at 30°, the knee is extended and the ankle is at a neutral position. As the loading response approaches with the foot flat, the hip continues in a flexed mode as the knee starts flexing 5–10°, along with the ankle plantar flexing up to 20°, for the weight acceptance, shock absorption, and to propel the body forward. At the mid stance, the hip is extended, the knee flexed by 5–10° and the ankle is dorsi-flexed, with the purpose to move the body over the stationary foot. As the heel rises, with the ankle dorsi-flexing at 15°, the hip is extended at 15–30° and the knee is extended and then flexing. At the last point of the stance phase, in the toe off moment, the hip is flexing, the knee is also flexing at 30–40° and the ankle has a plantar flexing of 20–30°, in the preparation for the swing phase and the transfer of the load to the other limb [61].

At the initial swing, the hip continues flexing at 15°, the knee is flexing up to 65°, and the ankle is plantar flexed at 10° to clear the foot from the floor and advance the

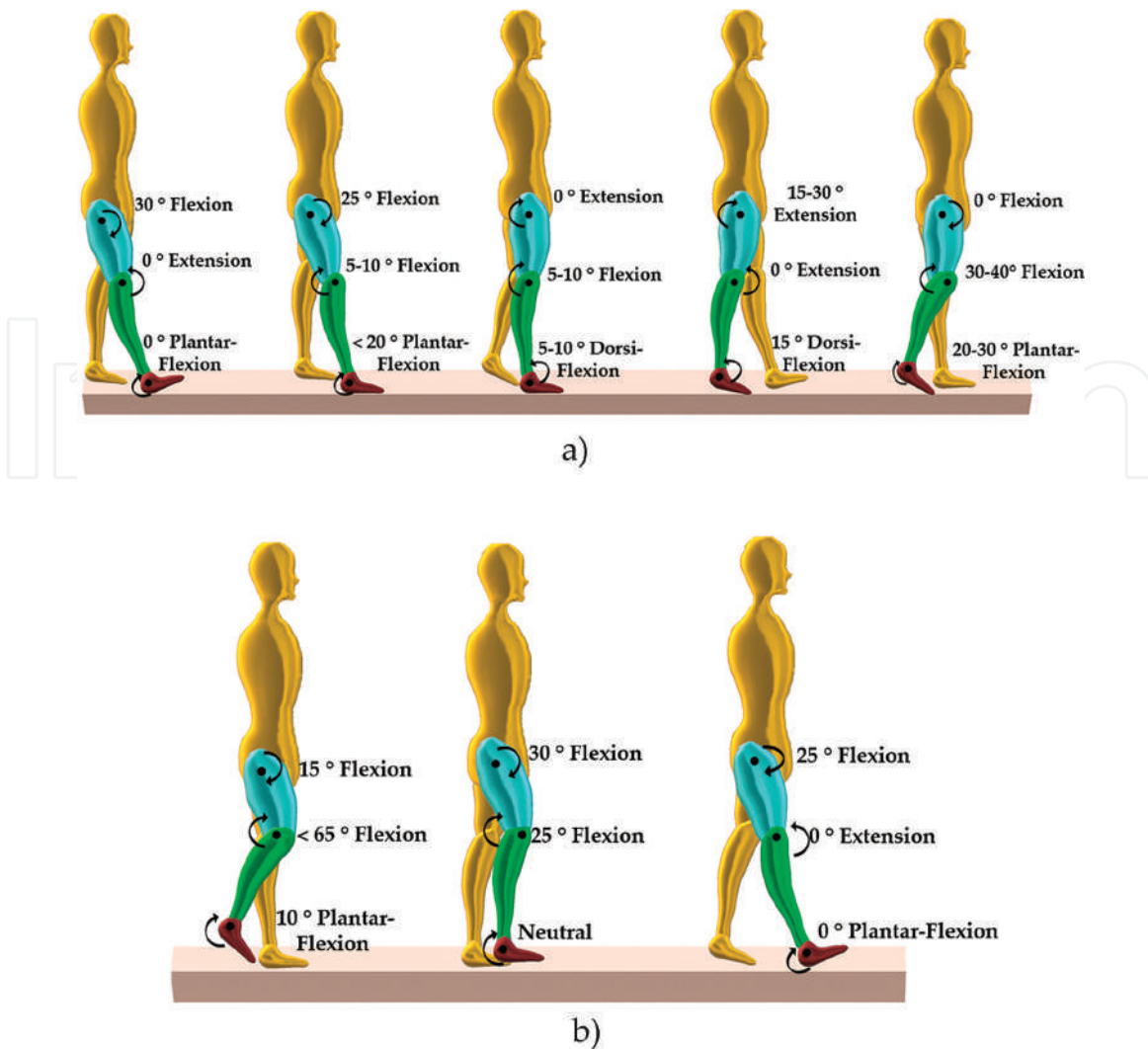


**Figure 10.** Schematic representation of the lower limbs kinematics involved in the: (a) stance and (b) swing phases.

limb. At the mid swing, the hip is flexed at 30°, while the knee is flexing at 25°, and the ankle is at a neutral position. At the terminal swing, the hip is flexed at 25°, the knee is extended, and the ankle is at a 0° plantar flexion, to prepare the next heel contact at the beginning of the new stance phase [61].

The use of objective techniques to evaluate the health conditions of the knee can be a powerful tool for researchers and medical staff, providing relevant information about tendon-ligament strains and vibration, pressure, angular range of movements, and even temperature [62, 63].

There are numerous conventional techniques that can be used to monitor the joint conditions, such as stereo-optic, solid state, and piezo-resistive sensing methods, which employ accelerometers, magneto-resistive sensors, flexible goniometers, electromagnetic tracking systems, among others [24, 62, 64]. However, these techniques usually require complex and expensive electronics, which are susceptible to magnetic interferences and also cannot be used in humid/wet environments. Therefore, they do not represent an ideal solution for wearable sensing configurations, where the human transpiration may influence the sensors performance. So, the increasing research in the field of optical fiber sensors has also been focusing in the introduction of FBG technology in monitoring the lower limb joints during walking. Optical fiber sensors can be easily adapted to curved surfaces and various contours of the human body, especially the knee, a joint with complex anatomy [62, 63, 65–67].

The ideal technology to monitor limb joints should be able to measure curvature, being useful not only to monitor the motion of the lower limb segments, as well

as to evaluate all the corporal posture [65]. The development of a smart garment, based on FBGs and flex sensing technologies, to monitor the body posture and lower and upper limbs' movements, was reported. An FBG-based sensing belt was produced by encapsulating FBG sensors inside a synthetic silica gel, as depicted in **Figure 11**, which was afterward attached to a garment for monitoring joints and body posture. The encapsulation of the FBG was made with an applied pre-stress, so the sensor is able to monitor both extension and compression deformations. The proposed FBG belt, fixed near the limb joints, is influenced by the body posture shifts, and the consequent sensor's Bragg wavelength shift was correlated with the angles at the limb joint [65]. Although the results presented by Abro et al. are only related to tests made at the upper limbs, the reasonable results obtained within the tests and exercises are a good indication of its potential application for the monitoring of the lower limbs motion.

#### 4.1 Knee flexion-extension monitoring

From the lower limb three joints (ankle, knee, and hip), the knee is one of the body joints most prone to develop osteoarthritis [68]. Therefore, the supervision and monitoring of the motion of the knee are of crucial importance in the medical and physical rehabilitation field [37, 62, 67, 69, 70].

Rocha et al. suggest a wearable knee motion sensor, designed with a single FBG, embedded in a stretchable band of polyvinyl chloride (PVC) material and placed in the center of the knee joint, as schematized in **Figure 12a** [67]. The objective is to measure the knee movements from the straight leg to the maximum knee flexion and to obtain graphically the pattern of human gait, by monitoring flexion and extension, with the joint acting as a rotation axis, as represented in **Figure 12b**. The PVC band with the FBG was attached to an elastic ribbon (knee brace), by metallic pressure-buttons that ensure the stability of the sensing band while walking or running. In the reported work, the authors tested the proposed solution on a treadmill, under different types of run and speed, accompanied by video recorder [67]. The video was used to define the starting time of the stance and swing phases in order to correlate the data provided by the FBG sensor to the different phases of the walking routine [67, 71, 72].

When the leg is straight, the FBG sensor is in the resting position since there is neither flexion nor extension in the optical fiber. Once the bending movement of the knee starts, during walking, it results in an extension of the optical fiber, inducing a strain in the FBG sensor, positioned at the center of the knee joint. Consequently, a positive shift of the reflected Bragg wavelength is obtained. The reverse bending movement, from the maximum knee flexion point to straight leg, leading to a relaxation of the FBG, return to its initial Bragg wavelength value [67]. By monitoring the wavelength shift during these movements, the gait pattern of the patient could be characterized.

Although the researchers Rocha et al. show a clear characterization of the movement of the knee joint during the gait cycle, they also point out, as a drawback, the noise induced in the signal by vibration, considering that better results are achieved at lower speed, softening the influence of the elastic factor of the knee band [67].

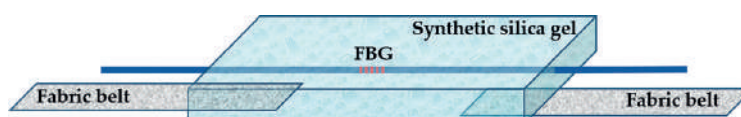


**Figure 11.**  
 Schematic representation of the FBG belt proposed by Abro et al. (adapted from [65]).



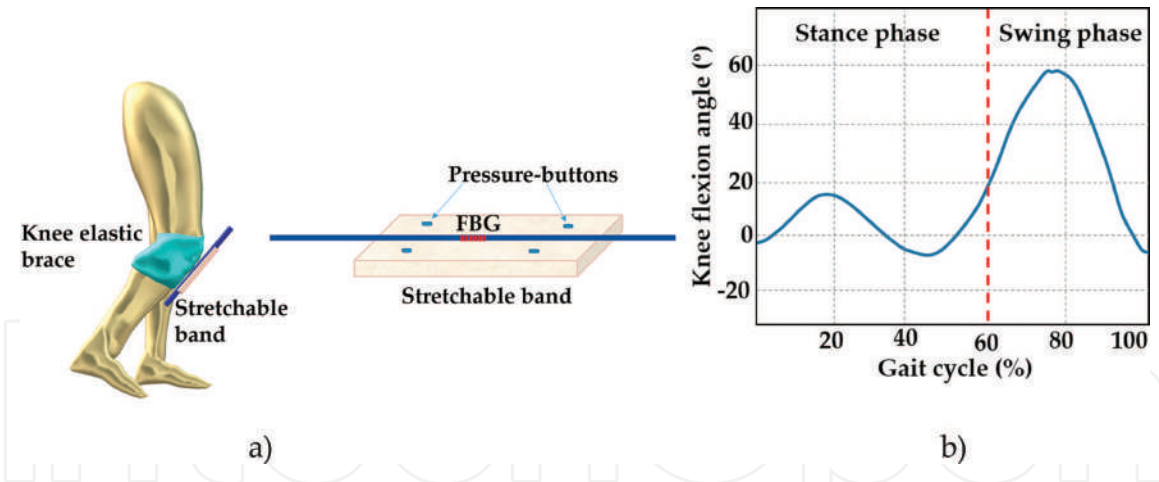


**Figure 12.**

(a) Schematic representation of an FBG-based solution for knee movements monitoring (adapted from [67]); and (b) typical knee angle pattern during gait.

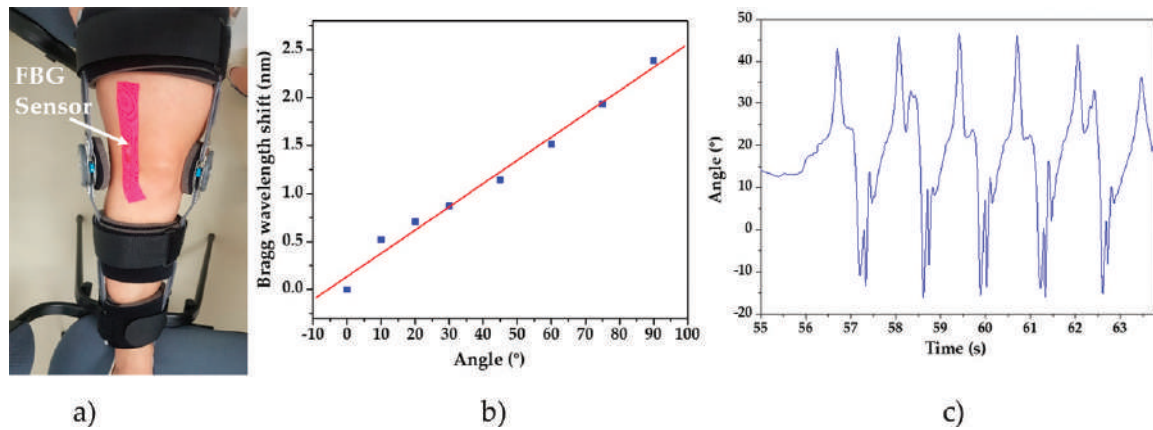


**Figure 13.**

(a) Photograph of the kinesio tape with an embedded FBG for knee angle monitoring; (b) Bragg wavelength shift dependence with the knee flexion angle; and (c) knee flexion/extension angle during six gait cycles.

Similar results can be achieved using kinetic tape (elastic adhesive tape) with an embedded FBG. The kinetic tape is attached to the lower limb, starting at the quadriceps area and ending at the beginning of the tibia, with the FBG placed just a few centimeters above the knee rotation axis, as shown in **Figure 13a**. Such configuration is a more stable solution, since the fiber containing the FBG is only actuated by the rotation of the knee, which stretches the kinetic tape inducing a strain and consequent positive wavelength shift in the FBG. During the calibration process, using an angle lock goniometer for angles ranging between 0 and 90°, a direct relation between the knee angle and the Bragg wavelength shift was found as displayed in **Figure 13b**. In **Figure 13c** is presented the flexion/extension angles, along time for six gait cycles, obtained with the solution represented in **Figure 13a**, and which as a similar behavior as reported by the authors in Ref. [67], but with a considerable reduced noise level.

#### 4.2 Ankle flexion and dorsi-flexion monitoring

Umesh et al. proposed an FBG goniometer based on the deflection produced in an optical fiber by variation of the angle of the goniometer [73]. The purpose of the sensor is to measure the range of movement (ROM), which for the ankle joint the movement can be classified as ROM plantar-flexion and ROM dorsi-flexion. Plantar flexion is described as the rotation that increments the angle described between

foot and the shin, and the dorsi-flexion is the rotation that results in a lower angle. The sensor is an assembly of two discs of 30 mm, overlapped by two discs with smaller diameter (5 mm). The two pairs of discs are circled by a rubber belt, to ensure synchronized rotation between them. The optical fiber with the FBG sensor is placed in a cantilever, connected to the upper belt. The rotation arm is linked to the side of the foot and its movement motivates the rotation of the correspondent disc. This rotation moves the cantilever and creates strain in the FBG, which can be rewritten in angle values, by proper calibration. The characterization of these two rotations has crucial importance in clinical diagnosis, helping the evaluation of the limitations of this joint. Furthermore, it is a noninvasive method of measurement with the advantages that optical fibers offer, and that can counteract to limitations of conventional electro-goniometers and video tracking systems as electromagnetic interference, size, and fragility [73].

### **4.3 Tendons and ligaments monitoring**

Beyond their ability to measure the flexion, dorsiflexion, and extension of the joints involved in gait, FBGs can broaden their usage to applications related to the tendons and muscles monitoring. Although it may fall a bit out of the scope of e-Health, it is worth mentioning the application of FBGs to perform pressure mapping, and monitor strain and length of tendons and ligaments, when under load or locomotion. Ren et al. presented an FBG sensor embedded in a micro-shape memory alloy tube which is able to measure the displacement of the tendon [74]. To verify the performance of the sensor, the initial tests were made in the Achilles tendon and the results compared with the ones obtained simultaneously with a two-camera stereovision sensor. The fiber-based sensor was also applied to a cadaver knee tendon, in the medial and lateral collateral ligament, to record the deformation of the ligaments in simulated postures. The results proved that the FBG sensor has high sensitivity and low signal-to-noise ratio, without loss of accuracy. It is also easily implemented and minimally invasive to the biological tissues, projected to be applied *in-vivo*, after some improvements [74].

## **5. Prosthetic and exoskeletons applications**

For severe impaired citizens, it is common to adapt prosthetic lower limbs, in order to offer patients mobility. The interface pressure inside the prosthetic sockets is of major relevance, in order to avoid ulcerations in the patients and evaluate its suitability. Moreover, the application of robotics technology to improve the wellbeing of debilitated patients has been highly investigated in the past few years. In particular, exoskeletons can be wearable devices prone to be used to restore functional movements of amputees and persons with paralysis. Therefore, this section surveys the use of FBG sensors for the development and evaluation of prosthetic limbs, in addition to control and automation of exoskeletons.

### **5.1 Prosthetic limbs**

The partial or total limb amputation is one of the oldest treatment options available in medicine. Unfortunately, the frequency of the lower limb amputation is growing worldwide. Traffic accidents, particularly motorcycle accidents, health problems (including diabetes, arterial hypertension, chronic renal failure, and hypercoagulability), and advanced age are the main causes. Additionally, this is a predominant incident in countries affected by landmines and other natural



disasters, including, for instance, earthquakes. Due to the socioeconomic impact (with the consequent inability to work and socialize), the interference on the life quality, and other complications, such as hematoma, infections, necrosis, contractures, neuromas, and phantom pain; this is a relevant public health problem.

The key element of amputee rehabilitation is the engineering of solutions, appropriated for individuals to recover their physical capabilities. A prosthesis or artificial limb is a device, whose function is to substitute the limb that was lost, with cosmetic and functionality for the amputee. A lower limb prosthesis results from the assembly of several components, including socket, shank, ankle, and foot, as schematized in **Figure 14**.

The socket is the most relevant component of the artificial limb, since it constitutes the critical interface between the amputee's stump and the amputee. The design and fitting of the socket are also the most difficult processes, due to the particularity of each amputee's stump. When wearing the prostheses, the appropriated fit and comfort are critical factors that contribute to its successful use. Nevertheless, many amputees still complain about discomfort or pain, reporting a set of problems, including edema, pressure ulcers, dermatitis, and skin irritation, due to the use of the prostheses [76]. This is particularly related with the changes in the residual limb soft tissues (volume, shape, sensitivity, composition, among others), which vary during the day due to factors such as temperature, activity, and hydration.

As result, in the last years, several measurement systems have been proposed to assess the interface pressure between the residual limb and the prosthetic socket [77]. This includes electrical strain gauge [78], F-socket transducer arrays [79, 80], and finite element analysis [81–83]. The output from these systems has been used to improve the socket design. Nevertheless, despite the technological advances in the existing socket design and the measurement systems, available sockets still exhibit many weaknesses. For instance, apart from the high accuracy and sensitivity provided, the use of strain gauges requires modifying the sockets with openings for accommodation of the device. This procedure interferes in the socket shape, and consequently in the accuracy of the pressure measurements.

In the case of the F-sockets, these systems present flexibility, good sensitivity, and ease of use. Additionally, in contrast to strain gauges, no change in the

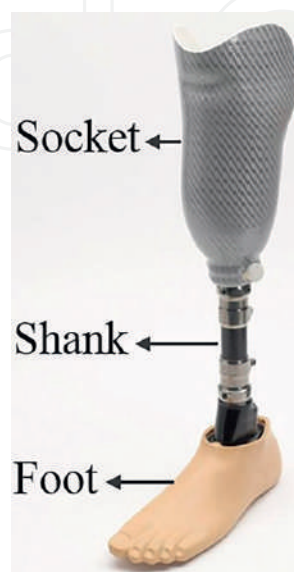


**Figure 14.**  
*Typical transtibial prosthesis (adapted from [75]).*

socket shape is required, since F-sockets are quite thin, which can be placed *in-situ* between the residual limb and the prosthetic socket. Nevertheless, the nonlinearity, hysteresis, drift, and vulnerability to electromagnetic interferences are the main limitations. Additionally, the shear stresses are not accounted for, when this system is used.

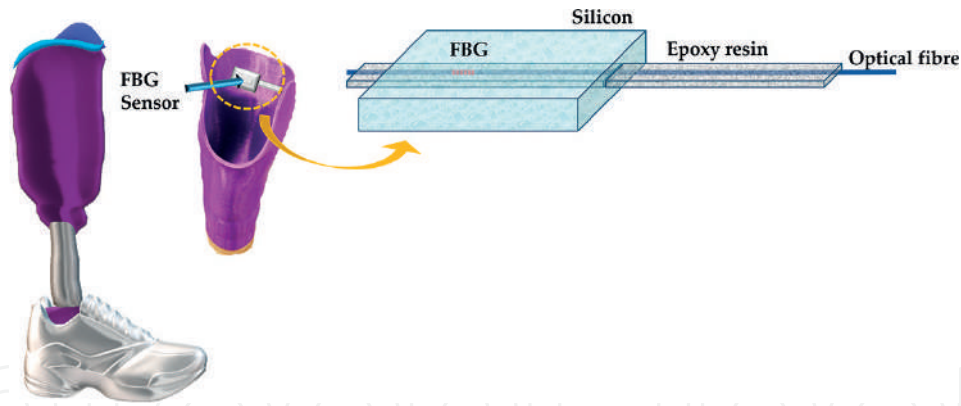
The finite element analysis is a numerical modeling alternative, which, when applied to the residual limb, predicts the soft tissues load distributions and magnitudes. This information has been assisting the technicians during the socket design. Nonetheless, although some models already considered thresholds for tissue injury and adverse adaptation, and other researchers have included in the models parameters, such as comfort and pain threshold, several complaints are still reported from the use of the prostheses, due to the subjectivity, difficulty to evaluate these factors, and the inter- and intra-individual loading [83].

Consequently, new sensing methodologies with minimal limitations toward accurate measurements of the interface pressure within prosthetic sockets are essentially required. Thereby, the FBG technology was pointed out as a potential alternative to conventional methodologies [84]. In 2010, Kanellos et al. proposed a 2D optical FBG-based pressure sensor, predicting to be suitable for several biomedical applications, namely biomechanics, rehabilitation, and orthotics, including amputee sockets [85]. The device consists of FBGs embedded into a thin polymer layer of PDMS, with the minimum thickness of the sensing pad set to 2.5 mm. The sensor exhibited a maximum fractional pressure sensitivity of  $12 \text{ MPa}^{-1}$ , with a spatial resolution of  $1 \times 1 \text{ cm}^2$ , also revealing no hysteresis and real-time operation possibility. Due to the elasticity and ductility of the polymer, which match human skin behavior, the system becomes a flexible 2D pressure sensing surface. This configuration is appropriate to be attached or anchored to irregular shaped objects/bodies, allowing to translate more accurately all the phenomena that may occur in them. These properties meet the requirements of human machine interfaces, comprising amputee sockets, as initially predicted.

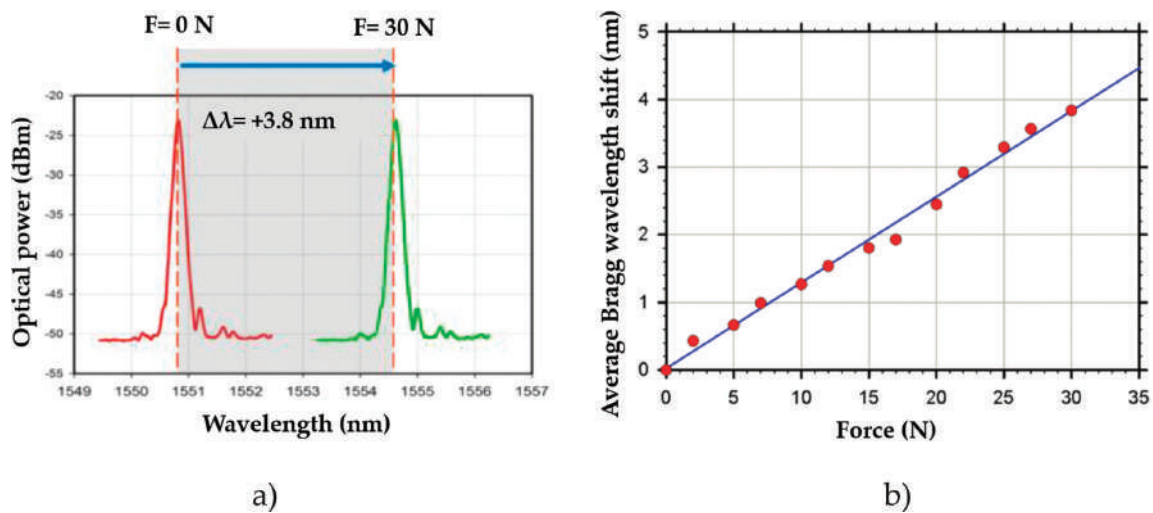
Apart from the medical requirements imposed on the FBG embedded-based sensor pads, which include real time acquisition, high sensitivity and resolution, and increased dynamic range, these systems also need to comply with a set of demands related to fabrication and packaging processes. These conditions result from the diversity of the patients to be treated, and also from their real life conditions. Thus, the influence of the fiber embedding depth (center and top position of pad cross-section), the thickness of the polymer sheet (2 and 3 mm), and the fiber type (hydrogenated SMF-28 and nonhydrogenated GF1B) were assessed in [86]. The results of this study reveal that the sensor pads rigidity and durability are enhanced, when the Bragg grating, inscribed into nonhydrogenated fiber, is embedded at the polymer center, with a thickness of 3 mm.

Results of the first investigation of the ability of FBGs to measure interface pressure between the stump of a trans-tibial amputee and a patellar tendon bearing (PTB) prosthetic sockets are presented in [75]. The patellar tendon (PT) bar was the key analyses' area since this supports the majority of the transtibial amputee's body weight, when the subject is using the PTB socket. In Ref. [75], the FBGs were first embedded into an epoxy material (NOA 61), aiming to acquire the required protection to withstand the high pressure values up to 230 kPa at the PT bar [78]. After that, this sensing pad was placed between two silicone polymeric sheets forming the pressure sensor, as schematized in **Figure 15**.

Since the initial contact of the PT with the sensor surface is mostly pressure concentrated, this behavior was imitated using a ball bearing, and positive wavelength shift of 3.8 nm was observed for a maximum load of 30 N, **Figure 16a**.

**Figure 15.**

Schematic representation of an FBG-based system for monitor the interface pressure between the socket and the amputee (adapted from [75]).

**Figure 16.**

(a) Representation of the maximum Bragg wavelength shift for maximum load applied (adapted from [75]); and (b) average Bragg wavelength shift as function of the applied force (adapted from [75]).

Thereafter, an experimental set up was designed to assess, *in-situ*, the sensor performance, while attached to the inner socket wall. Although there was no subject involved in these tests, consideration was taken to reproduce a real-life situation, as much as possible. The results obtained for the different load cycles reveal the suitability of the sensor to accomplish pressure measurements on the socket stump interface, especially in the PT region. From the calibration procedure, a proportional wavelength shift dependence with the load applied was found **Figure 16b**.

Toward using these sensors *in-situ*, the performance of these sensing pads was broadly assessed concerning the sensitivity, durability, and hysteresis error [87]. Similar to the work of Kanellos et al., three production parameters were investigated, which are the FBG embedding depth (top, bottom, and neutral layers of the sensing pad), the sensing pad thickness (1, 2, and 3 mm), and the type/hardness of sensing pad materials [PDMS (harder) and silicone rubber (softer)]. The best sensor's performance (highest sensitivity and accuracy) was obtained for the FBG embedded in the neutral layer of PDMS and with the thicker sensing pads. An FBG array was produced with these conditions and used for interface pressure measurements within prosthetic sockets. Additionally, to further assess the performance of the proposed sensing pad, these were evaluated *in-situ*, in a traumatic transtibial amputee using a total surface bearing socket, with 6 mm silicone liner. The results were validated comparing the data obtained with the FBG technology

to the pressure measurements acquired by the F-socket sensors. Although the data obtained for the 8 sub-regions of the amputees' residual limb follow the same tendency; higher pressure values were registered by the FBG sensors. The difference was attributed to the sensors' thickness, which is 3 mm in the case of the FBG sensing pads and 0.2 mm in the F-socket sensing mats.

Aiming to eliminate the previous limitations and provide a simpler and more practical sensing procedure, Al-Fakih et al. proposed an innovative customized FBG-instrumented silicone liner, which consists of two silicone layers with 12 FBGs embedded between them, with the gratings located in clinical interest points [88]. In this study, a custom gait simulation machine was built to test the performance of the sensing system during an amputee's simulation gait. The data were validated with the findings obtained using an F-socket. The FBG technology revealed sensitivity and accuracy similar to the ones obtained with the F-socket technology. Nevertheless, this new design can be used repeatedly in clinical and research setting, which is an important benefit compared to the F-socket mats that, due to drift and calibration issues, are usually discarded after each utilization.

Recently, the technologies used to assess the interface pressure between the residual limb and the prosthetic socket, and the challenges found concerning the development of new solutions of sockets for limb prostheses were reviewed in [89]. In this chapter, FBGs are pointed out as one of these technologies. Additionally, the study observes that due to the high risk of the damaging of fibers, their applications are still limited, with further studies still required to confirm their suitability in this field. Nevertheless, the shown advantages of this technology over other sensing methodologies, especially regarding drift and linearity, and the constant low satisfaction level of the amputees, are enough motivations to continue investing on this technology.

## **5.2 Rehabilitation exoskeletons**

The application of robotics, in particular robotic exoskeleton systems, to improve the wellbeing of debilitated patients is already being adopted. This technology is being used in human power augmentation, and its application has become more prominent, as to provide alternative solutions for physically limited people support in their daily movements [90].

Exoskeletons are known to be wearable robots (robotic exoskeletal structures), with a strict physical and cognitive interaction with the human user, since, typically, it operates alongside human limbs. Although the scientific and technological research on the development and implementation of exoskeletons began in the early 60s, only recently, its application in rehabilitation and functional substitution of movements have been implemented in patients with motor disorders [91].

Robotic exoskeletons provide unique methods for rehabilitation, by promoting the patient engagement in its training, and retrieving better quantitative feedback and improved functional outcome for patients. In a future perspective, the development of more effective exoskeletons is insight, with solutions for a real-time biological synergy-based exoskeleton, which will allow disabled patients to regain normal mobility capabilities [92, 93].

The exoskeleton feedback is based on the information, which is retrieved from the embedded sensors in its structure. The current exoskeleton designs can have up to several dozens of sensors, to monitor variables, such as rotation, torque, tilt, pressure, position, velocity, neurological signals, among others. As the sensing systems integrated in the robot are the key devices for its proper performance, the research field on robotics already has a mature and overspread technology, offering good sensitivity, precise measurements, and competitive price, with



sensing systems often based on solid-state sensing [64]. Nevertheless, this technology has also shown some drawbacks, due to its susceptibility to electromagnetic interferences resulting from the electric inertial motors. This interference could be enough to degrade the sensors signal, sending erroneous information to the control devices, leading the exoskeleton to perform erratically, and risking injuring the patient.

Rehabilitation robotics applications also require the analysis of the body motion, in order to close control loops around defined joints. Commercial optical systems, such as Vicon, are considered the standard in human motion analysis. Although Vicon provides accurate position information, it has some significant limitations, such as high costs and limited measure volume, since it has to be used in laboratories with fixed equipment, which prevents its use in rehabilitation robotics applications [94]. On the other hand, soft exoskeletons require even more imperceptible sensors, typically sensor heads with thicknesses below 0.5 mm, in which electronic devices present some drawbacks, including long term instability, inconsistency, excessive drift, and the restriction to a small sensing area requiring the use of more sensors to monitor larger areas [64]. As an alternative to these electronic and optical sensors, the optical fiber sensors offer a small and robust solution, able to acquire kinematic and kinetic measurements, enhancing the exoskeleton performance by adding further responsiveness, controllability, and flexible motion. Nevertheless, the use of FBG sensors in exoskeletons is not yet widely explored, with only a limited number of studies reported. Recently, Domingues et al. reported the instrumentation of an insole with FBG sensors for plantar pressure monitoring [12, 32]. The reported wearable device is able to be adapted to exoskeletons structures, and dynamically retrieve the gait pattern of the patient.

Although there is a shortage of studies regarding the adaptation of FBG sensing technologies to exoskeletons, for gait aid there are already some reports focusing on its application in robot fingers and glove-based devices [95–97]. Park et al. presented an FBG-based solution to monitor the force in exoskeleton fingers [95]. The authors embedded the optical fiber sensors in a finger-like plastic 3D mesh, inspired in the design of arthropod limbs, near the fingers base, for enhanced sensitivity. With the developed structure, it is possible to detect forces down to 0.02 N, with a resolution of  $\sim 0.15$  N. The robot hand instrumented by Park et al. was able to be operated in a hybrid control scheme, with the fingers being capable to sense small forces, with the advantage of being able to have all the FBG sensors in one single fiber, due to FBGs multiplexing ability [95].

Jiang et al. also described the design and production of an instrumented robotic hand with three fingers that enable both pinch and power grips. The optical FBG sensors were embedded in both the rigid plastic and soft skin material that constitutes the hand bone structure. In the rigid plastic material, the authors included eight FBGs for force sensing, while in the soft skin, they integrated six FBGs strain sensors for tactile monitoring, providing information on the location of the contact points [96]. Although there are already some studies related to the upper limbs motion aid, some work is still needed concerning the application of FBG technology to exoskeletons for gait rehabilitation of patients, which demands a direct focus on the lower limbs synergy between the patient and the exoskeleton.

Key topics for further development of exoskeletons in rehabilitation scenarios include the need for robust human-robot multimodal cognitive interaction, safe and dependable physical interaction, true wearability and portability, and user aspects such as acceptance and usability [91]. It should be able to augment the ability and/or to treat skeletal parts, which are weak, ineffective, or injured due to a disease or a neurological condition. Therefore, the exoskeleton should be designed to work in parallel with human body and be actuated either passively and/or actively [98].

## 6. Conclusion

e-Health has been widely investigated in recent years, building on technological advances, especially in fields such as sensing and networking. Building on such gains, more innovations are expected to enhance the life quality of citizens, especially debilitated and elder ones. Gait analysis stands out as one promising solution, which can help in the rehabilitation of locomotive impairments, in addition to early diagnosis of other pathologies, such as ulcers in patients with diabetes. Various solutions have been proposed in the literature for close monitoring and analysis of gait. However, recently, FBGs have been pointed out as a promising alternative for a sensing technology to analyze gait movement, building on advantages such as small size, rigidity, low-cost, low power consumption, and minimally invasive. Due to its recent adoption and promising advantages, this chapter has provided a thorough review of research and design efforts of FBG-based sensors for gait analysis. The chapter initially explains the sensing principle underlying the FBG technology, after that the topic of gait analysis and the different phases of gait cycle are described, and then moves toward required e-Health monitoring solutions. Efforts toward the design of solutions to monitor plantar pressure and shear forces are discussed. Monitoring of plantar pressure, independently, is first presented, then simultaneous monitoring of plantar and shear forces is further elaborated. The chapter then moves toward monitoring of lower limb joints, which also play key roles in the gait analysis, since their wellbeing affects the gait cycle pattern. The use of optical fiber sensing in prosthetic and exoskeletons concludes the topics discussed in the chapter. This chapter represents a thorough review of research efforts in the design of optical fiber-based sensors in gait analysis, covering all related topics of monitoring plantar pressure, shear forces, knee and joints, and integration in prosthetic and exoskeletons.

## Acknowledgements

This work is funded by FCT/MEC through national funds and when applicable co-funded by FEDER – PT2020 partnership agreement under the projects, UID/EEA/50008/2013, UID/CTM/50025/2013 and 5G-AHEAD IF/FCT- IF/01393/2015/CP1310/CT0002. Nélia Alberto acknowledges PREDICT (FCT-IT-LA) scientific action; Cátia Tavares acknowledges her PhD grant PD/BD/142787/2018. The financial support from FCT through the fellowships SFRH/BPD/101372/2014 (M. Fátima Domingues) and SFRH/BPD/109458/2015 (Carlos Marques) is also acknowledged.

IntechOpen

### Author details

Maria de Fátima Domingues<sup>1\*</sup>, Cátia Tavares<sup>2</sup>, Tiago Leite<sup>1,2</sup>, Nélia Alberto<sup>1</sup>,  
Cátia Leitão<sup>1,2</sup>, Carlos Marques<sup>1,2</sup>, Ayman Radwan<sup>1</sup>, Eduardo Rocon<sup>3</sup>,  
Paulo Antunes<sup>1,2</sup> and Paulo André<sup>4</sup>

1 Instituto de Telecomunicações, Campus Universitário de Santiago, Aveiro,  
Portugal

2 Department of Physics & I3N, University of Aveiro, Campus Universitário de  
Santiago, Aveiro, Portugal

3 Centro de Automática y Robótica, CSIC-UPM, Madrid, Spain

4 Department of Electrical and Computer Engineering, Instituto de  
Telecomunicações, Instituto Superior Técnico, University of Lisbon, Lisbon,  
Portugal

\*Address all correspondence to: fatima.domingues@ua.pt

### IntechOpen

© 2018 The Author(s). Licensee IntechOpen. This chapter is distributed under the terms of the Creative Commons Attribution License (<http://creativecommons.org/licenses/by/3.0>), which permits unrestricted use, distribution, and reproduction in any medium, provided the original work is properly cited. 

## References

- [1] Kawasaki B, Hill K, Johnson D, et al. Narrow-band Bragg reflectors in optical fibers. *Optics Letters*. 1978;**3**:66-68. DOI: 10.1364/OL.3.000066
- [2] Lam D, Garside B. Characterization of single-mode optical fiber filters. *Applied Optics*. 1981;**20**:440-445. DOI: 10.1364/AO.20.000440
- [3] Hill K, Meltz G. Fiber Bragg grating technology fundamentals and overview. *Journal of Lightwave Technology*. 1997;**15**:1263-1276. DOI: 10.1109/50.618320
- [4] Kashyap R, editor. *Fiber Bragg Gratings*. 2nd ed. San Diego: Academic Press; 2009. 632 p. ISBN: 9780080919911
- [5] Meltz G, Morey W, Glenn W. Formation of Bragg gratings in optical fibers by a transverse holographic method. *Optics Letters*. 1989;**14**:823-825. DOI: 10.1364/OL.14.000823
- [6] Hill K, Malo B, Bilodeau F, et al. Bragg gratings fabricated in monomode photosensitive optical fiber by UV exposure through a phase mask. *Applied Physics Letters*. 1993;**62**:1035-1037. DOI: 10.1063/1.108786
- [7] Muro-de-la-Herran A, Garcia-Zapirain B, Mendez-Zorrilla A. Gait analysis methods: An overview of wearable and non-wearable systems, highlighting clinical applications. *Sensors*. 2014;**14**:3362-3394. DOI: 10.3390/s140203362
- [8] Gehlsen G, Beekman K, Assmann N, et al. Gait characteristics in multiple sclerosis: Progressive changes and effects of exercise on parameters. *Archives of Physical Medicine and Rehabilitation*. 1986;**67**:536-539. DOI: 10.5555/uri:pii:0003999386905496
- [9] Kerrigan D, Tidd M, Croce U, et al. Biomechanical gait alterations independent of speed in the healthy elderly: Evidence for specific limiting impairments. *Archives of Physical Medicine and Rehabilitation*. 1998;**79**:317-322. DOI: 10.1016/S0003-9993(98)90013-2
- [10] Stolze H, Klebe S, Getersen G, et al. Typical features of cerebellar ataxic gait. *Journal of Neurology, Neurosurgery and Psychiatry*. 2002;**73**:310-312. DOI: 10.1136/jnnp.73.3.310
- [11] Afilalo J, Eisenberg M, Morin J-F, et al. Gait speed as an incremental predictor of mortality and major morbidity in elderly patients undergoing cardiac surgery. *Journal of the American College of Cardiology*. 2010;**56**:1668-1676. DOI: 10.1016/j.jacc.2010.06.039
- [12] Domingues M, Tavares C, Leitão C, et al. Insole optical fibre Bragg grating sensors network for dynamic vertical force monitoring. *Journal of Biomedical Optics*. 2017;**22**:091507(8pp). DOI: 10.1117/1.JBO.22.9.091507
- [13] Sutherland D. The evolution of clinical gait analysis part I: Kinesiological EMG. *Gait and Posture*. 2001;**14**:61-70. DOI: 10.1016/S0966-6362(01)00100-X
- [14] Sutherland D. The evolution of clinical gait analysis. Part II kinematics. *Gait Posture*. 2002;**16**:159-179. DOI: 10.1016/S0966-6362(02)00004-8
- [15] Sutherland D. The evolution of clinical gait analysis part III–Kinetics and energy assessment. *Gait and Posture*. 2005;**21**:447-461. DOI: 10.1016/j.gaitpost.2004.07.008
- [16] Mummolo C, Mangialardi L, Kim J. Quantifying dynamic characteristics of human walking for comprehensive gait cycle. *Journal of Biomechanical*



- Engineering. 2013;**135**: 091006 (10pp). DOI: 10.1115/1.4024755
- [17] Soames R. Foot pressure patterns during gait. *Medical Engineering and Physics*. 1985;**7**:120-126. DOI: 10.1016/0141-5425(85)90040-8
- [18] Marasović T, Cecic M, Zanchi V. Analysis and interpretation of ground reaction forces in normal gait. *WSEAS Transactions on Systems*. 2009;**8**: 1105-1114. ISSN: 1109-2777
- [19] Perry J, Davids J. Gait analysis: Normal and pathological function. *Journal of Pediatric Orthopaedics*. 1992;**12**:815. DOI: 10.1097/01241398-199211000-00023
- [20] Vaughan C, Davis B, O'Connor J, editors. *Dynamics of Human Gait*. 2nd ed. South Africa: Kiboho Publishers; 1999. 137p. ISBN: 0-620-23558-6
- [21] Perttunen J. Foot loading in normal and pathological walking [thesis]. Jyväskylä: University of Jyväskylä; 2002
- [22] Prakash C, Kumar R, Mittal N. Recent developments in human gait research: Parameters, approaches, applications, machine learning techniques, datasets and challenges. *Artificial Intelligence Review*. 2018;**49**: 1-40. DOI: 10.1007/s10462-016-9514-6
- [23] Whittle M. Gait analysis. In: McLatchie G, Lennox C, editors. *The Soft Tissues – Trauma and Sports Injuries*. Oxford: Butterworth-Heinemann; 1993. pp. 187-199. ISBN: 0 7506 0170 1
- [24] Tao W, Liu T, Zheng R, et al. Gait analysis using wearable sensors. *Sensors*. 2012;**12**:2255-2283. DOI: 10.3390/s120202255
- [25] Shi DL, Wang YB, Ai ZS. Effect of anterior cruciate ligament reconstruction on biomechanical features of knee level in walking: A meta-analysis. *Chinese Medical Journal*. 2010;**123**:3137-3142. DOI: 10.3760/cma.j.issn.0366-6999.2010.21.034
- [26] Langer S. *A Practical Manual of Clinical Electrodynography*. 2nd ed. New York, USA: The Langer Foundation for Biomechanics and Sports Medicine Research; 1989. ISBN: 0936445025
- [27] Kyriazis V. Gait analysis techniques. *Journal of Orthopaedics and Traumatology*. 2001;**2**(1):1-6. DOI: 10.1007/PL00012205
- [28] Terrier P, Schutz Y. How useful is satellite positioning system (GPS) to track gait parameters? A review. *Journal of NeuroEngineering and Rehabilitation*. 2005;**2**:28(11pp). DOI: 10.1186/1743-0003-2-28
- [29] Frigo C, Rabuffetti M, Kerrigan D, et al. Functionally oriented and clinically feasible quantitative gait analysis method. *Medical and Biological Engineering and Computing*. 1998;**36**:179-185. DOI: 10.1007/BF02510740
- [30] Al-Fakih E, Osman N, Adikan F. The use of fibre Bragg grating sensors in biomechanics and rehabilitation applications: The state-of-the-art and ongoing research topics. *Sensors*. 2012;**12**:12890-12926. DOI: 10.3390/s121012890
- [31] Domingues M, Tavares C, Alberto N, et al. Non-invasive insole optical fibre sensor architecture for monitoring foot anomalies. In: *Proceedings IEEE Global Communications Conference (GLOBECOM 2017)*; 4-8 December 2017; Singapore. New York: IEEE; 2018. 6p. DOI: 10.1109/GLOCOM.2017.8255026
- [32] Domingues M, Alberto N, Leitão C, et al. Insole optical fibre sensor architecture for remote gait analysis-an eHealth solution. *IEEE Internet of Things Journal*. DOI: 10.1109/JIOT.2017.2723263

- [33] Farahani B, Firouzi F, Chang V, et al. Towards fog-driven IoT eHealth: Promises and challenges of IoT in medicine and healthcare. *Future Generation Computer Systems*. 2018;**78**(part 2):659-676. DOI: 10.1016/j.future.2017.04.036
- [34] Aging and Health, Fact sheet n°404 (World Health Organization) [Internet]. Available from: <http://www.who.int/mediacentre/factsheets/fs404/en/> [Accessed: February 13, 2018]
- [35] McWilliams A. Global markets and technologies for home medical equipment. bccResearch [Internet]. 2016. Available from: <https://www.bccresearch.com/market-research/healthcare/home-medical-equipment-technologies-market-report-hlc054d.html> [Accessed: July 27, 2018]
- [36] Eskofier B, Lee S, Baron M, et al. An overview of smart shoes in the internet of health things: Gait and mobility assessment in health promotion and disease monitoring. *Applied Sciences*. 2017;**7**:986(17pp). DOI: 10.3390/app7100986
- [37] Mignani A, Baldini F. Biomedical sensors using optical fibres. *Reports and Progress in Physics*. 1996;**59**:1-28. DOI: 10.1088/0034-4885/59/1/001
- [38] Grattan K, Sun T. Fibre optic sensor technology: An overview. *Sensors and Actuators: A*. 2000;**82**:40-61. DOI: 10.1016/S0924-4247(99)00368-4
- [39] Alberto N, Bilro L, Antunes P, et al. Optical fibre technology for eHealthcare. In: Cruz-Cunha M, Miranda I, Gonçalves P, editors. *Handbook of Research on ICTs and Management Systems for Improving Efficiency in Healthcare and Social Care*. Hershey, USA: IGI Global; 2013. pp. 180-200. DOI: 10.4018/978-1-5225-5484-4.ch069
- [40] Demarré L, Lancker A, Hecke A, et al. The cost of prevention and treatment of pressure ulcers: A systematic review. *International Journal of Nursing Studies*. 2015;**52**:1754-1774. DOI: 10.1016/j.ijnurstu.2015.06.006
- [41] Rahman S, Rahman T, Ismail A, et al. Diabetes-associated macrovasculopathy: Pathophysiology and pathogenesis. *Diabetes, Obesity and Metabolism*. 2007;**9**:767-780. DOI: 10.1111/j.1463-1326.2006.00655.x
- [42] Cobb J, Claremont D. Transducers for foot pressure measurement: Survey of recent developments. *Medical and Biological Engineering Computing*. 1995;**33**:525-532. DOI: 10.1007/BF02522509
- [43] Lord M, Hosein R. Study of in-shoe plantar shear in patients with diabetic neuropathy. *Clinical Biomechanics*. 2000;**15**:278-283. DOI: 10.1016/S0268-0033(99)00076-5
- [44] Najafi B, Mohseri H, Grewal G, et al. An optical-fibre-based smart textile (smart socks) to manage biomechanical risk factors associated with diabetic foot amputation. *Journal of Diabetes Science and Technology*. 2017;**11**:668-677. DOI: 10.1177/1932296817709022
- [45] Antunes P, Marques C, Varum H, et al. Biaxial optical accelerometer and high-angle inclinometer with temperature and cross-axis insensitivity. *IEEE Sensors Journal*. 2012;**12**:2399-2406. DOI: 10.1109/JSEN.2012.2190763
- [46] Leitão C, Antunes P, Pinto J, et al. Carotid distension waves acquired with a fiber sensor as an alternative to tonometry for central arterial systolic pressure assessment in young subjects. *Measurement*. 2017;**95**:45-49. DOI: 10.1016/j.measurement.2016.09.035
- [47] MacWilliams B, Armstrong P. Clinical applications of plantar pressure measurement in pediatric orthopedics.

In: *Pediatric Gait: A new Millennium in Clinical Care and Motion Analysis Technology*. 22 July 2000; Chicago, USA. New York: IEEE; 2002. pp. 143-150. DOI: 10.1109/PG.2000.858886

[48] Hao J, Tan K, Tjin S, et al. Design of a foot-pressure monitoring transducer for diabetic patients based on FBG sensors. In: *Proceedings the 16th Annual Meeting of the IEEE Lasers and Electro-Optics Society*; 27-28 October 2003; Tucson, USA. New York: IEEE; 2004. pp. 23-24. DOI: 10.1109/LEOS.2003.1251581

[49] Suresh R, Bhalla S, Tjin S, et al. Plantar stress monitoring using fibre Bragg grating sensors. In: *Proceedings of the 9th International Symposium on Advanced Science and Technology in Experimental Mechanics*; 1-6 November 2014; New Delhi, India

[50] Suresh R, Bhalla S, Hao J, et al. Development of a high resolution plantar pressure monitoring pad based on fibre Bragg grating (FBG) sensors. *Technology and health care: Official journal of the European Society for Engineering and Medicine*. 2015;**23**:785-794. DOI: 10.3233/THC-151038

[51] Liang T-C, Lin J-J, Guo L-Y. Plantar pressure detection with fibre Bragg gratings sensing system. *Sensors*. 2016;**16**:1766(13pp). DOI: 10.3390/s16101766

[52] Vilarinho D, Theodosiou A, Leitão C, et al. POFBG-embedded cork insole for plantar pressure monitoring. *Sensors*. 2017;**17**:2924(15pp). DOI: 10.3390/s17122924

[53] Zhang YF, Hong CY, Ahmed R, et al. A fibre Bragg grating based sensing platform fabricated by fused deposition modeling process for plantar pressure measurement. *Measurement*. 2017;**112**:74-79. DOI: 10.1016/j.measurement.2017.08.024

[54] Tjin S, Suresh R, Ngo N. Fibre Bragg grating based shear-force sensor: Modeling and testing. *Journal of Lightwave Technology*. 2017;**22**:1728-1733. DOI: 10.1109/JLT.2004.831171

[55] Suresh R, Bhalla S, Singh C, et al. Combined application of FBG and PZT sensors for plantar pressure monitoring at low and high speed walking. *Technology and Health Care*. 2014;**23**(1):47-61. DOI: 10.3233/THC-140867

[56] Koulaxouzidis A, Holmes M, Roberts C, et al. A shear and vertical stress sensor for physiological measurements using fibre Bragg gratings. In: *Proceedings of the 22nd Annual International Conference of the IEEE Engineering in Medicine and Biology Society (Cat. No.00CH37143)*; 23-28 July 2000; Chicago, USA. New York: IEEE; 2002. pp. 55-58. DOI: 10.1109/IEMBS.2000.900666

[57] Zhang Z, Tao X, Zhang H, et al. Soft fibre optic sensors for precision measurement of shear stress and pressure. *IEEE Sensors Journal*. 2013;**13**:1478-1482. DOI: 10.1109/JSEN.2012.2237393

[58] Chethana K, Prasad A, Omkar S, et al. Design and development of optical sensor based ground reaction force measurement platform for gait and geriatric studies. *World Academy of Science, Engineering and Technology, International Journal of Mechanical, Aerospace, Industrial, Mechatronic and Manufacturing Engineering*. 2015;**10**:60-64. DOI: 10.1999/1307-6892/10003366

[59] Tavares C, Domingues M, Frizera-Neto A, et al. Biaxial optical fibre sensor based in two multiplexed Bragg gratings for simultaneous shear stress and vertical pressure monitoring. In: *Proceedings of the SPIE Photonics Europe*; 22-26 April 2018; Strasburg,



France. Bellingham: SPIE; 2018. DOI: 10.1117/12.2306889

[60] Najafi B, Wrobel J, Grewal G, et al. Plantar temperature response to walking in diabetes with and without acute Charcot: The Charcot activity response test. *Journal of Aging Research*. 2012;140968(5pp). DOI: 10.1155/2012/140968

[61] Uustal H. Prosthetics and orthotics. In: Cooper G, editor. *Essential Physical Medicine and Rehabilitation*. United States: Humana Press; 2006. pp. 101-118. DOI: 10.1007/978-1-59745-100-0

[62] Mishra V, Singh N, Tiwari U, et al. Fibre grating sensors in medicine: Current and emerging applications. *Sensors and Actuators: A*. 2011;167:279-290. DOI: 10.1016/j.sna.2011.02.045

[63] Saggio G, Quitadamo L, Albero L. Development and evaluation of a novel low-cost sensor-based knee flexion angle measurement system. *The Knee*. 2014;21:896-901. DOI: 10.1016/j.knee.2014.04.014

[64] Roriz P, Carvalho L, Frazão O, et al. From conventional sensors to fibre optic sensors for strain and force measurements in biomechanics applications: A review. *Journal of Biomechanics*. 2014;47:1251-1261. DOI: 10.1016/j.jbiomech.2014.01.054

[65] Abro Z, Yi-Fan Z, Cheng-Yu H, et al. Development of a smart garment for monitoring body postures based on FBG and flex sensing technologies. *Sensors and Actuators A: Physical*. 2018;272:153-160. DOI: 10.1016/j.sna.2018.01.052

[66] Mohanty L, Tjin S, Lie D, et al. Fibre grating sensor for pressure mapping during total knee arthroplasty. *Sensors and Actuators: A*. 2007;135:323-328. DOI: 10.1016/j.sna.2006.07.021

[67] Rocha R, Silva A, Carmo J, et al. FBG in PVC foils for monitoring

the knee joint movement during the rehabilitation process. In: *Proceedings of the 33rd Annual International Conference of the IEEE Engineering in Medicine and Biology Society*; 30 August–3 September 2011; Boston, USA. New York: IEEE; 2011. pp. 458-461. DOI: 10.1109/IEMBS.2011.6090064

[68] Deluzio K, Wyss UP, Zee B, et al. Principal component models of knee kinematics and kinetics: Normal vs. pathological gait patterns. *Human Movement Science*. 1997;16:201-217. DOI: 10.1016/S0167-9457(96)00051-6

[69] Anderson D, Sidaway B. Coordination changes associated with practice of a soccer kick. *Research Quarterly for Exercise and Sport*. 1994;65:93-99. DOI: 10.1080/02701367.1994.10607603

[70] Rocha L, Correia J. Wearable sensor network for body kinematics monitoring. In: *Proceedings 2006 10th IEEE International Symposium*; 11-14 October 2006; Montreux, Switzerland. New York: IEEE 2007. pp. 137-138. DOI: 10.1109/ISWC.2006.286364

[71] Skelly M, Chizeck H. Real-time gait event detection for paraplegic FES walking. *IEEE Transactions on Neural Systems and Rehabilitation Engineering*. 2001;9:59-68. DOI: 10.1109/7333.918277

[72] Castro M, Abreu S, Sousa S, et al. In-shoe plantar pressures and ground reaction forces during overweight adults' overground walking. *Research Quarterly for Exercise and Sport*. 2014;85:188-197. DOI: 10.1080/02701367.2014.893055

[73] Umesh S, Padma S, Srinivas T, et al. Fibre Bragg grating goniometer for joint angle measurement. *IEEE Sensors Journal*. 2018;18:216-222. DOI: 10.1109/JSEN.2017.2770176

[74] Ren L, Song G, Conditt M, et al. Fibre Bragg grating displacement



sensor for movement measurement of tendons and ligaments. *Applied Optics*. 2007;**46**:6867-6871. DOI: 10.1364/AO.46.006867

[75] Al-Fakih E, Osman N, Eshraghi A, et al. The capability of fibre Bragg grating sensors to measure amputees' trans-tibial stump/socket interface pressures. *Sensors*. 2013;**13**:10348-10357. DOI: 10.3390/s130810348

[76] Dou P, Jia X, Suo S, et al. Pressure distribution at the stump/socket interface in transtibial amputees during walking on stairs, slope and non-flat road. *Clinical Biomechanics*. 2006;**21**:1067-1073. DOI: 10.1016/j.clinbiomech.2006.06.004

[77] Al-Fakih E, Osman N, Eshraghi A. Techniques for interface stress measurements within prosthetic sockets of transtibial amputees: A review of the past 50 years of research (Review). *Sensors*. 2016;**16**:1119(30pp). DOI: 10.3390/s16071119

[78] Osman N, Spence W, Solomonidis S, et al. The patellar tendon bar! Is it a necessary feature? *Medical Engineering and Physics*. 2010;**32**:760-765. DOI: 10.1016/j.medengphy.2010.04.020

[79] Buis A, Convery P. Calibration problems encountered while monitoring stump/socket interface pressures with force sensing resistors: Technique adopted to minimize inaccuracies. *Prosthetic and Orthotics International*. 1997;**21**:179-182. DOI: 10.3109/03093649709164552

[80] Dumbleton T, Buis A, McFadyen A, et al. Dynamic interface pressure distributions of two transtibial prosthetic socket concepts. *Journal of Rehabilitation Research and Development*. 2009;**46**:405-415. DOI: 10.1682/JRRD.2008.01.0015

[81] Portnoy S, Yarnitzky G, Yizhar Z, et al. Real-time patient-specific finite

element analysis of internal stresses in the soft tissues of a residual limb: A new tool for prosthetic fitting. *Annals of Biomedical Engineering*. 2007;**35**:120-135. DOI: 10.1007/s10439-006-9208-3

[82] Moo E, Osman N, Pingguan-Murphy B, et al. Interface pressure profile analysis for patellar tendon-bearing socket and hydrostatic socket. *Acta of Bioengineering and Biomechanics*. 2009;**11**:37-43. Available from: <http://www.ncbi.nlm.nih.gov/pubmed/20405814>

[83] Dickinson A, Steer J, Worsley P. Finite element analysis of the amputated lower limb: A systematic review and recommendations. *Medical Engineering and Physics*. 2017;**43**:1-18. DOI: 10.1016/j.medengphy.2017.02.008

[84] Tsiokos D, Kanellos G, Papaioannou G, et al. Fibre-optic-based pressure sensing surface for skin health management in prosthetic and rehabilitation interventions. In: Hudak R, editor. *Biomedical Engineering—Technical Applications in Medicine*. United Kingdom: IntechOpen; 2012. pp. 245-268. DOI: 10.5772/50574

[85] Kanellos G, Papaioannou G, Tsiokos D, et al. Two dimensional polymer-embedded quasi-distributed FBG pressure sensors for biomedical applications. *Optics Express*. 2010;**18**:179-186. DOI: 10.1364/OE.18.000179

[86] Kanellos G, Tsiokos D, Pleros N, et al. Enhanced durability FBG-based sensor pads for biomedical applications as human-machine interface surfaces. In: *Proceeding of the International Workshop on BioPhotonics*; 8-10 June 2011; Parma, Italy. New York: IEEE; 2011. 3pp. DOI: 10.1109/IWBP.2011.5954848

[87] Al-Fakih E, Osman N, Adikan F, et al. Development and validation of fibre Bragg grating sensing pad

for interface pressure measurements within prosthetic sockets. *IEEE Sensors Journal*. 2016;**16**:965-974. DOI: 10.1109/JSEN.2015.2495323

[88] Al-Fakih E, Arifin N, Pirouzi G, et al. Optical fibre Bragg grating-instrumented silicone liner for interface pressure measurement within prosthetic sockets of lower-limb amputees. *Journal of Biomedical Optics*. 2017;**22**:087001(8pp). DOI: 10.1117/1.JBO.22.8.087001

[89] Paternò L, Ibrahimi M, Gruppioni E, et al. Sockets for limb prostheses: A review of existing technologies and open challenges. *IEEE Transactions on Biomedical Engineering*. 2018;**65**:1996-2010. DOI: 10.1109/TBME.2017.2775100

[90] Norhafizan A, Ghazilla R, Kasi V, et al. A review on lower-limb exoskeleton system for sit to stand, ascending and descending staircase motion. *Applied Mechanics and Materials*. 2014;**541**:1150-1155. DOI: 10.4028/www.scientific.net/AMM.541-542.1150

[91] Rocon E, Pons J, editors. *Exoskeletons in Rehabilitation Robotics-Tremor Suppression*. Berlin: Springer Tracts in Advanced Robotics; 2011. DOI: 10.1007/978-3-642-17659-3

[92] Chen G, Chang C, Guo Z, et al. A review of lower extremity assistive robotic exoskeletons in rehabilitation therapy. *Critical Review in Biomedical Engineering*. 2013;**41**:343-363. DOI: 10.1615/CritRevBiomedEng.2014010453

[93] Blank A, French J, Pehlivan A, et al. Current trends in robot-assisted upper-limb stroke rehabilitation: Promoting patient engagement in therapy. *Current Physical Medicine and Rehabilitation Reports*. 2014;**2**:184-195. DOI: 10.1007/s40141-014-0056-z

[94] Ayoade M, Morton L, Baillie L. Investigating the feasibility of a wireless

motion capture system to aid in the rehabilitation of total knee replacement patients. In: *Proceedings of the IEEE 5th International Conference on Pervasive Computing Technologies for Healthcare (PervasiveHealth) and Workshops*; 23-26 May 2011; Dublin. New York: IEEE; 2011. pp. 404-407. DOI: 10.4108/icst.pervasivehealth.2011.246132

[95] Park YL, Ryu S, Black R, et al. Exoskeletal force-sensing end-effectors with embedded optical fibre-Bragg-grating sensors. *IEEE Transactions on Robotics*. 2009;**25**:1319-1331. DOI: 10.1109/TRO.2009.2032965

[96] Jiang L, Low K, Cost J, et al. Fibre optically sensorized multi-fingered robotic hand. In: *Proceedings of the International Conference on Intelligent Robots and Systems*; 28 September-2 October 2015; Hamburg, Germany. New York: IEEE; 2015. pp. 1763-1768. DOI: 10.1109/IROS.2015.7353606

[97] Fujiwara E, Miyatake D, Santos M, et al. Development of a glove-based optical fibre sensor for applications in human-robot interaction. In: *Proceedings of the 8th ACM/IEEE International Conference on Human-robot Interaction (HRI)*; 3-6 March 2013; Tokyo, Japan. New York: IEEE; 2013. pp. 123-124. DOI: 10.1109/HRI.2013.6483532

[98] Aram K, Al-Jumaily A. Active exoskeleton control systems. *State of the art. Proceeding Engineering*. 2012;**41**:988-994. DOI: 10.1016/j.proeng.2012.07.273

# We are IntechOpen, the world's leading publisher of Open Access books Built by scientists, for scientists

6,300

Open access books available

171,000

International authors and editors

190M

Downloads

Our authors are among the

154

Countries delivered to

TOP 1%

most cited scientists

12.2%

Contributors from top 500 universities



WEB OF SCIENCE™

Selection of our books indexed in the Book Citation Index  
in Web of Science™ Core Collection (BKCI)

Interested in publishing with us?  
Contact [book.department@intechopen.com](mailto:book.department@intechopen.com)

Numbers displayed above are based on latest data collected.  
For more information visit [www.intechopen.com](http://www.intechopen.com)



# Distributed, Advanced Fiber Optic Sensors

*Sanjay Kher and Manoj Kumar Saxena*

## Abstract

India is poised to use nuclear energy in a big way. The safety of these systems depends upon monitoring various parameters in hazardous environment like high radiation, high temperature exceeding 1000°C, and gas/coolant leakages. In this chapter, we shall dwell on basics of distributed sensing, related instrumentation, device fabrication, and actual advanced field applications. Techniques like Raman scattering, resonance response of fiber gratings, and selective absorption are employed for design, development, and fabrication of distributed sensors and devices. Raman distributed sensors with advanced data processing techniques are finding increasing applications for fire detection, coolant leak detection, and safety of large structures. The systematic investigations related to portable systems developed at the author's lab have been described. Wavelength-encoded fiber gratings are the attractive candidate for high gamma radiation dose measurements in environment such as particle accelerators, fission reactors, food processing facilities, and ITER-like installations. The basics of fiber gratings, their operational designs, and devices based on fiber gratings have been described with advanced applications like high temperature sensing, strain measurements at cryogenic temperatures, and strain in nuclear environment. Finally, novel approaches are described for distributed hazardous gas monitoring for large areas such as airports, train stations, and reactor containment buildings.

**Keywords:** Raman optical fiber distributed temperature sensor, fiber Bragg grating sensor, long period grating sensor, dynamic self-calibration, strain sensors for nuclear environment

## 1. Introduction

The discovery of lasers in the 1960s and development of low loss silica optical fiber opened a new era of fiber optic sensors. Intrinsic insensitivity to electromagnetic interference (EMI), remote detection, operational ability in hazardous environment, and potential for distributed sensing make them especially useful for monitoring large nuclear infrastructures such as coolant monitoring, reactor containment buildings, nuclear waste storage sites etc. [1–5]. Radiation tolerant fibers can be used in various configurations for distributed sensing of temperature, strain, and several other parameters avoiding the requirement of positioning many discreet sensors [6–11]. Further, the radiation sensitive fibers can be used for radiation dose monitoring for local dose deposition measurements, hot spot dose monitoring in waste storage facilities, surveillance at airports and ports of entry, etc. With the



availability of lasers, fibers, and low noise detectors in the mid-IR region, it has become possible to design novel distributed sensor devices for sensing hazardous volatile compounds for homeland security especially at airports, underground metro stations, and big event areas.

A wide range of techniques such as intensity modulation, wavelength encoding, and polarization provide powerful sensing capabilities. Further, several detection techniques have been investigated for development of optical fiber-based distributed sensors. Radiation-induced absorption, scintillation, fluorescence, optically stimulated luminescence, and induced refractive index changes have been used for real-time dose measurements. Optical fiber grating [12–15]-based specialty sensors have been used for distributed strain measurements in very low temperature, very high temperature, or high radiation environment. Raman and Brillouin scattering-based techniques are used for distributed temperature measurements for fire and hot spot detection. Mid-IR and near-IR absorption measurements coupled with hollow core fibers are used for leak detection of hazardous gases. This chapter will describe the basic principles, main components, various sensing systems for advanced applications, and future potential of distributed fiber sensors.

2. What is distributed sensing?

Distributed sensing is a technique whereby one sensor cable is capable to collect data (continuous/quasi-continuous profiling) that are spatially distributed over many individual measurement points. The various modes of sensing can be understood from **Figure 1** [3, 4]. Briefly, a point sensor means monitoring a parameter at a discreet point; a quasi-distributed sensor system involves an arrangement of a finite number of discreet sensors as a linear array, while in fully distributed sensing mode, the measuring parameter of interest is monitored continuously along the fiber path, providing a spatial mapping of the parameter along fiber.

In conventional sensing, say for temperature, an individual sensor such as a thermocouple or platinum probe is needed for each point of interest whereas distributed sensing addresses many points simultaneously along with their spatial location [5]. With proper design architecture, it can contribute to enhanced safety and security by providing early warnings of gas and coolant leakages, structural cracks, onset of fire, hot spot detection in pipelines, radiation leaks, etc. Two techniques such as optical time-domain reflectometry (OTDR) [4, 16–23] and

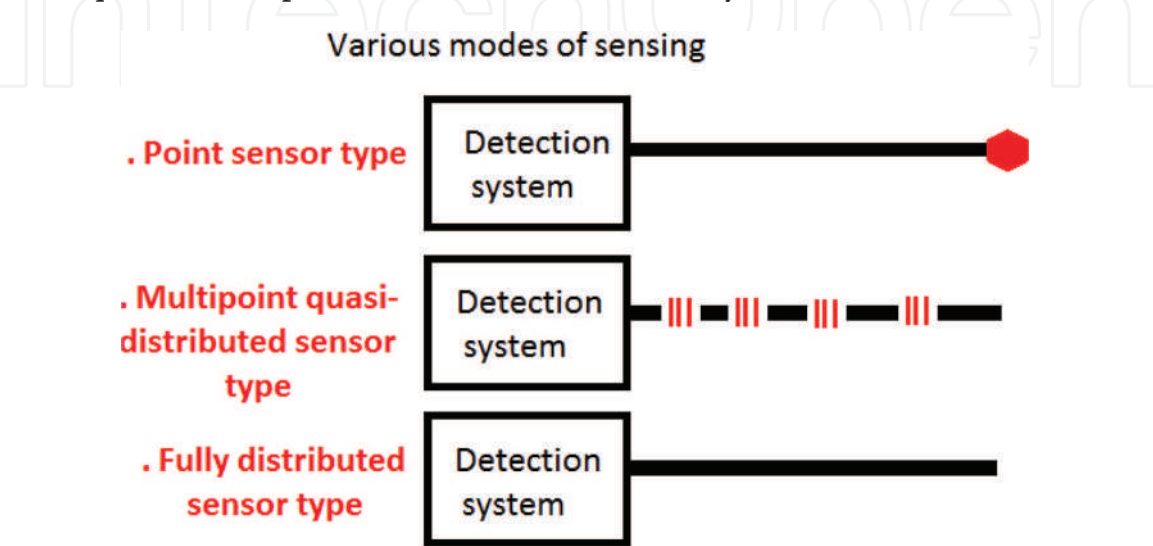


**Figure 1.**  
*Various modes of sensing: point, multipoint quasi-distributed, and fully distributed.*

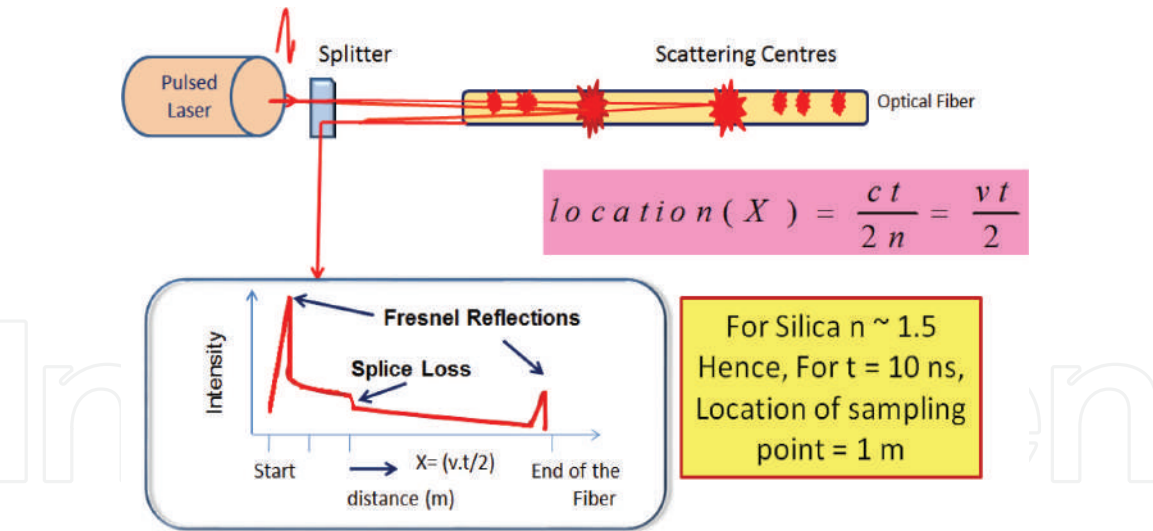


**Figure 2.**  
*Schematic diagram of OTDR.*

wavelength division multiplexing (WDM) are generally used for distributed sensing. In OTDR (**Figure 2**), a pulsed laser is coupled to an optical fiber through a directional coupler/splitter. The backscattered light originating from density and composition variation is monitored continuously in time. The spatial location of an event is determined from time of flight measurements, that is, the device calculates the distance of the measuring point based on the time it takes for the reflected light to return.

For example, if the backscattered light is detected after 10 ns from the starting point, it is set to originate from 1 m distance from origin of fiber. This can be easily calculated from OTDR equation  $X = ct/2n$ , where  $X$  is the distance from origin (start of fiber taken as zero time),  $t$  is the time of event detection,  $c$  ( $3 \times 10^8$  m/s) is the velocity of light in the vacuum, and  $n$  is the refractive index of fiber for wavelength of operation. If we use a sensing fiber with core refractive index ( $n$ ) of 1.5 and wish to measure distance ( $X$ ) traveled after  $t = 10$  ns, then it is easy to calculate that  $X = 1.0$  m by putting the values in OTDR equation [21, 23].

In wavelength multiplexing, a device such as Bragg grating is used to encode a series of resonant wavelengths in the fibers [12–15]. The wavelengths in turn are monitored by wavelength interrogator. The resonant wavelengths are affected by measuring parameters and are thus monitored in a quasi-distributed manner.

### 3. All fiber Raman optical fiber distributed temperature sensor with dynamic self-calibration

Temperature sensors are ubiquitous devices that permeate our daily lives. Many areas of temperature measurements require a large area of coverage with high localization accuracy. Raman optical fiber-based distributed temperature sensors (ROFDTSs) are equipped with the ability of providing temperature values as a continuous function of distance along the fiber. In an ROFDTS, every bit of fiber works as a sensing element as well as data transmitting medium, to substitute the role played by several point sensors, thus allowing reduced sensor network cost. ROFDTSs have attracted the attention as a means of temperature monitoring and fire detection in power cables, long pipelines, bore holes, tunnels, and critical installations like oil wells, refineries, induction furnaces, and process control industries. The basic principle of temperature measurement using ROFDTS involves

Raman scattering [10] in conjunction with OTDR. The ratio of Raman anti-Stokes (AS) and Stokes (St) intensities is used for determination of unknown temperature. The AS signal is strongly dependent on temperature, while the Stokes signal is slightly dependent on temperature. Based on time of flight and intensity of Stokes and anti-Stokes signals, location and temperature information can be retrieved. The backscattered light has many spectral components as shown in **Figure 3** [24]. For temperature measurements, Raman components are analyzed.

The OTDR principle allows estimation of the location of hot zone whereas Raman scattering permits measurement of temperature of the hot zone. Sensing fiber is coupled to short interrogating laser pulses, and backscattered AS and St components are monitored for signal changes. Unknown temperature of hot zones can be estimated from the ratio ( $R$ ) of AS and St using the following expression [11]

$$R = \frac{I_{as}}{I_s} = \left( \frac{\lambda_s}{\lambda_{as}} \right)^4 \exp \left( -\frac{hc\nabla}{kT} \right) \quad (1)$$

where  $\lambda_s$  and  $\lambda_{as}$  are the Stokes and anti-Stokes optical signal wavelengths,  $\nabla$  is their wave number separation from the pump laser wavelength,  $h$  is Planck's constant,  $c$  is the velocity of light, and  $k$  is Boltzmann's constant. AS is the main signal which carries the signature of temperature variation whereas St provides reference and eliminates a number of effects common to both the signals. One can simplify Eq. (1) by replacing known terms by  $B$  where,

$$B = \frac{hc\nabla}{k} \quad (2)$$

Since values of  $h$ ,  $c$ , and  $k$  are known, the numerical value of  $B$  is found to be 631.3 for silica fiber having  $\nabla = 440 \text{ cm}^{-1}$ .

One can simplify the profile analysis by referencing the ratio profile at unknown temperature to the ratio value at known temperature of a pre-selected calibration zone of fiber. The temperature of a given zone  $T$  ( $^{\circ}\text{C}$ ) is then given by the following expression [25].

$$T(^{\circ}\text{C}) = B \cdot \left[ \frac{1}{\left( B \cdot \frac{1}{\theta} - \ln R_T + \ln R_{\theta} \right)} \right] - 273 \quad (3)$$

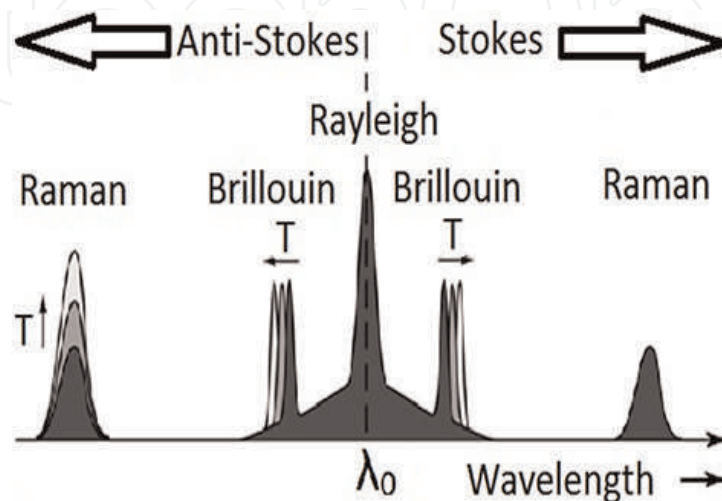


**Figure 3.**

Backscattered laser light from optical fiber in the case of Raman and Brillouin scattering (source: [https://www.google.co.in/search?q=BACKSCATTERED+LASER+LIGHT&source=lnms&tbm=isch&sa=X&ved=0ahUKEwiCvf-iq9jcAhWKT3oKHdJ4CjYQ\\_AUICigB&biw=1093&bih=530](https://www.google.co.in/search?q=BACKSCATTERED+LASER+LIGHT&source=lnms&tbm=isch&sa=X&ved=0ahUKEwiCvf-iq9jcAhWKT3oKHdJ4CjYQ_AUICigB&biw=1093&bih=530)) (images) [24].

Here, the calibration zone is kept at some known absolute room temperature ( $\theta$ ). Eq. (3) can be deduced after taking the quotient of the ratio profile at unknown temperature ( $R_T$ ) for an arbitrary zone and the ratio value at the calibration zone ( $R_\theta$ ) and solving it for  $T$ . Parameter ( $R_\theta$ ) is the ratio value of AS to St signal (AS/St) for the calibration zone (at temperature  $\theta$ ) of length 1 m chosen from sensing fiber at the laser end. In Eq. (3), parameters  $B$  and  $\theta$  are known. Therefore, Eq. (3) will yield temperature profile ( $T$  in  $^{\circ}\text{C}$ ) for complete fiber length, provided that profiles of  $R_T$  and value of  $R_\theta$  are available.

**Figure 4** shows the block diagram of Raman optical fiber distributed temperature sensor.

Further, **Figure 5** gives an idea of averaged anti-Stokes Raman signal for a 2.5 m long zone heated by a proportional integral derivative (PID) controlled heating oven.

To determine the unknown temperature profile with certain accuracy for complete fiber length by using Eq. (1), appropriate measures are to be devised and implemented to address several error-causing issues. These issues are described as below [21, 23]. The author's laboratory has successfully solved these issues and designed a field portable unit.

3.1 Issue no. 1

The first issue is the difference in theoretical and experimental values of the ratio ( $R$ ) at various temperature values. For example, at room temperature ( $25^{\circ}\text{C}$ , say), the theoretical and experimental values of  $R$  are 0.1693 and 0.55, respectively. At  $50^{\circ}\text{C}$ , the theoretical and experimental values of  $R$  are found to be 0.1995 and 0.658, respectively. On the other hand, the theoretical and experimental values are 0.2415 and 0.8279, respectively, at  $85^{\circ}\text{C}$ . The reason for this difference is explained below [23].

At  $25^{\circ}\text{C}$  (for example), obtaining a theoretical value of 0.1693 for  $R$  requires that the optoelectronic conversion using photomultiplier tube (e.g. PMT-R5108, Hamamatsu) detectors, the beam splitting, and the subsequent light coupling into AS and St detectors are in such a way that the relation  $\text{St} = 5.906 \times \text{AS}$  is maintained for backscattered AS and St signals while traveling the path from fiber to the final stage of detection. However, due to nonideal behavior of various optical components in

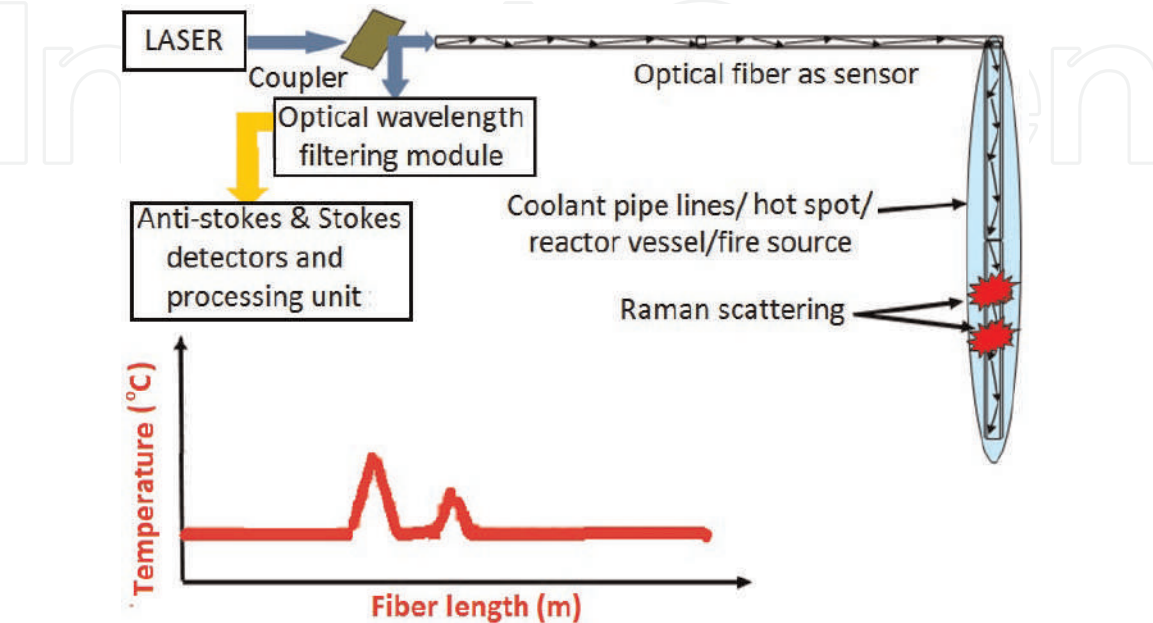


**Figure 4.**  
*Block diagram of Raman optical fiber distributed temperature sensor.*



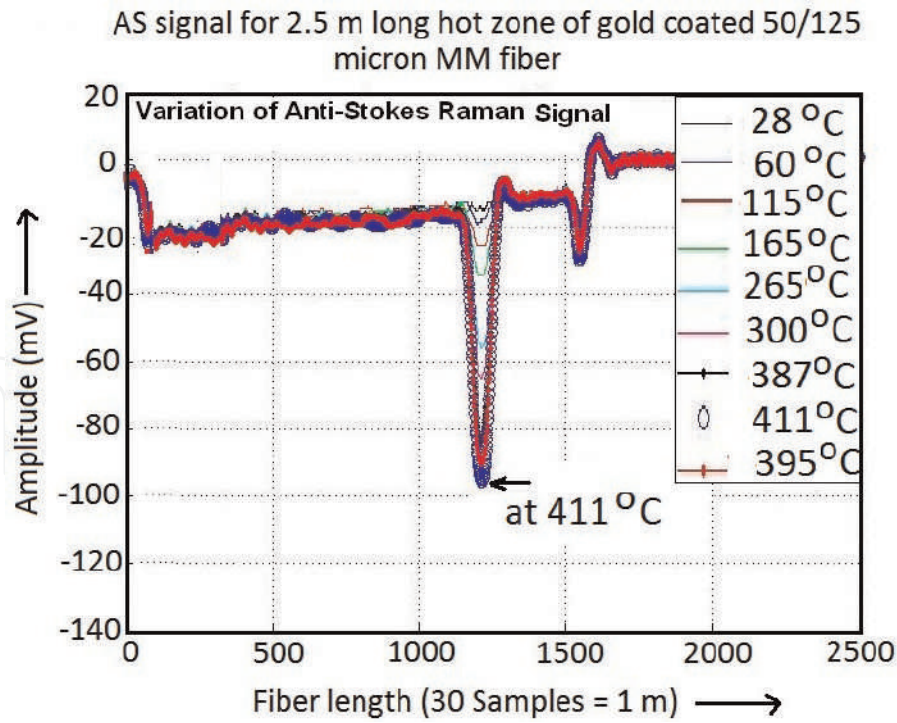


**Figure 5.**  
The anti-Stokes Raman signal profile at various temperatures.

the path and band nature of AS and St signals, the above relation does not hold. The relation gets deteriorated at every stage in the path. For example, the cathode radiant sensitivity of a PMT for AS wavelength (1018 nm) and St wavelength (1109 nm) is 0.95 mA/W and 0.2mA/W, respectively, which causes St current to be approximately 5 times less compared to AS current. Nonideal performance of beam splitters and optical filters also does not support the above ideal relation. As a result, the cumulative effect of various components makes experimental values of  $R$  to be different from the theoretical one.

Direct use of experimental values of  $R$  in Eq. (1) will yield highly erroneous and unacceptable temperature profile ( $T$ ). Hence, Eq. (1) needs to be modified to obtain correct values. Modification is done by referencing the experimentally obtained ratio values with respect to the ratio value at some known temperature of calibration zone which is chosen from sensing fiber itself.

### 3.2 Issue no. 2

The second issue is the nonidentical fiber attenuation along the fiber length for Raman AS and St signals due to difference in their wavelengths [9, 11]. In a typical system using 1064 nm excitation laser, the difference between two wavelengths is  $\sim 90$  nm. The lower optical wavelength signal (AS) experiences higher attenuation in comparison to higher optical wavelength signal (St) while traveling in sensing optical fiber. This attenuation difference results in an unwanted downward slope in ratio ( $R$ ) profile and finally in unknown temperature ( $T$ ) profile with respect to fiber length. It may be noted that downward slope in ratio ( $R$ ) profile causes additional errors in unknown temperature ( $T$ ) profile of fiber and should be corrected.

### 3.3 Issue no. 3

While de-noising Raman AS and St signals for better signal-to-noise ratio (SNR), conventional finite impulse response/infinite impulse response (FIR/IIR)-based

Fourier filtering causes spatial inaccuracy in locating the hot-zones which in turn yields erroneous information about the location of hot zones [18].

### 3.4 Issue no. 4

The amplitude of AS and St signals varies with time due to slow variations/drifts in laser power and laser-fiber coupling. Also, the temperature of calibration zone itself may change unless it is controlled by a dedicated setup. Therefore, any previously stored reference values of AS and St signals and calibration zone temperature can no longer be used as a reference for temperature measurement at a later stage.

### 3.5 Approaches to solve the problematic issues

Stoddart et al. [20] proposed to use Rayleigh instead of St from the backscattered spectrum to avoid the temperature measurement error in hydrogen-rich environments due to differential attenuation caused by the optical fiber for AS and St signal wavelengths. This resulted in better results but could not eliminate the error caused by the differential attenuation completely. The dual-ended (DE) configuration [26] (i.e. both ends of sensing fiber are connected to ROFDTS unit) and dual laser source schemes [27, 28] have also been proposed to take care of the difference in attenuation between AS and St. These schemes have resulted in improvements but add complexity and need double length of fiber, extra distributed temperature sensor (DTS) with an optical switch, and two costly lasers. A correction method to take care of the difference in attenuation for AS and St signals has been proposed with only one light source and one light detector but requires attachment of a carefully designed reflective mirror at the far fiber-end of the sensing fiber [29]. Recently, a more sophisticated correction technique [30] based on detection of AS signal alone in combination with DE configuration has been investigated. ROFDTSs based on the above schemes are important and to a certain extent become mandatory in situations where sensing fiber is exposed to the severe radiation environment or hydrogen darkening in oil wells. Requirements for less demanding situations like temperature measurement in steam pipelines of turbines, electrical cables and temperature profiling of big buildings, gas pipelines and mines etc. can be met by the technique based on digital signal processing.

In order to address the above issues satisfactorily, a discrete wavelet transform (DWT)-based dynamic self-calibration and de-noising technique is used and implemented by the authors as given in detail [23]. Briefly, wavelets are mathematical functions that can be used to segregate data into various frequency components. Each component can then be studied with a resolution matched to its scale. In DWT, a signal may be represented by its low frequency component and its high frequency component.

The DWT-based technique is simpler, more automatic, and provides a single solution to address all the above issues simultaneously. The DWT technique takes care of the difference in optical attenuation for AS and St signals by using their trend and also de-noises the AS and St signals while preserving spatial locations of peaks. Also, this technique requires just 1 m long calibration zone which is much less than the 100 m required in the previous technique. Moreover, the dynamic measurement of calibration zone's temperature eliminates the requirement of keeping the calibration zone at a constant temperature, and thus, complicated heating arrangement is avoided. Actual wavelet transform-based processed signal profile is shown in **Figure 6**. **Table 1** presents the comparison of error in temperature measurement at various zones using Eq. (3) with unprocessed and processed Raman signals. Both absolute errors and percentage errors (in brackets) are

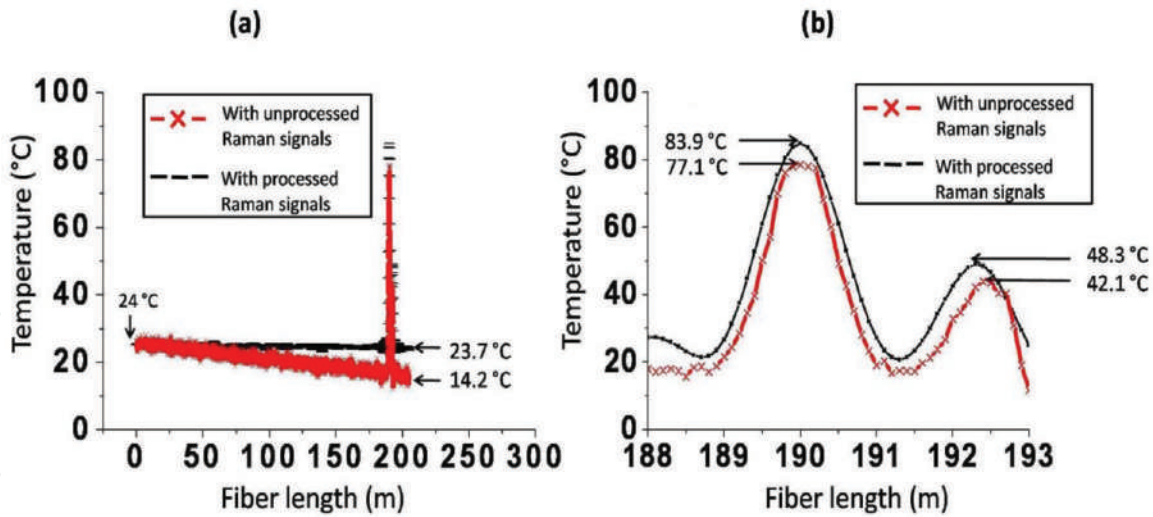


**Figure 6.** Distributed temperature profile with processed (black color) and unprocessed (red color) Raman signals: (a) view for complete fiber length and (b) zoomed view for hot zones.

Zone (location)	Reference temperature	Measured temperature	
		Unprocessed	Processed
Start of fiber (location: 0 m)	24.5°C	24°C	24°C
	Error	−0.5°C (−2.04%)	−0.5°C (−2.04%)
Hot zone-1 (location: 190 m)	85°C	77.1°C	83.9 °C
	Error	−7.9 °C (−9.29%)	−1.1 °C (−1.29%)
Hot zone-2 (location: 192.4 m)	50°C	42.1°C	48.3°C
	Error	−7.9°C (−15.8%)	−2.4°C (−3.4%)
End of fiber (location: 205 m)	25°C	14.2 °C	23.7°C
	Error	−10.8°C (−43.2%)	−1.3°C (−5.2%)

**Table 1.** Comparison of error in temperature measurement at various zones with unprocessed and processed Raman signals.

reported to appreciate the improvement achieved after processing of Raman signals.

Fiber Sensors Lab., Raja Ramanna Centre for Advanced Technology (RRCAT), Indore, India has developed a Raman scattering-based OFDTS [23] with the following specifications, and the developed OFDTS is capable of working in high accelerating voltage (1.5 MV), magnetic field (1.5 T), and bremsstrahlung radiation present in accelerator systems.

(a) Temperature range: 25–300°C, (b) temperature resolution: 3°C, (c) spatial resolution: 1 m (over a length of 500 m); can be improved to few cm with special fiber-laying techniques, (d) distance (dynamic range for distance covered): 500 m, (e) fire alarm: audio-visual alarms can be generated, and (f) gamma field operation; can operate up to a gamma dose of 1 MGy.

For more ruggedness and field deployability, an all-fiber ROFDTS scheme is desirable. The schematic design of one such scheme is depicted in **Figure 7**.

Recently, a distributed sensor using a superconducting nanowire single photon detector and chalcogenide fiber has been proposed. This scheme has the potential to

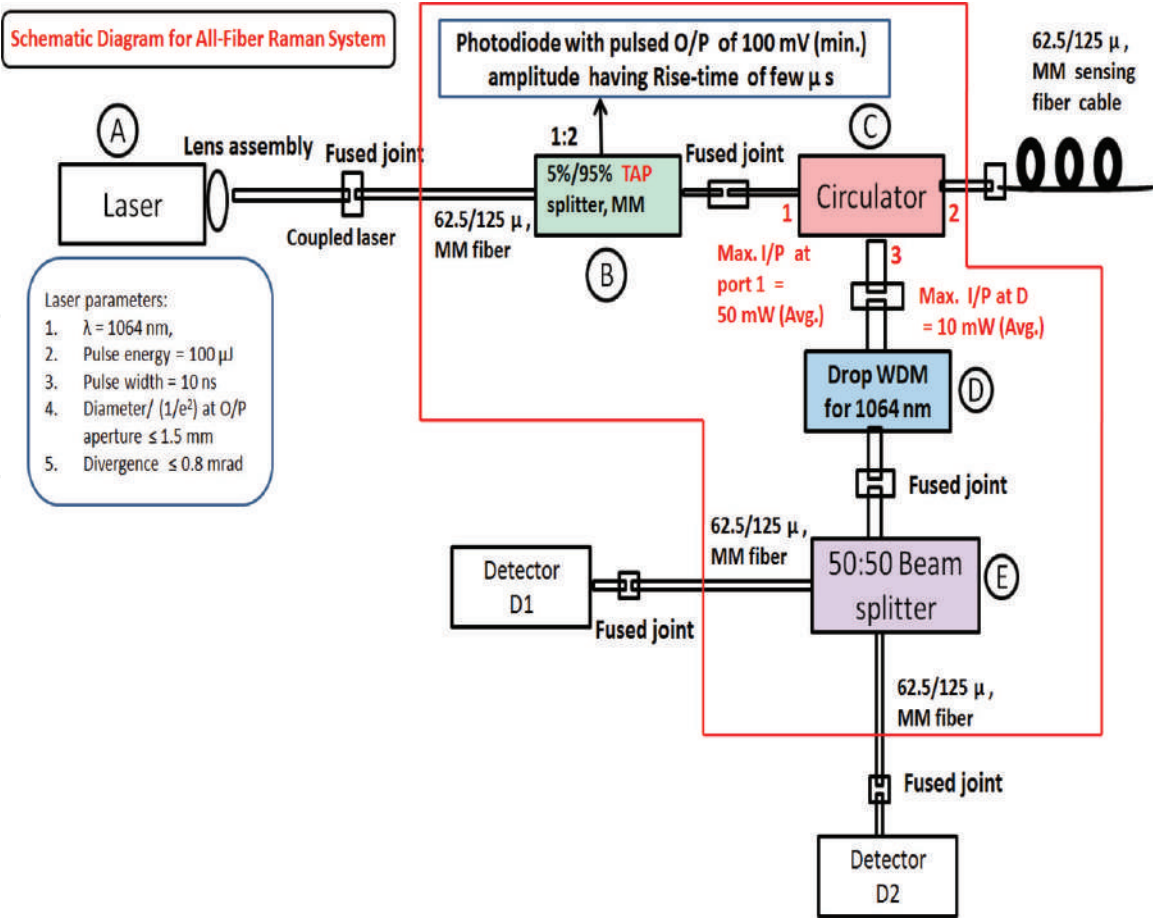


**Figure 7.**  
*Schematic diagram of an all-fiber-based ROFDTS scheme.*

offer sub-centimeter spatial resolution sensor, below  $1^\circ\text{C}$  temperature resolution over a distance of few hundreds of meters.

#### 4. Quasi-distributed sensors for temperature and strain measurements

The fiber Bragg gratings (FBG) were first written by Hill et al. [12] who discovered the breakthrough phenomena of photosensitivity in optical fiber. As a result of this development, FBG-based strain and temperature sensors came into existence. The method of writing FBG in sensing fiber's section involves creation of periodic modulation of fiber core's refractive index. The refractive index is modulated by spatial pattern of ultraviolet (UV) light between 240 and 260 nm. The periodic structure in fiber's core can be created by phase mask method [13, 15]. A particular pattern in a particular segment of fiber will correspond to a specific Bragg reflection wavelength. The multiple gratings can be fabricated by using a specific phase mask with different initial Bragg wavelength gratings in the same fiber causing creation of several point sensors in a single sensing fiber. Such FBG-based sensors are quasi-distributed temperature sensors where temperature sensing by fiber is possible only where grating was created.

According to Bragg's law, when a broad band light is injected into the optical fiber consisting of FBG sensors, a specific wavelength of light is reflected by FBG [15]. The Bragg wavelength is determined by the product of effective refractive



index ( $n_{eff}$ ) of the grating and the grating period ( $\Lambda$ ) (also called pitch length) as given by the following equation:

$$\lambda_B = 2n_{eff}\Lambda \quad (4)$$

**Figure 8** depicts the basic principle of FBG reflection spectra and interrogation technique [12–15]. The Bragg wavelength depends on grating period of FBG and the refractive property of optical fiber.

It is clear from Eq. (4) that any change in the pitch length or refractive index will induce a shift in the resonant wavelength. Consequently, temperature, strain or deformations of the fiber can be monitored by the corresponding resonant wavelength shift. The Bragg wavelength is strain- and temperature-dependent through physical elongation or thermal change of the sensor and through the change in the fiber refractive index due to photoelastic and thermo-optic effects.

There are essentially three types of gratings which vary in photosensitivity. They are known as type I, II, and IIA with the details of each type given in [15]. Type I gratings are written with moderate intensities and exhibit an index grating right across the core. Type II gratings can be written with much higher intensities within very short times, often with a single nanosecond pulse from an excimer laser (single shot damage gratings). Type IIA gratings are regenerated gratings (RGs) specifically designed for high temperature operation. In addition, there are different physical types of gratings such as long period gratings (LPGs), chirped gratings, tilted (blazed) gratings, and micro-structured FBGs. Typical temperature sensitivity of FBG is 10 pm/°C (at 1550 nm in standard silica-based single mode fiber) and strain sensitivity is 1.2 pm/micro-strain [13].

A strong point of FBGs is their capability of multiplexing in wavelength that enable multiple points or quasi-distributed sensing. The schematic diagram of the distributed FBG sensor is shown in **Figure 9**.

There have been significant developments in two of the areas that have constrained the progress of fiber grating technology. Firstly, the issue of temperature and strain isolation has been overcome by using various techniques reported in the literature, from simply having collocated sensors that are exposed to the same temperature fluctuations to isolate stress and strain, to more complex methods, such as using tilted or chirped gratings to distinguish between the different measurands. Secondly, with improved data processing methods, simpler interrogation techniques are being utilized such that the optical signal can easily be transposed into the electrical domain, allowing the optical networks to be interfaced seamlessly with electronic systems. In addition, the production of FBGs has improved significantly through draw tower processes and automated manufacturing. One of the main advantages of FBG sensors is their ability to be easily

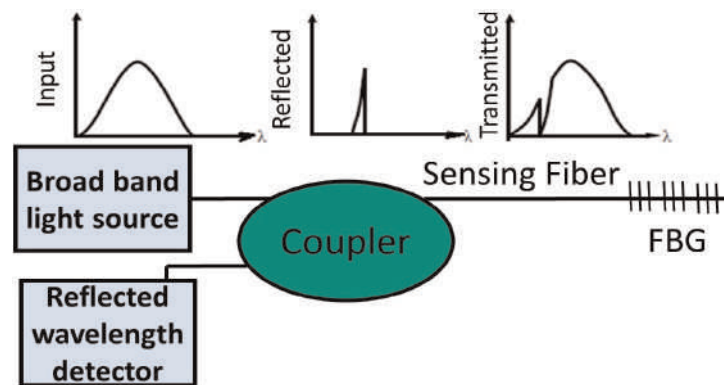


**Figure 8.**  
Schematic representation of FBG sensor.

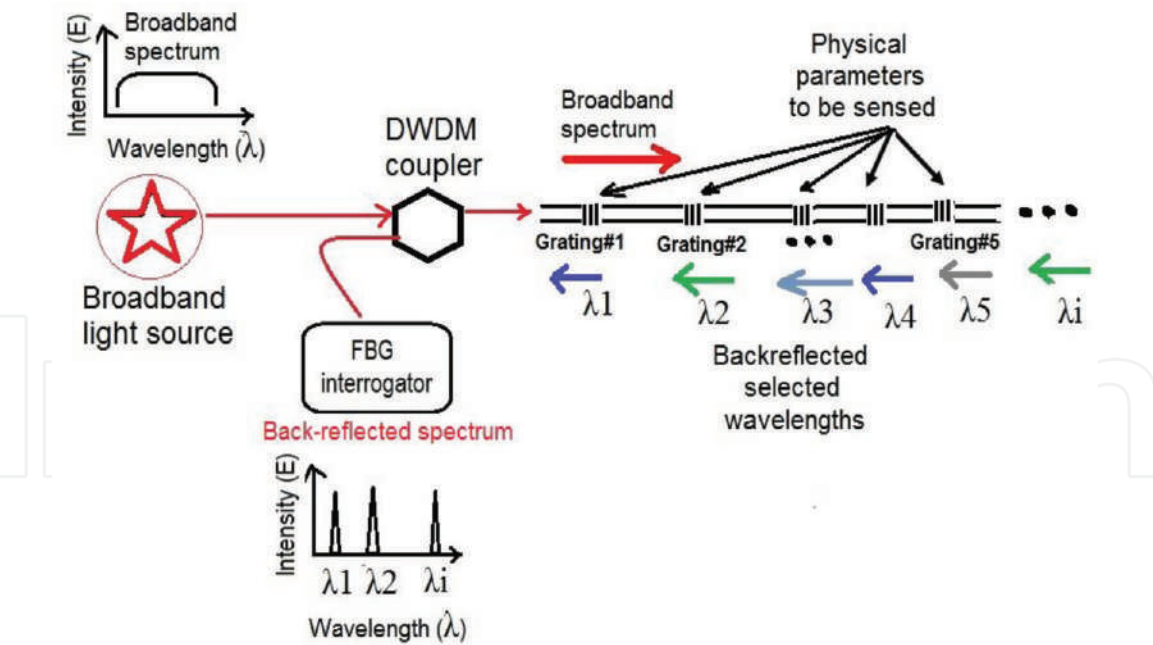


**Figure 9.**  
*Schematic diagram of the distributed FBG sensor.*

multiplexed through time division multiplexing (TDM) and wavelength division multiplexing (WDM). The information from each sensor must be separated and interpreted, which requires an interrogator system to interrogate many FBGs connected in series.

A series of wavelength-encoded FBGs are used for quasi-distributed sensing applications. Several groups developed quasi-distributed FBG sensors for temperature and strain monitoring [31–33]. Central Glass & Ceramic Research Institute (CGCRI), Kolkata, India recently developed specially packaged FBGs for strain/force monitoring of electric railway engine pantographs. However, very special packaging or specialty fibers were required for advanced applications such as strain monitoring at high temperature, strain monitoring at cryogenic temperature, and very high temperature monitoring exceeding 1000°C. FBG strain sensor for health monitoring of structure at 600°C have also been developed.

### 5. Ultra-high temperature distributed sensors

The dynamic range of ROFDTS is restricted by coating on the optical fiber. Polyimide coatings can permit measurement up to 350°C while the gold coating may allow the measurement up to 600°C. Beyond this, distributed sensing is possible by specialized gratings made in specialized fibers. For ultra-high temperature sensing, type II-IR gratings in silica optical fiber withstand a temperature of up to 1000°C, which are usually fabricated by using a femto-second laser with power density near the damage threshold of the fiber glass. These gratings however have disadvantages as sensing elements because of asymmetric reflection spectrum and a large spectral width of more than 0.6 nm. These create problems during distributed sensing. Gratings written on a different host material, namely sapphire gratings, can be used as a temperature-sensing probe up to 1900°C. However, the material and mode mismatch with normal silica-based optical fiber and high cost of fabrication restricts its use in distributed sensing. Identification of structural changes on a molecular scale involved with the formation of a new type of FBG named

regenerated Bragg grating based on annealing a conventional Type-I FBG to create a new, more robust one seems to be a promising candidate to achieve better sustainability at high temperature. However, in standard photosensitive silica fiber, RG gratings were found to be stable only below 950°C.

CGCRI, Kolkata, India in collaboration with RRCAT, Indore, India has taken up the development of a new glass composition-based photosensitive fiber to fabricate RG for temperature  $\sim 1400^\circ\text{C}$ . The fiber is likely to be based on yttrium-stabilized zirconia-calcium-alumina-phospho silica glass. The motivation of the choice of such kind of multi-material glass-based optical fiber is to increase the photosensitivity along with thermal stability of fabricated RG. The regeneration takes place near the fiber glass transition temperature, in which the transformation of the glass from monoclinic structure to tetragonal structure occurs. The ultra-high temperature sustainability of RG will be evaluated for the special composition through material study, which definitely is not achievable in a standard germano-silicate fiber. This work is expected to provide a new degree of freedom in the design of optical fiber sensor for ultra-high temperature sensing. This will open up opportunities in sectors such as power plants, turbines, combustion, and aerospace engineering where often the environments are too harsh for existing FBG sensor technology and will offer a new degree of freedom in the design of optical fiber sensors.

## **6. Strain sensors for nuclear environment**

### **6.1 Wavelength encoded strain sensors**

A long period fiber grating sensor in photonic crystal fiber with a strain sensitivity of  $-2.0 \text{ pm}/\mu\epsilon$  and negligible temperature sensitivity is fabricated by use of  $\text{CO}_2$  laser beam. Such a strain sensor can effectively reduce the cross sensitivity between strain and temperature. Due to single material (pure silica) construction, they have been shown to be resistant to nuclear radiation and are thus useful for applications in secondary loops of nuclear reactors. The authors' lab has designed and developed such sensor devices.

### **6.2 Design principle**

Photonic crystal fibers (PCFs) also known as holey fibers are a new class of optical fibers that have attracted intense scientific research during past few years. Typically, these fibers incorporate a number of air holes that run along the length of the fiber, and the size, shape, and distribution of the holes can be designed to achieve various novel wave-guiding properties that may not be possible in conventional fibers. Various PCFs have been demonstrated so far that exhibit remarkable properties such as endlessly single mode fiber, large mode area, and highly nonlinear performance. Temperature-insensitive long period gratings have attracted much attention because of their potential applications in achieving stable optical filters and gain flatteners as well as in realizing temperature-insensitive sensors for industrial and nuclear applications. Conventional fibers contain at least two different glasses, each with a different thermal expansion coefficient, thereby giving rise to high temperature sensitivity. PCFs are virtually insensitive to temperature because they are made of only one material (and air hole). This property can be used to obtain temperature-insensitive PCF-based devices. Long period gratings (LPGs) in PCF fibers have not yet been reported in India. Besides, the effect of high nuclear radiation on such PCF-based grating sensors has not been reported by any group to the best of our knowledge.

### 6.3 Theory

An LPG is formed by introducing periodic modulation of the refractive index along a single mode fiber. Such a grating induces light coupling from the fundamental guided mode to co-propagating cladding modes at discrete resonant wavelengths. LPGs in conventional fibers have been extensively used as band rejection filters, gain flattening filters, tunable couplers, and sensors. In general, as fiber devices and sensing elements, LPGs offer low back reflection, insensitivity to electromagnetic interference, and low insertion loss and cost effectiveness. For a long period grating with periodicity  $\Lambda$ , the wavelength  $\lambda^{(m)}$  at which mode coupling occurs is given by

$$\lambda^{(m)} = (n_{eff} - n_{cl,m})\Lambda \quad (5)$$

where  $n_{eff}$  is the effective refractive index of the propagating core mode at wavelength  $\lambda$ , and  $n_{cl,m}$  is the effective refractive index of the  $m$ th cladding mode. The variation in the grating period and modal effective indices due to strain and temperature causes the coupling wavelength to shift. This spectral shift is distinct for each loss band and is a function of the order of corresponding cladding mode.

The axial strain sensitivity of LPGs may be examined by expanding Eq. (5) to yield

$$\frac{d\lambda}{d\varepsilon} = \frac{d\lambda}{d(\delta n_{eff})} \left( \frac{dn_{eff}}{d\varepsilon} - \frac{dn_{cl}}{d\varepsilon} \right) + \Lambda \frac{d\lambda}{d\Lambda} \quad (6)$$

where  $\delta n_{eff} = (n_{eff} - n_{cl})$  is the differential effective index; ordinal  $m$  has been dropped for the sake of simplicity. The two terms on the right side can be divided into material (first term) and waveguide (second term) contributions. The temperature sensitivity of LPG grating is given by

$$\frac{d\lambda}{d\varepsilon} = \frac{d\lambda}{d(\delta n_{eff})} \left( \frac{dn_{eff}}{dT} - \frac{dn_{cl}}{dT} \right) + \Lambda \frac{d\lambda}{d\Lambda} \frac{1}{L} \frac{dL}{dT} \quad (7)$$

where  $\lambda$  is the central wavelength of the attenuation band,  $T$  is the temperature,  $L$  is the length of the LPG, and  $\Lambda$  is the period of the LPG. For standard long period gratings with periodicity of hundreds of micrometers, the material effect dominates the waveguide contribution. Hence, only the first term in Eqs. (6) and (7) is considered for evaluation of sensitivity. For photonic crystal fibers which are single material fibers, the first term in Eq. (7) becomes negligible, resulting in very low temperature sensitivity. This term is an order smaller than that of B-Ge-doped photosensitive fiber. This opens-up the field for PCF-based temperature-insensitive sensors.

### 6.4 Device designs

Inscription of LPGs has been demonstrated using various techniques such as UV treatment, heat treatment with a CO<sub>2</sub> laser, or by applying mechanical pressure. Formation of LPG in pure-silica core PCF fibers is not straightforward because there is no photosensitivity provided by Ge-O<sub>2</sub> vacancy defect centers. The LPGs in PCF are primarily formed due to modification of glass structure. However, any geometrical deformation results in flaws or cracks that result in fracture of the fiber, and therefore, LPGs in PCF require high precision systems. Our fully automated CO<sub>2</sub> laser-based grating writing system can set the grating period in the range of



200–800  $\mu\text{m}$  with a precision of 1  $\mu\text{m}$  while laser intensity can be stabilized within  $\pm 5\%$ . **Figure 10** shows the schematic diagram of our grating writing system. The fiber is exposed to  $\text{CO}_2$  laser for a predetermined period and the beam is scanned repeatedly over the fiber until grating of sufficient strength is formed. This operation is performed through an AutoCAD program in which the period and length of the grating are selected as per the design requirement. This method is more accurate and free from vibration related uncertainties in the grating period. The spectral response is recorded using an optical spectrum analyzer (OSA) (86142B, Agilent) which is connected to LPG through patch-cords as shown in **Figure 10**.

During application of LPG-based strain sensors, one of the main difficulties is the cross sensitivity between strain and the temperature [34]. The common methods for cross sensitivity reduction are using temperature compensation and simultaneous strain and temperature measurement. Conventional fibers contain at least two different glasses, each with a different thermal expansion coefficient, thereby giving rise to high temperature sensitivity. By use of the  $\text{CO}_2$  laser method, an LPG sensor with strain sensitivity of  $-0.45 \text{ pm}/\mu\epsilon$  and a temperature sensitivity of  $59.0 \text{ pm}/^\circ\text{C}$  was written in corning SMF-28 fiber 2. Another LPG with a strain sensitivity of  $-0.19 \text{ pm}/\mu\epsilon$  and a temperature sensitivity of  $10.9 \text{ pm}/^\circ\text{C}$  was described in PCF fiber. In this paper, we present a LPG-PCF sensor fabricated in ESM-PCF with a high strain sensitivity ( $-2.0 \text{ pm}/\mu\epsilon$ ) and negligible temperature sensitivity.

For the preparation of LPFG in an endless-single-mode photonic crystal fiber (ESM-PCF), both ends of the PCF are fusion spliced to SMFs [34]. The loss for each splice is about 0.74 dB. An X-Y scanning  $\text{CO}_2$  laser is used for the fabrication of LPGs in the ESM-PCF. The  $\text{CO}_2$  laser operates at a frequency of 2 kHz and has a maximum power of 10 W. The laser power is controlled by the mark-speed of the laser pulses. The typical grating length and period in our experiment is 23.4 mm and 450  $\mu\text{m}$ , respectively. **Figure 11** shows the transmission characteristics of a LPG fabricated on an ESM-PCF. Attenuation bands in the range of 1300–1700 nm have been investigated by an Optical spectrum analyzer.

The device has been tested on a standard strain calibration platform. **Figure 12** shows the strain-dependent wavelength shift of the fabricated device.

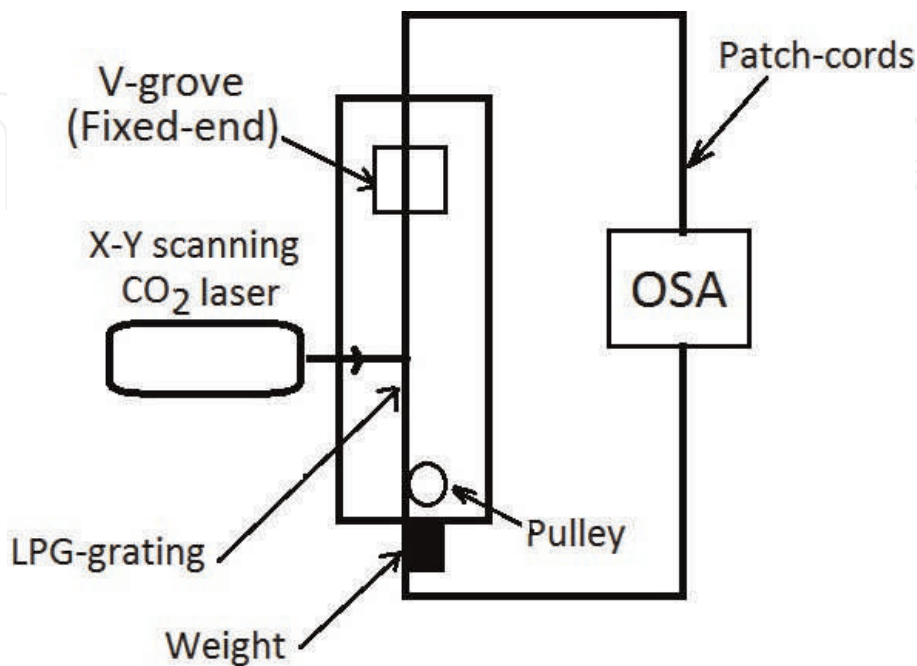


**Figure 10.** Schematic diagram of long period grating fabrication set-up [34].

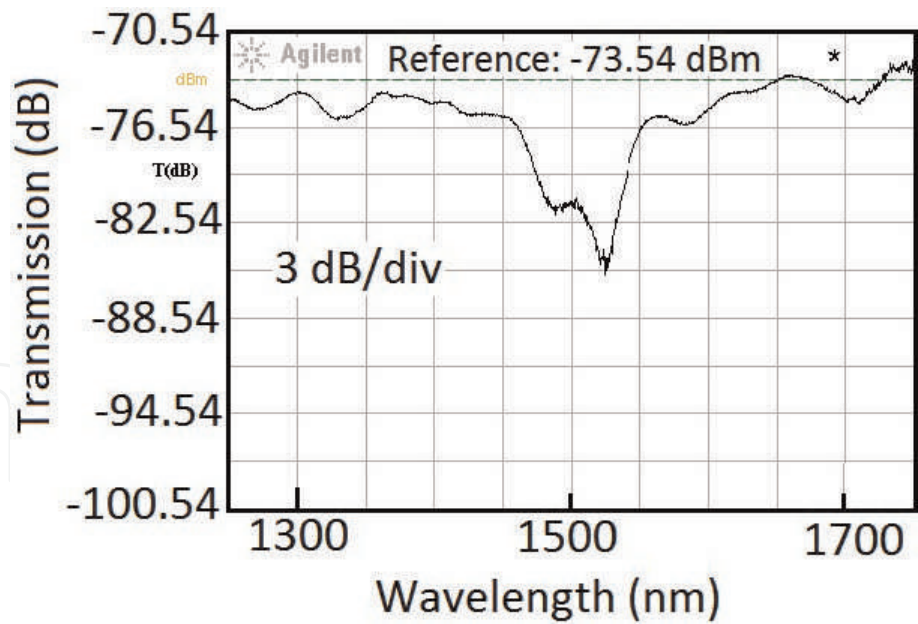


**Figure 11.**  
*Transmission characteristics of a LPG fabricated on an ESM-PCF with a period of 450  $\mu\text{m}$  [34].*

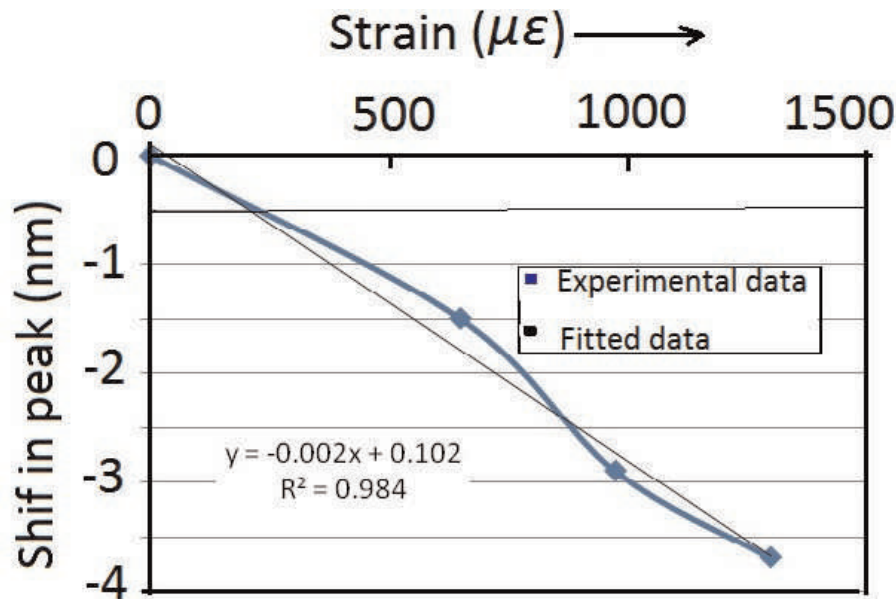


**Figure 12.**  
*Strain-dependent wavelength shift of LPG [34].*

### 6.5 Strain sensors for cryogenic environment

The tendency of superconducting magnet coils to quench prematurely, at relatively low fractions of the critical current, or to exhibit training behavior, is often attributed to mechanical issues. Knowledge of stress, strain, and displacement of the windings is therefore central to the design of the superconducting magnet. The resistive foil strain gauge has remained the device most commonly used for measuring the strain on cryogenic structures. The nonlinear thermal apparent strains and measurement sensitivity to electromagnetic noise remain the most significant limitations to its successful implementation. FBG sensor has a number of distinct advantages over other sensors, such as EMI immunity, high sensitivity, and compact size. Furthermore, the wavelength-encoded nature allows the distributed sensing of strain. Fiber Bragg gratings are used to monitor temperature and strain in

engineering structures; to date, however, their use has been limited to ambient and high temperatures, typically in the range of 273–773 K.

There exist very few published reports on FBG strain sensors that have been functional at liquid nitrogen temperature. Zhang et al. have reported one such FBG sensor used to strain sensing at 77 K and used in high temperature superconducting magnet [29]. To date, an FBG sensor used to strain sensing at 4.2 K and used in low temperature superconducting magnet has not been reported. RRCAT, Indore is also working on FBG strain and temperature sensors for cryogenic applications. The sensors show linearity in strain range from 50 to 500 micro-strain at liquid nitrogen temperature.

#### *6.5.1 Nuclear radiation sensors*

Optical fibers offer a unique capability for remote monitoring of radiation in hazardous locations such as nuclear reactors and waste storage sites. Increase of attenuation, luminescence, and radiation-induced index change have been used to design dose sensors for dose ranges up to 100 kGy. The attenuation-based sensors based on specialty doped fibers reach a saturation level above 10 kGy. To overcome this limitation, alternative techniques such as changes in fiber gratings are explored. The wavelength-encoded operation of fiber gratings can solve many measurement problems such as radiation-induced broadband transmission loss in optical fibers, source fluctuation, etc. Most Bragg grating-based sensors, reported till date, are either less sensitive or reach a saturation level near 50–150 kGy depending on the composition and grating writing technique [29–33]. Recent publications have reported measurements only up to 100 kGy. The authors Henchel et al. [35] used specialty chiral gratings and reported measurements up to 100 kGy. However, the mode orders and fiber composition in sensitive gratings were not known. Rego et al. [36] have performed gamma dose measurements on arc-induced long period fiber gratings up to 500 kGy but found no measurable shift in the resonance wavelength. Gusarov et al. [16, 17, 37] have conducted high dose measurements on FBGs but did not find high sensitivity. We have discovered sensitive gratings in commercially available single mode fibers with known composition and mode orders [38, 39]. Our results and approach are described. These are believed to be the first studies of CO<sub>2</sub> written long period gratings up to 1 MGy.

#### *6.5.2 Optical fiber composition optimization for high gamma dose and temperature sensing applications*

Following requirements explain the need for novel radiation dose sensors:

- a. Measurement of precise dose delivery is very crucial for treatment of cancer (40–50 Gy in about 20 sittings).
- b. In the case of gamma source misplacement by universities or hospitals, it is important that state-of-the-art sensors away from the source are required.
- c. Accelerators, fusion reactors, nuclear waste sites, and accidental leaks in reactors all require a sensitive, large area but remote dose sensors. Typically, the dose in various conditions and installations are: Tokamak Fusion reactor system, Japan (behind coils: 2 kGy, behind tiles: 200 MGy, 1.1 m behind port plug: 15 Gy). For space-based systems, total 10 year dose is around 100 kGy.

To cover a broad dose range from few Gy to 1 MGy, novel sensor systems like gratings are desirable. For most fibers, the increase in attenuation with dose saturates near few kGy which is accumulated within a relatively short time at certain critical locations and so they need to be replaced frequently. Even space-based systems are qualified for a dose up to 100 kGy.

6.5.3 Novel devices, fabrication technology, and testing for high radiation dose detection

Specialty doped fibers are required to measure high dose gamma radiation. These fibers should have negligible radiation-induced attenuation in IR but should show high index changes upon irradiation. Wavelength encoded fiber gratings are attractive candidates for high level gamma dose measurements in nuclear environment. This paper explains for the first time how arc-induced long period fiber gratings can be optimally designed for gamma dose measurements ranging from 1 kGy to 1 MGy.

We have investigated the gamma radiation effects on parameters of electric-arc-induced long period fiber gratings in high Ge doped and B/Ge co-doped single mode fibers. The grating resonance wavelength shifts and amplitude of the dips of various cladding modes were monitored on-line to study the role of grating fabrication and fiber chemical composition. These studies lead to identification of boron as a critical core dopant for high radiation sensitivity. After a Co-60 gamma dose of 1 MGy, the optimized gratings show radiation-induced changes of their transmission dip wavelength up to 20 nm which is comparable to CO<sub>2</sub> laser-induced gratings reported by us previously [39]. These gratings also show very high temperature sensitivity specially when operated in dispersion turn-around-point (TAP) mode [38].

Fibers doped with different boron contents in SiO<sub>2</sub>-GeO<sub>2</sub>-B<sub>2</sub>O<sub>3</sub> host were fabricated indigenously under collaboration with CGCRI, Kolkata, India. The gratings in such fibers were modeled and analyzed. We have also designed and fabricated a stable and robust sensor package unit for remote gamma dose measurements up to a dose of 1 MGy. Lab trials of such units have been carried out, and the experience in using such devices for dose estimation is discussed. These devices make arc-induced LPGs and CO<sub>2</sub> laser-induced LPGs in Boron doped fibers a strong candidate for applications in super Large Hadron Collider (LHC) and International Thermonuclear Experimental Reactor (ITER). **Table 2** shows the experimental results of such online measurements.

**Figure 13** shows our on-line gamma dose effect measurements using specialty turn-around-point (TAP) long period fiber grating.

Wavelength before exposure (nm)	Wavelength measured after 4.30 h of dose (dose of 3.6 kGy) after removal from gamma chamber (nm)
1161	1165.4
1229.6	1231
1250	1253.6
1364	1366.4
1546.7	No significant dip

**Table 2.**  
*Gamma radiation exposure data for LPG of a 400 micron grating period inscribed in Fiber Logix, SM G652 fiber. Total dose: 65 kGy.*



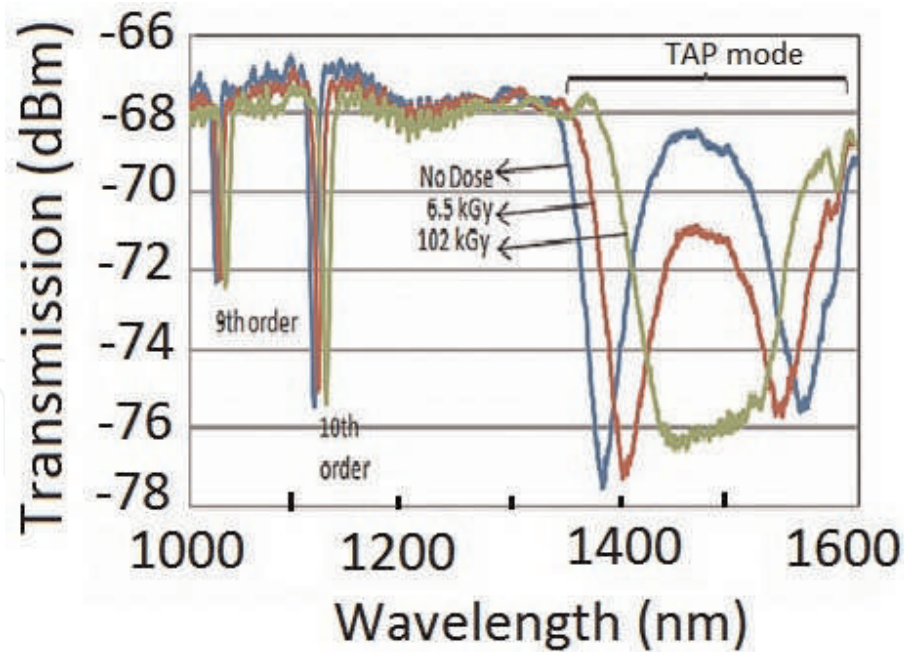


**Figure 13.**  
Real-time resonance spectral measurements of TAP-LPG in gamma field [38].

The requirement of such sensors is divergent: for radiotherapy, we need very compact needle-like disposable tip sensors with very weak annealing properties. Once a patient is given a certain dose, the tip is discarded and a new dose sensing tip is used for other patients. For high dose sensing applications, the probe with high or low annealing may be desirable depending on application. For example, for long-term monitoring of integrated dose in waste storage facility will need very low annealing dose sensors while for repetitive dose measurements like gamma pencil fabrication, a high annealing rate sensor will be required.

## 6.6 Distributed gas sensors

The detection and identification of hazardous volatile compounds with low false alarm probability in large areas such as airports, underground metro stations, mines, bus stands, and major event arenas are a very daunting task. Other strategic applications include multi-point hydrogen leak detection systems for commercial and military launch vehicles that use cryogenic hydrogen as the main propellant. This gas is highly volatile, extremely flammable, and highly explosive. Hundreds of point gas sensors with electronic circuits are needed to cater big areas. Current detection systems use transfer tubes at a small number of locations through which gas samples are drawn and stream analyzed by a mass spectrometer. They are complex and costly systems and do not provide leak location.

Among several sensing systems, absorption-based systems are extensively explored and successfully employed. There have been serious efforts to develop absorption-based fiber optic systems for gas detection with higher sensitivity, fast response, and distributed sensing capability. They are based on measurement of VIS-IR-mid IR absorption by intended chemical species. The characteristic absorption spectra can be used as a fingerprint to identify a particular gas species. For example, many gas molecules have absorption lines in 0.8–1.8  $\mu\text{m}$  band which is also a low loss transmission window of the silica fiber.

The spectral region of mid-IR is also a finger print region for most of the volatile compounds and nerve gases which is under investigation due to availability of compact tunable lasers in this band. The general principles of quantitative measurement of gas concentration have been described extensively in the literature [40, 41]. The basic principle is that the absorption is wavelength-dependent and compound specific. Initial systems used open path gas absorption cells comprising a pair of graded index collimator lenses with fiber pigtails [42]. The optical fibers here perform a passive role like transfer of light to and from absorption cell but play no active role in gas sensing. The National Aeronautics and Space Administration (NASA) reported a multi-point fiber optic multi-point hydrogen micro-sensor system for leak detection for launch vehicles [43]. The system consists of a multiplexed system having palladium coated micro lens attached to fiber tips. These chemically reactive coatings undergo changes in reflection in proportion to hydrogen concentration and are used as leak detectors. The invention of PCF or Holey fiber in 1990 opened new opportunities for exploiting the interaction of light with gases either through evanescent field or through hollow core region [44, 45]. The PCF family includes index guided PCF, hollow core photonic bandgap-fiber, and suspended core fiber.

#### *6.6.1 Index guided photonic crystal fiber*

Index-guided photonic crystal fibers are made with stack-and-draw process in fiber draw tower. They contain a periodic array of air holes running in cladding region and light is confined to solid core due to reduced effective index of the cladding. A fraction of evanescent field of power is extended into the holey region where it is absorbed by gas species and the gas concentration is obtained from intensity attenuation through the Beer-Lambert law. It is possible to design an IG-PCF that has a large fraction of evanescent power located within air-holes. This provides a good platform for gas sensing applications. Gas detectors based on absorption spectroscopy with IG-PCFs were experimentally demonstrated by Hoo et al. [46].

One concern in using IG-PCF as evanescent field sensors is the limited response time due to time required for sample gas to diffuse into holes from two open ends. Hoo et al. [46] have numerically calculated response time for acetylene gas in IG-PCF fiber ( $\lambda = 1.55 \mu\text{m}$ ,  $d = 1.4 \mu\text{m}$ ) of length  $l$  with two ends open. When the fiber sensor length is 1 m, the time required to reach 90% concentration of exposed gas in surrounding is 200 min. This shows that we have to take a very short fiber if we require a response time of 1 min governed by diffusion time. However, this will reduce the sensitivity of the device due to limited path length. It is also observed that the relative sensitivity is also about 6% of that of open path cell per equal length. To achieve fast response time, one has to introduce periodic openings along the sensing fiber and measures like micro-pumping of sampling gases. To improve sensitivity, hollow core fibers may be a better choice as efficient interaction of guided light with gas molecules would be possible.

#### *6.6.2 Hollow core photonic crystal fiber*

Hollow core photonic crystal fiber is composed of a hollow core and a cladding with holes. The light is guided through the bandgap effect due to a proper design of hole sizes and gaps. They allow simultaneous confinement of optical mode and

gas phase materials within the hollow core. This provides an excellent means for strong light/molecular interaction inside the fiber core over long distance.

### *6.6.3 Enabling technologies*

Critical issues related to distributed, high sensitivity, fast response sensors are mainly governed by the time required for gas to diffuse into the holes and open ends of the sensor fiber. One can introduce a number of transverse holes by using micro-structuring techniques. Various techniques for transverse micro-structuring have been reported. Hensley et al. [45] have reported gas cell fabrication using femtosecond micro-machining. Tightly focused laser pulses are used to produce micro-meter diameter radial channels in hollow core photonic crystal fiber, and through these micro-channels, the core of the fiber is filled with test gas. There are some reports about fabrication of microchannel by using 193 nm ArF laser. Viola et al. [43] have reported micro-hole drilling in hollow core mid-IR transmitting fibers by means of high power CO<sub>2</sub> laser shots.

### *6.6.4 Recent developments and existing fiber-based systems*

Distributed gas sensors rely on depositing specific gas sensitive coatings as cladding in multi-mode fibers or gratings and OTDR method. Recently, many designs and configurations using PCFs have been reported which targeted better sensitivity and distributed detection capability. The advantage of waveguide-based sensors over open path multiple reflection cells included low gas volume, high photon to molecular interaction, and reduction of fringe effects. Whitenett et al. [47] reported the operation of a 64 point fiber optic methane sensor installed on a landfill site in Glasgow, UK. Though the environmental conditions are harsh, the sensor has performed satisfactorily, detecting methane in the range of ~50 ppm to 100% methane. Viola et al. [42] have reported development of a distributed nerve gas sensor based on mid-IR spectroscopy. This has been possible due to availability of tunable quantum cascade lasers in the 9–10  $\mu\text{m}$  range, suitable hollow fibers for this band, and low noise cooled detectors.

## **7. Conclusion**

India is poised to use nuclear power in a big way. The safety of these power stations will depend on monitoring the radiation levels near plant and at waste disposal sites. In such environments, conventional sensors have certain limitations. Fiber-based sensors are being developed all over the world and are expected to make significant contribution to safe operation of nuclear fuel cycle. New technologies of laser micro- and nano-processing, mid-IR transmitting fibers, and hollow fibers have opened development of new structures and devices like fast response PCF-based gas sensors, high temperature Bragg gratings, distributed nerve gas sensors, and distributed nuclear radiation sensors for home land security. On the other hand, availability of all silica nuclear resistant fibers and nano-fibers and possibility of grating writing in such fibers using focused ion beam source and femto-sec lasers have attracted their use for different parameter monitorings like structural health monitoring in nuclear reactors, tokamaks, and storage facilities.

## Acknowledgements

The authors are thankful for the help received from Shri Jai Kishore, Smt. Smita Chaubey, and Shri Sanjai Kumar of Fiber Sensors Lab., RRCAT, Indore, in conducting various experiments.

## List of acronyms

AS	anti-Stokes
CGCRI	Central Glass & Ceramic Research Institute
DE	dual-ended
DNA	deoxyribonucleic acid
DWT	discrete wavelet transform
EMI	electromagnetic interference
ESM-PCF	endless-single-mode photonic crystal fiber
FBG	fiber Bragg gratings
FIR	finite impulse response
IIR	infinite impulse response
ITER	International Thermonuclear Experimental Reactor
LHC	Large Hadron Collider
LPGs	long period gratings
MOSFET	metal-oxide semiconductor field-effect transistor
NASA	National Aeronautics and Space Administration
OSA	optical spectrum analyzer
OTDR	optical time domain reflectometry
PCFs	photonic crystal fibers
RGs	regenerated gratings
ROFDTs	Raman optical fiber-based distributed temperature sensors
RRCAT	Raja Ramanna Centre for Advanced Technology
SNR	signal-to-noise ratio
St	Stokes
TAP	turn-around-point
TDM	time division multiplexing
TLD	thermoluminescent dosimeter
UV	ultraviolet
WDM	wavelength division multiplexing



IntechOpen

IntechOpen

### **Author details**

Sanjay Kher\* and Manoj Kumar Saxena  
Fiber Sensors Lab., FSOSS, Raja Ramanna Centre for Advanced Technology, Indore,  
India

\*Address all correspondence to: [kher@rrcat.gov.in](mailto:kher@rrcat.gov.in)

### **IntechOpen**

---

© 2019 The Author(s). Licensee IntechOpen. This chapter is distributed under the terms of the Creative Commons Attribution License (<http://creativecommons.org/licenses/by/3.0>), which permits unrestricted use, distribution, and reproduction in any medium, provided the original work is properly cited. 

## References

- [1] Zhao XF, Li L, Ba Q, Ou JP. Scour monitoring system of subsea pipeline using distributed Brillouin optical sensors based on active thermometry. *Optics and Laser Technology*. 2012;**44**: 2125-2129
- [2] Lopez RM, Spirina VV, Miridonova SV, Shlyagina MG, Beltran G, Kuzin EA. Fiber optic distributed sensor for hydrocarbon leak localization based on transmission/reflection measurement. *Optics and Laser Technology*. 2012;**34**: 465-469
- [3] Culshaw B, Kersey A. Fiber-optic sensing: A historical perspective. *Journal of Lightwave Technology*. 2008;**26**: 1064-1078
- [4] Grattan KTV, Sun T. Fiber optic sensor technology: An overview. *Sensors and Actuators A Physical*. 2000; **82**:40-61
- [5] Dakin JP. Distributed optical fiber sensor systems. In: Culshaw B, Dakin J, editors. *Optical Fiber Sensors: Systems and Applications*. Vol. 2. Norwood, MA: Artech House; 1989. pp. 575-588
- [6] Rogers AJ. Distributed optical-fiber sensors for the measurements of pressure, strain and temperature. *Physics Reports*. 1988;**169**:99-143
- [7] Yilmaz G, Karlik SE. A distributed optical fiber sensor for temperature detection in power cables. *Sensors and Actuators A Physical*. 2006;**125**:148-155
- [8] Hurtig E, Großwig S, Kühn K. Fiber optic temperature sensing: Application for subsurface and ground temperature measurements. *Tectonophysics*. 1996; **257**:101-109
- [9] Höbel M, Ricka J, Wüthrich M, Binkert T. High-resolution distributed temperature sensing with the multiphoton-timing technique. *Applied Optics*. 1995;**34**(16):2955-2967
- [10] Long DA. *The Raman Effect*. England: John Wiley; 2002. pp. 49-131
- [11] Dakin JP, Pratt DJ, Bibby GW, Ross JN. Distributed optical fiber Raman temperature sensor using a semiconductor light source and detector. *Electronics Letters*. 1985; **21**(13):569-560
- [12] Hill KO et al. Photosensitivity in optical fiber waveguides: Application to reflection fiber fabrication. *Applied Physics Letters*. 1978;**32**:647-649
- [13] Kersey AD, Davis MA, Patrick HJ, LeBlanc M, Koo KP, Askins CG, et al. Fiber grating sensors. *Journal of Lightwave Technology*. 1997;**15**(8): 1442-1463
- [14] Shimada Y, Nishimura A. Development of optical fiber Bragg grating sensors for structural health monitoring. *Journal of Laser Micro/Nano Engineering*. 2013;**8**(1):110-114
- [15] Kashyup R. *Fiber Bragg Gratings*. San Diego, CA, USA: Academic Press; 1999
- [16] Kher S, Srikanth G, Chaube S, Chakraborty AL, Nathan TPS, Bhawalkar DD. Design, development and studies on Raman based fiber-optic distributed temperature sensor. *Current Science*. 2002;**83**(11):1365-1368
- [17] Kher S, Srikanth G, Saxena MK, Nathan TPS. Development of distributed fiber optic temperature sensor with sub-meter resolution. *Current Science*. 2004;**86**(9):1202-1204
- [18] Chakraborty AL, Sharma RK, Saxena MK, Kher S. Compensation for temperature dependence of Stokes signal and dynamic self-calibration of a

Raman distributed temperature sensor. *Optics Communication*. 2007;**274**: 396-402

[19] Chakraborty AL, Kher S, Chaubey S, Nathan TPS. Bidirectional frequency-domain digital filtering to simultaneously improve temperature resolution and eliminate spatial inaccuracy of a distributed temperature sensor. *Optical Engineering*. 2004; **43**(11):2724-2729

[20] Stoddart PR, Cadusch PJ, Pearce JB, Vukovic D, Nagrajah CR, Booth DJ. Fiber optic distributed temperature sensor with an integrated background correction function. *Measurement Science and Technology*. 2005;**16**(6): 1299-1304

[21] Saxena MK, Raju SDVSJ, Kher S, Arya R, Ravindranath SVG, Kher S, et al. Optical fiber distributed temperature sensor using short term Fourier transform based simplified signal processing of Raman signals. *Measurement*. 2014;**47**:345-355

[22] Guang-yong X, Jian-ping Y, Kun-jun Z, Wen M. Monitoring data processing of distributed optical fiber temperature sensor based on multi-wavelet. In: *Proceedings of the International Workshop on Education Technology and Training & International Workshop on Geoscience and Remote Sensing*. 2008. pp. 203-206

[23] Saxena MK, Raju SDVSJ, Arya R, Pachori RB, Ravindranath SVG, Kher S, et al. Raman optical fiber distributed temperature sensor using wavelet transform based simplified signal processing of Raman backscattered signals. *Optics & Laser Technology*. 2015;**65**:14-24

[24] [www.google.co.in/search?q=BACKSCATTERED+LASER+LIGHT&source=lnms&tbm=isch&sa=X&ved=0ahUKEwiCvf-iq9jcAhWKT30KHdJ4CjYQ\\_AUICigB&biw=1093&bih=530](http://www.google.co.in/search?q=BACKSCATTERED+LASER+LIGHT&source=lnms&tbm=isch&sa=X&ved=0ahUKEwiCvf-iq9jcAhWKT30KHdJ4CjYQ_AUICigB&biw=1093&bih=530)

[25] Fukuzawa T, Shida H, Oishi K, Takeuchi N, Adachi S. Performance improvements in Raman distributed temperature sensor. *Photonic Sensors*. 2013;**3**(4):314-319

[26] Fernandez AF, Rodeghiero P, Brichard B, Berghmans F, Hartog AH, Hughes P, et al. Radiation-tolerant Raman distributed temperature monitoring system for large nuclear infrastructures. *IEEE Transaction on Nuclear Science*. 2005;**52**(6):2689-2694

[27] Lee CE. Self-calibrating technique enables long-distance temperature sensing. *Laser Focus World*. 2007;**43**: 101-117

[28] Suh K, Lee C. Auto-correction method for differential attenuation in a fiber-optic distributed-temperature sensor. *Optics Letters*. 2008;**33**(16): 1845-1847

[29] Zhang H, Wang Q, et al. Fiber Bragg grating sensor for strain sensing in low temperature superconducting magnet. *IEEE Transactions on Applied Superconductivity*. 2010;**20**(3): 1798-1801

[30] Marcelo M, Allil RCSB, de Nazar FVB. 14. Chapter "A Guide to Fiber Bragg Grating Sensors": In: *Current Trends in Short- and Long-period Fiber Gratings*. 2013

[31] Gusarov AI, Starodubov DS, et al. Comparative study of MGy dose level  $\gamma$ -radiation effect on FBGs written in different fibers. In: *Proceedings of the OFS-13*; April 12-16, 1999; Kyongju, Korea

[32] Gusarov AI, Chojetzkib C, et al. High total dose radiation effects on temperature sensing Fiber Bragg gratings. *IEEE Photonics Technology Letters*. 1999;**11**(9):1159-1161

[33] Krebber K et al. Fiber Bragg gratings as high dose radiation sensors.

Measurement Science & Technology.  
2006;**17**:1095-1102

[34] Kher S, Chaube S, et al. Fiber optic temperature-insensitive, strain sensors for nuclear applications. *International Journal of Applied Engineering and Technology*. 2011;**1**(1):61-67. Available from: <http://www.cibtech.org/J-ENGINEERING-TECHNOLOGY/PUBLICATIONS/2011/Vol%201%20No.%201/16-03-JET-Kher.pdf>

[35] Henschel H et al. High radiation sensitivity of Chiral long period gratings. *IEEE Transactions on Nuclear Science*. 2010;**57**(5):2915-2922

[36] Rego G et al. Effect of ionizing radiation on the properties arc-induced long period fiber gratings. *Applied Optics*. 2005;**44**(29):6258-6263

[37] Gusarov AI et al. Comparative study of MGy dose level  $\gamma$ -radiation effect on FBGs written in different fibers. In: *Proceedings of the OFS-13*; April 12–16, 1999; Kyongju, Korea

[38] Kher S, Chaubey S, Kashyap R, Oak SM. Turnaround-point long period fiber gratings (TAP-LPGs) as high radiation dose sensors. *IEEE Photonics Technology Letters*. 2012;**24**(9):742-744

[39] Kher S, Chaubey S, Oak SM. Long period fiber grating based nuclear radiation sensors for high level dose applications. *Journal of Instrumentation Science & Technology*. 2013;**41**(2): 135-142

[40] Bernath FP. *Spectra of Atoms and Molecules*. New York: Oxford University Press; 2005

[41] Svanburg S. *Atomic and Molecular Spectroscopy: Basic Aspects & Practical Applications*. Berlin: Springer; 2004

[42] Ho HL, Jim W, Demoken MS. Quantitative measurement of acetylene by using external cavity tunable diode

laser. In: *Proc. SPIE 3852, Harsh Environment Sensors II*; Boston, US. 1999. pp. 124-133

[43] Viola R, Liberatore N, et al. Distributed nerve gases sensor based on IR absorption in hollow optical fiber. *SPIE Proceedings*. 2010;**7838**:78380H

[44] Kazemi AA, Goepp JW, et al. Fiber optic microsensors hydrogen leak detection system on aerospike X-33. In: *SPIE Proceedings 6758, Photonics in the Transportation Industry: Auto to Aerospace*; Oct. 2007

[45] Hensley CJ, Broaddus DH, et al. Photonic bandgap fiber gas cell fabricated using fs micromachining. *Optics Express*. 2007;**15**(11):6690-6695

[46] Hoo YL, Jin W, et al. Design and modeling of a photonic crystal fiber gas sensor. *Applied Optics*. 2003;**22**(18): 3509-3515

[47] Whitenett G et al. Optical fibre instrumentation for environmental monitoring applications. *IOP Journal of Optics A: Pure and Applied Optics*. 2003;**5**:S140-S145